論文 / 著書情報
Article / Book Information

題目(和文)	反平行磁場中の引力相互作用するフェルミ気体の物理
Title(English)	Physics of an attractive Fermi gas in antiparallel magnetic fields
著者(和文)	安斎貴昭
Author(English)	Takaaki Anzai
出典(和文)	学位:博士(理学), 学位授与機関:東京工業大学, 報告番号:甲第11363号, 授与年月日:2020年3月26日, 学位の種別:課程博士, 審査員:西田 祐介,齋藤 晋,村上 修一,古賀 昌久,相川 清隆
Citation(English)	Degree:Doctor (Science), Conferring organization: Tokyo Institute of Technology, Report number:甲第11363号, Conferred date:2020/3/26, Degree Type:Course doctor, Examiner:,,,,
学位種別(和文)	博士論文
Type(English)	Doctoral Thesis

Dissertation

Physics of an attractive Fermi gas in antiparallel magnetic fields

Takaaki Anzai
Department of Physics, Tokyo Institute of Technology

February 18, 2020

Abstract

Ceaseless progress in ultracold atom experiments allows us to control system parameters at will. For example, the strength of the interaction between atoms can be arbitrarily tuned by varying a magnetic field via Feshbach resonances, which is unprecedented in other fields of physics. This technique applied to two-component Fermi gases led to the realization of smooth evolution from a Bardeen-Cooper-Schrieffer (BCS) superfluid of Cooper pairs to a Bose-Einstein condensation (BEC) of tightly bound molecules. This phenomenon is called "BCS-BEC crossover." Furthermore, the dimensionality can be tuned by confining atoms with an optical lattice generated by two counterpropagating laser beams. By confining Fermi gases in the two-dimensional (2D) space, the BCS-BEC crossover in 2D has also come to the reach of experimental investigation. In addition to tuning the interaction and dimensionality at will, we can control the quantum statistics and internal degrees of freedom. Therefore, ultracold atoms provide an ideal platform to study quantum many-body systems.

In general, phenomena induced by magnetic fields are important in various fields of physics. Therefore, by taking advantage of the experimental abilities to control system parameters of ultracold atoms at will, it is worthwhile to investigate phenomena induced by magnetic fields with ultracold atoms. However, atoms are electrically neutral, so that their orbital motion does not occur by magnetic fields. So far, enormous research efforts have been devoted to developing experimental techniques to create synthetic magnetic fields. One approach is to optically couple internal states of atoms so that neutral atoms can behave like charged particles in a magnetic field, which provided a new route towards the realization of topological physics with ultracold atoms. This approach was further extended to create "antiparallel" magnetic fields which are equal in magnitude but opposite in directions for different spin components of atoms.

In this thesis, we investigate the ground-state properties of an attractive Fermi gas with two spin components subjected to antiparallel magnetic fields in the mean-field approximation. Whereas the attractive interaction generally favors the Cooper pairing, the antiparallel magnetic fields lead to the Landau-level formation with opposite chiralities for different spin components of atoms. Therefore, we can expect

interesting physics to be realized by competition or cooperation between the Cooper pairing and antiparallel magnetic fields. Moreover, attractively interacting Fermi gases with two spin components in antiparallel magnetic fields may be viewed as a simulator of analogous phenomena in other fields of physics, such as exciton condensation and chiral condensation in a magnetic field, where two particles forming a pair have opposite charges and thus experience opposite Lorentz forces.

Firstly, we study a 2D spin-balanced Fermi gas in antiparallel magnetic fields. We find that the mean-field phase diagram at zero temperature consists of superfluid and quantum spin Hall insulator phases and closely resembles that of the Bose-Hubbard model, which consists of superfluid and Mott insulator phases. The resulting two phases are separated by a second-order quantum phase transition classified into the universality class of either the dilute Bose gas or XY model. We also calculate some physical quantities to elucidate the ground-state properties in the superfluid phase. In particular, we show that the pairing gap is enhanced by antiparallel magnetic fields as a consequence of magnetic catalysis.

Next, we study a 2D spin-imbalanced Fermi gas in antiparallel magnetic fields. By employing the mean-field approximation, we find that the Fulde-Ferrell (FF) state is energetically favored over the Larkin-Ovchinnikov (LO) state in the weak-coupling limit. We then clarify the mean-field phase diagram at zero temperature in the space of the attraction, average chemical potential, and Zeeman field analytically at weak coupling as well as numerically beyond it. We find that the resulting phase diagram shows the rich structures consisting of quantum Hall insulator, unpolarized superfluid, and FF phases separated by various first-order and second-order quantum phase transitions. Moreover, we show that the FF phases occupy the reasonable portions of the phase diagram, so that they may, in principle, be realized by ultracold atom experiments.

Finally, we study a three-dimensional (3D) spin-imbalanced Fermi gas in antiparallel magnetic fields with the ansatz of the FF state. Under the condition that fermions occupy the lowest Landau level, we find that the mean-field thermodynamic potential of a 3D spin-imbalanced Fermi gas in the magnetic fields corresponds to that of a one-dimensional (1D) spin-imbalanced Fermi gas without magnetic fields at weak coupling. We then clarify that the ground-state phase diagram consists of fully polarized normal, unpolarized superfluid, and FF phases. By calculating the collective excitation spectrum, we show that the long-range order exists in the weak-coupling limit, where our system is effectively described by a 1D spin-imbalanced Fermi gas without the magnetic fields.

Contents

Chapter 1

Introduction

Attractively interacting fermions with two spin components appear in various fields of physics such as condensed matter physics and nuclear physics. When the attractive interaction between fermions is weak, two fermions with different spin components form a Cooper pair by the BCS mechanism. Therefore, the ground state exhibits superconductivity or superfluidity by the condensation of Cooper pairs. On the other hand, when the attractive interaction is strong, two fermions form a bound molecule, which obeys the Bose-Einstein statistics. Therefore, the ground state also exhibits superconductivity or superfluidity by the BEC of tightly bound molecules. It is known that these weak and strong coupling regimes in the ground state are connected without phase transitions. Such smooth evolution from a condensation of Cooper pairs to a BEC of tightly bound molecules is called "BCS-BEC crossover" [1, 2].

Originally, the problem of the BCS-BEC crossover was studied by Eagles in the context of superconductivity in metals with a low electron density [3]. Leggett also considered the crossover problem in the context of superfluid ^{3}He [4, 5]. Nozières and Schmitt-Rink extended Leggett's study to investigate the evolution of the critical temperature across the BCS-BEC crossover [6]. Whereas authors in Refs. [3, 4, 5, 6] focused on the 3D case, early studies of the crossover problem in 2D was carried out by Miyake [7] and Randeria [8, 9]. Despite these theoretical studies, the BCS-BEC crossover was not realized until 2004.

In 2004, the 3D BCS-BEC crossover was firstly observed in ultracold gases of fermionic ^{40}K and ^{6}Li atoms [10, 11]. In these experiments, the strength of the attractive interaction between fermions can be arbitrarily tuned by varying a magnetic field via Feshbach resonances [12, 13], which is unprecedented in other fields of physics. Moreover, the dimensionality can be tuned by confining atoms with an optical lattice generated by two counterpropagating laser beams [14]. Therefore, by confining Fermi gases in the 2D space [15, 16, 17], the 2D BCS-BEC crossover has also come to the reach of experimental investigation [18, 19, 20, 21, 22, 23,

24, 25, 26, 27, 28, 29, 30, 31, 32]. Until now, for example, the observation of the Berezinskii-Kosterlitz-Thouless (BKT) transition [33, 34, 35, 36] and the measurement of the thermodynamic equation of state have been reported in Refs. [28, 29] and Refs. [26, 30, 31], respectively. More recently, motivated by the experimental realization of a spin-imbalanced Fermi gas in 3D [37, 38] and 2D [27], the ground-state phase diagram of a spin-imbalanced Fermi gas in 2D has been studied theoretically by several authors [39, 40, 41, 42]. They were interested in elucidating how much area in the ground-state phase diagram is occupied by the Fulde-Ferrell-Larkin-Ovchinnikov (FFLO) state, where the Cooper pairing takes place with nonzero momentum [43, 44]. In addition to tuning the interaction, dimensionality, and population imbalance at will, we can also control the quantum statistics and internal degrees of freedom. Therefore, ultracold atoms provide an ideal platform to study quantum many-body systems.

In general, phenomena induced by magnetic fields are important in various fields of physics. Therefore, by taking advantage of the experimental abilities to control system parameters of ultracold atoms at will, it is worthwhile to investigate phenomena induced by magnetic fields with ultracold atoms. However, atoms are electrically neutral, so that their orbital motion does not occur by magnetic fields. So far, enormous research efforts have been devoted to developing experimental techniques to create synthetic magnetic fields [45, 46, 47, 48, 49]. In a synthetic magnetic field, neutral atoms can behave like charged particles in a magnetic field. A simple way of creating synthetic magnetic fields is to rotate ultracold gases [45, 46]. This utilizes the fact that a Coriolis force in a rotating system corresponds to a Lorentz force in a magnetic field. Rotating atomic gases were observed by several groups [50, 51, 52, 53]. Another approach to creating synthetic magnetic fields is to couple internal states of atoms by laser beams [47, 48, 49]. In this approach, synthetic magnetic fields were firstly implemented for ^{87}Rb BECs [54, 55]. Recently, this approach was further extended to create "antiparallel" magnetic fields, which act on two different spin components of atoms with the same magnitude but in opposite directions [56, 57, 58]. In particular, Beeler *et al.* implemented antiparallel magnetic fields for ^{87}Rb BECs with two spin components and observed the spin Hall effect [56]. Although antiparallel magnetic fields have not been implemented for Fermi gases, there is a proposal to use fermionic ^{40}K atoms confined in a quasi-2D space [56]. If fermions with two spin components in antiparallel magnetic fields are realized in ultracold atom experiments, we can expect the quantum spin Hall insulator composed of two quantum Hall states with opposite chiralities for different spin components [59, 60, 61]. We note that attractively interacting Fermi gases with two spin components in antiparallel magnetic fields may be viewed as a simulator of analogous phenomena in other fields of physics, such as exciton condensation and chiral condensation in a magnetic field, where two particles forming a pair have opposite charges and thus experience opposite Lorentz forces [62, 63, 64].

In the context of the chiral condensation in a magnetic field, the magnetic catalysis and inverse magnetic catalysis have been known as interesting phenomena induced by a magnetic field [63, 64]. The magnetic catalysis means an enhancement of dynamical symmetry breaking by a magnetic field [63, 64]. In the mechanism of the magnetic catalysis, a magnetic field enhances the condensation of pairs of a fermion and an antifermion with opposite charges, which is in contrast to the case of superconductivity. In a superconductor, a magnetic field tends to break a charged Cooper pair of two electrons with opposite magnetic moments because a magnetic field induces the orbital motion of a charged Cooper pair and the frustration of the magnetic moment pointing in the opposite direction from the magnetic field. It was revealed in Refs. [65, 66, 67] that the essence of the magnetic catalysis is the dimensional reduction, $D \to D-2$, in the low-energy dynamics of the pairing fermions in a magnetic field. This reduction results from the fact that the motion of fermions is restricted in the directions perpendicular to the magnetic field. More recently, the lattice studies of quantum chromodynamics revealed that the critical temperature for the chiral symmetry restoration phase transition decreases with an external magnetic field, although the chiral condensation at $T = 0$ increases with an external magnetic field. This suppression is referred to as "inverse magnetic catalysis" [64].

In this thesis, we investigate the ground-state properties of an attractive Fermi gas with two spin components subjected to antiparallel magnetic fields in the mean-field approximation. Whereas the attractive interaction generally favors the Cooper pairing, the antiparallel magnetic fields lead to the Landau-level formation with opposite chiralities for different spin components of atoms. Our purpose is to deeply understand how the antiparallel magnetic fields and Cooper pairing compete or cooperate to give rise to interesting physics. Many theoretical works have been made on ultracold gases in antiparallel magnetic fields. For 2D Bose gases, the ground-state phase diagram was investigated in Refs. [68, 69, 70] and Yoshino *et al* studied collective modes [71]. For 3D Fermi gases, the superfluid transition temperature was investigated in Ref. [72]. For ultracold gases in optical lattices, the ground-state phase diagram of 2D Fermi gases was investigated in Refs. [73, 74, 75, 76, 77]. The critical BCS and BKT transition temperatures of 2D Fermi gases were studied in Refs. [77, 78, 79]. Zeng *et al.* proposed a way to realize higher-order topological superfluidity by using ultracold atoms in optical lattices [80]. We note that our continuum model of an attractive Fermi gas with two spin components in antiparallel magnetic fields is related to the time-reversal invariant Hofstadter-Hubbard model in the flat-band regime [77, 78]. In Ref. [78], it was shown that a pairing gap and superfluid density are proportional to the coupling constant at weak coupling.

This thesis is organized as follows. In Chapter 2, we review the previous works for 2D quantum systems: BCS-BEC crossover, Bose-Hubbard model, and magnetic catalysis. In Chapter 3, we investigate a 2D spin-balanced Fermi gas in antiparallel magnetic fields. We determine the ground-state phase diagram and discuss

the universality class of quantum phase transitions. We also calculate some physical quantities to clarify ground-state properties. In Chapter 4, we investigate a 2D spin-imbalanced Fermi gas in antiparallel magnetic fields and determine the ground-state phase diagram analytically at weak coupling as well as numerically beyond it. In particular, we elucidate how much area in the ground-state phase diagram is occupied by the FFLO state. In Chapter 5, we investigate a 3D spin-imbalanced Fermi gas in antiparallel magnetic fields with the ansatz of the FF state. We determine the ground-state phase diagram under the condition that fermions only occupies in the lowest Landau level. We also calculate the collective excitation spectrum to discuss the stability of the superfluid state. We summarize this thesis in Chapter 6. Throughout this thesis, we set $\hbar = 1$.

Chapter 2

Review of two-dimensional quantum systems

In this chapter, we review three topics on 2D quantum systems: BCS-BEC crossover, Bose-Hubbard model, and magnetic catalysis. These topics are useful to better understand our study of an attractive Fermi gas in antiparallel magnetic fields.

2.1 BCS-BEC crossover

In Section 2.1.1, we follow Ref. [81] and review the scattering problem in 2D. In Section 2.1.2, we follow Ref. [41] and review the ground-state phase diagram of a 2D Fermi gas with population imbalance under the ansatz of the FF state, where the order parameter has a spatially varying phase with a constant magnitude, $\Delta(\boldsymbol{x}) = \Delta_0 \mathrm{e}^{i\boldsymbol{Q}\cdot\boldsymbol{x}}$, within the mean-field approximation.

2.1.1 Scattering problem

We consider two fermions with two different spin components interacting via a short-range potential $V(r)$ with a range r_0, which is assumed to only depend on the magnitude of the relative coordinate $\boldsymbol{r}$. The 2D Schrödinger equation in the center-of-mass frame is given by

$$\left[-\frac{\boldsymbol{\nabla}}{m} + V(r)\right]\phi(\boldsymbol{r}) = E\phi(\boldsymbol{r}) \tag{2.1}$$

with the particle mass m and the energy E. The wave function can then be written as $\phi(\boldsymbol{r}) = R(r)T(\varphi)$ and the Schrödinger equation can be separated into two parts:

$$\frac{d^2}{d\varphi^2}T(\varphi) = -\ell^2 T(\varphi), \tag{2.2}$$

$$\left[-\frac{1}{mr}\frac{d}{dr}\left(r\frac{d}{dr}\right) + \frac{\ell^2}{mr^2} + V(r)\right] R(r) = ER(r). \tag{2.3}$$

The quantum number ℓ corresponds to the angular momentum around the axis perpendicular to the plane and takes integer because the wave function $T(\varphi)$ has to be single-valued.

In the asymptotic limit $r \to \infty$, the wave function can be written as a superposition of an incident plane wave and a scattered wave,

$$\phi(r) \to \mathrm{e}^{ikr\cos\varphi} - \sqrt{\frac{i}{8\pi kr}} f(\boldsymbol{k}) \mathrm{e}^{ikr}, \tag{2.4}$$

where $\boldsymbol{k} = k\hat{\boldsymbol{r}}$ is the relative momentum with its magnitude k defined by $E = k^2/m$. The scattering amplitude $f(\boldsymbol{k})$ can then be expanded in the partial waves as

$$f(\boldsymbol{k}) = \sum_{\ell=0}^{\infty} (2 - \delta_{\ell,0}) \cos(\ell\varphi) f_\ell(k), \tag{2.5}$$

where the function $f_l(k)$ is related to the phase shift δ_ℓ by the following expression:

$$f_\ell(k) = \frac{-4}{\cot\delta_\ell - i}. \tag{2.6}$$

In the low-energy limit, for example, the phase shift for the s-wave ($\ell = 0$) can be expanded as

$$\cot\delta_0(k) = -\frac{2}{\pi}\ln\left(\frac{1}{ka_{2\mathrm{D}}}\right) + \mathcal{O}\left(k^2\right), \tag{2.7}$$

where $a_{2\mathrm{D}} > 0$ is a 2D scattering length.

Now, we assume the attractive interaction, which has a range r_0 much shorter than the mean interparticle distance and the thermal de Broglie wavelength. Therefore, the attractive interaction can be effectively considered as a contact, s-wave interaction and the two-body problem is described by the following Hamiltonian:

$$H = \sum_{\boldsymbol{k}} \frac{k^2}{m} |\boldsymbol{k}\rangle \langle\boldsymbol{k}| - \frac{1}{L^2}\sum_{\boldsymbol{k},\boldsymbol{k}'} g(\boldsymbol{k},\boldsymbol{k}') |\boldsymbol{k}\rangle \langle\boldsymbol{k}'|, \tag{2.8}$$

where L is the linear size of the system. The contact interaction $g(\boldsymbol{k},\boldsymbol{k}') \equiv \langle \boldsymbol{k}|\hat{g}|\boldsymbol{k}'\rangle$ is taken to be constant $g > 0$ up to a large ultraviolet cutoff $k_\Lambda \sim 1/r_0$. It is convenient to describe the interaction between two fermions in terms of a T matrix, which is obtained from the following series,

$$T(E) = -g + (-g)\frac{1}{E - q^2/m}(-g) + \cdots \equiv \frac{1}{-g^{-1} + \Pi(E)}, \tag{2.9}$$

where the one-loop polarization bubble is given by

$$\Pi(E) = \frac{m}{2\pi}\int_0^\Lambda d\epsilon\, \frac{1}{2\epsilon - E} \tag{2.10}$$

with an energy cutoff $\Lambda \equiv k_\Lambda^2/(2m)$. When we set $E \equiv -\epsilon_b$ with $\epsilon_b > 0$, the relation between the coupling constant g and the binding energy ϵ_b is obtained by the pole of the T matrix,

$$\frac{1}{g} = \Pi(-\epsilon_b) = \frac{m}{2\pi}\int_0^\Lambda d\epsilon\, \frac{1}{2\epsilon + \epsilon_b}. \tag{2.11}$$

Therefore, a two-body bound state always exists for the attractive contact interaction in 2D and its binding energy ϵ_b is given by $\epsilon_b = 2\Lambda e^{-4\pi/(mg)}$. We can use Eq. (2.11) to remove the dependence on Λ in the physics beyond the two-body problem by replacing the coupling constant g with the two-body binding energy ϵ_b.

When we consider the on-shell scattering of two fermions at incoming momenta $\pm\boldsymbol{k}_i$ into outgoing momenta $\pm\boldsymbol{k}_f$ with $k = |\boldsymbol{k}_i| = |\boldsymbol{k}_f|$, the scattering amplitude $f(\boldsymbol{k})$ is related to the T matrix, $f(\boldsymbol{k}) = mT(k^2/m)$. Then, the relation between the binding energy ϵ_b and the 2D scattering length $a_{2\mathrm{D}}$ is given by $\epsilon_b = 1/(ma_{2\mathrm{D}}^2)$.

Finally, we note that the 2D scattering length $a_{2\mathrm{D}}$ is related to the 3D scattering length $a_{3\mathrm{D}}$, which is tuned via Feshbach resonances. In ultracold atom experiments, 2D atoms are realized by confining atoms in a highly anisotropic trapping potential $U(\boldsymbol{x}) = m\omega_z^2 z^2/2 + m\omega_\perp^2(x^2+y^2)/2$ with $\omega_\perp \ll \omega_z$ and the motion of trapped fermions along the z direction is restricted to their zero-point oscillation [15, 16, 17]. According to Refs. [1, 82], by considering the low-energy scattering, the 2D scattering length $a_{2\mathrm{D}}$ can be expressed as

$$a_{2\mathrm{D}} = a_z\sqrt{\frac{\pi}{0.905}}\exp\left(-\sqrt{\frac{\pi}{2}}\frac{a_z}{a_{3\mathrm{D}}}\right) \tag{2.12}$$

with a transverse harmonic-oscillator length $a_z \equiv 1/\sqrt{m\omega_z}$. In particular, if $a_z \gg -a_{3\mathrm{D}} > 0$, the dimensionless coupling constant mg can be approximated by

$$mg = -\sqrt{8\pi}\frac{a_{3\mathrm{D}}}{a_z} \tag{2.13}$$

within the Born approximation.

2.1.2 Ground-state phase diagram

We consider attractive 2D fermions with population imbalance, which are described by the following Hamiltonian:

$$H = \sum_{\sigma=\uparrow,\downarrow} \int d^2\boldsymbol{x}\, \phi_\sigma^*(\boldsymbol{x}) \left[-\frac{\boldsymbol{\nabla}^2}{2m} - \mu_\sigma \right] \phi_\sigma(\boldsymbol{x}) - g \int d^2\boldsymbol{x}\, \phi_\uparrow^*(\boldsymbol{x}) \phi_\downarrow^*(\boldsymbol{x}) \phi_\downarrow(\boldsymbol{x}) \phi_\uparrow(\boldsymbol{x}), \tag{2.14}$$

where m is the mass of fermions and μ_σ is the chemical potential for each spin component. To determine the ground-state phase diagram in the plane of the average chemical potential $\mu \equiv (\mu_\uparrow + \mu_\downarrow)/2$ and Zeeman field $h \equiv (\mu_\uparrow - \mu_\downarrow)/2$, we perform the standard mean-field approximation with the ansatz of the FF state, $\Delta(\boldsymbol{x}) = \Delta_0 \mathrm{e}^{i\boldsymbol{Q}\cdot\boldsymbol{x}}$. The resulting mean-field thermodynamic potential at zero temperature takes the form [41],

$$\Omega_{\mathrm{MF}} = -\frac{1}{4\pi^2} \int d^2\boldsymbol{k} \left(E_k - \widetilde{\xi}_k - \frac{\Delta_0^2}{2\epsilon_k + \epsilon_b} \right) + \frac{1}{4\pi^2} \sum_{\alpha=\pm} \int d^2\boldsymbol{k}\, E_{k\alpha} \theta(-E_{k\alpha}), \tag{2.15}$$

where we have used Eq. (2.11) to remove the logarithmic divergence. Here, we have defined

$$E_{k\pm} = E_k \pm \left(h - \frac{\boldsymbol{k}\cdot\boldsymbol{Q}}{2m} \right), \tag{2.16a}$$

$$E_p = \sqrt{\widetilde{\xi}_k^2 + \Delta_0^2}, \tag{2.16b}$$

$$\widetilde{\xi}_k = \epsilon_k - \widetilde{\mu} \tag{2.16c}$$

with $\epsilon_k = k^2/(2m)$ and $\widetilde{\mu} = \mu - Q^2/(8m)$. The pairing gap Δ_0 and momentum Q are determined so as to minimize the thermodynamic potential in Eq. (2.15).

For $h = 0$ and $Q = 0$, the BCS-BEC crossover in 2D is described by solving the gap and number equations simultaneously, $\partial\Omega_{\mathrm{MF}}/\partial\Delta_0 = 0$ and $n = -\partial\Omega_{\mathrm{MF}}/\partial\mu$. At the fixed μ, their solutions take simple forms [7, 8, 9],

$$\Delta_0 = \sqrt{\epsilon_b(\epsilon_b + 2\mu)}, \tag{2.17a}$$

$$\epsilon_F = \mu + \frac{\epsilon_b}{2} \tag{2.17b}$$

with the Fermi energy $\epsilon_F \equiv \pi n/m$, so that the ground state is unpolarized superfluid (SF) for $\mu > -\epsilon_b/2$.

Next, we consider the case $h > 0$ but $Q = 0$. The location of the minimum of Ω_{MF} for the unpolarized SF phase is unchanged with increasing h, although a second minimum corresponding to the polarized normal (N) phase appears at $\Delta_0 = 0$. By

substituting the solution in Eq. (2.17a) into Eq. (2.15), the local minimum $\Omega_{\rm SF}$ corresponding to the SF phase is found to be

$$\Omega_{\rm SF} = -\frac{m}{2\pi}\left(\mu + \frac{\epsilon_b}{2}\right)^2, \tag{2.18}$$

where we have assumed $\mu > -\epsilon_b/2$. On the other hand, the local minimum $\Omega_{\rm N}$ corresponding to the N phase with $\Delta_0 = 0$ becomes

$$\Omega_{\rm N} = -\frac{m}{4\pi}\left[(\mu - h)^2\theta(\mu - h) + (\mu + h)^2\theta(\mu + h)\right], \tag{2.19}$$

where the case $\mu + h < 0$ corresponds to the vacuum without fermions. For $\mu + h > 0$, the first term in Eq. (2.19) is zero if the polarized N phase has one Fermi surface (i.e., fully polarized N phase) and nonzero if the polarized N phase has two Fermi surfaces (i.e., partially polarized N phase). The critical Zeeman field h_c of a first-order quantum phase transition between the SF and N phases is determined by solving $\Omega_{\rm SF} = \Omega_{\rm N}$, which leads to

$$h_c(\mu) = \begin{cases} \dfrac{\epsilon_b}{\sqrt{2}} + (\sqrt{2} - 1)\mu & (\mu < \mu_c), \\ \sqrt{\epsilon_b\left(\mu + \dfrac{\epsilon_b}{4}\right)} & (\mu > \mu_c), \end{cases} \tag{2.20}$$

where $\mu_c \equiv (1 + \sqrt{2})\epsilon_b/2$ separates the fully and partially polarized N phases. We note that the polarized superfluid or Sarma phase [83] is always located at the local maximum of the thermodynamic potential in 2D [84, 85]. In contrast to the 2D case, the Sarma state becomes the stable ground state of a 3D Fermi gas in the strong-coupling limit [86, 87, 88, 89, 90, 91].

Next, we consider the case $h > 0$ and $Q \neq 0$. The author in Ref. [41] showed a continuous phase transition from the N phase with $\Delta_0 = 0$ to the FF phase with $\Delta_0 > 0$ and $Q \neq 0$. The critical Zeeman field $h_{\rm FF}$ of its continuous phase transition is determined by simultaneously solving $Q = Q_c(\mu, h_{\rm FF})$ and $S(h_{\rm FF}, Q, 0) = 0$, where $Q_c(\mu, h) = \sqrt{2(\mu + h)} - \sqrt{2(\mu - h)}$ is the difference in the Fermi wave vectors of two spin components and $S(h, Q, \Delta_0)$ is defined via $\partial\Omega_{\rm MF}/\partial\Delta_0 = -2\Delta_0 S(h, Q, \Delta_0)$. The function $S(h, Q, 0)$ can be obtained analytically [41],

$$S(h, Q, 0) = \begin{cases} \dfrac{1}{2\pi}\log\left(\dfrac{\sqrt{2\widetilde{\mu}\epsilon_b}}{h + \sqrt{h^2 - Q^2\widetilde{\mu}/2}}\right) & (Q < Q_c), \\ \dfrac{1}{4\pi}\log\left(\dfrac{4\epsilon_b}{Q^2}\right) & (Q > Q_c), \end{cases} \tag{2.21}$$

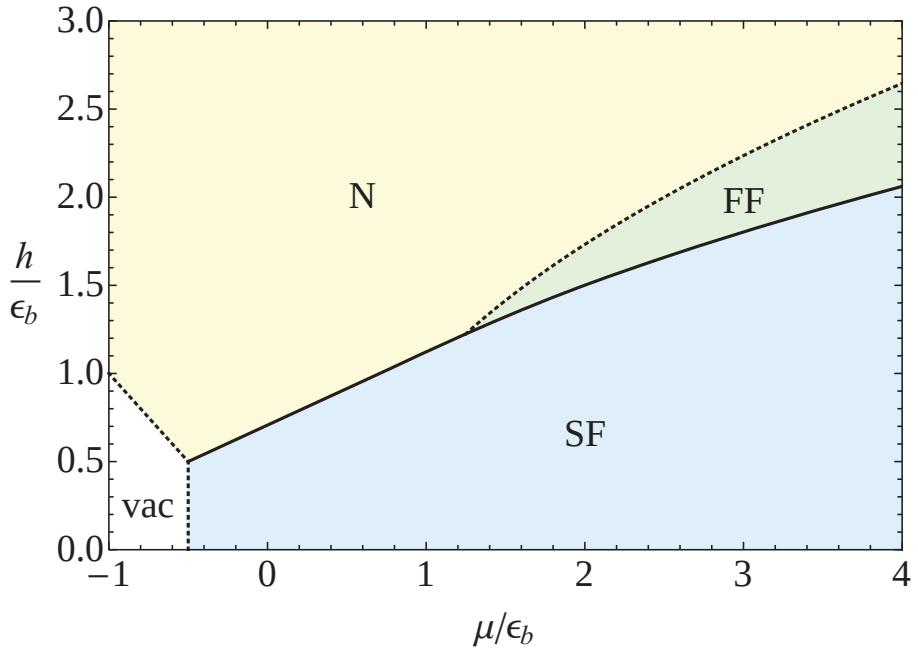

Figure 2.1: Mean-field ground-state phase diagram in the plane of the chemical potential μ and Zeeman field h in units of the two-body binding energy ϵ_b. The solid curve shows the boundary of the first-order phase transition, whereas the dotted curves show that of the second-order phase transition.

and therefore, we obtain

$$h_{\rm FF} = \sqrt{2\mu\epsilon_b - \epsilon_b^2}, \tag{2.22}$$

$$Q_c = 2\sqrt{\epsilon_b}. \tag{2.23}$$

The ground-state phase diagram within the mean-field approximation is depicted in Fig. 2.1. It consists of polarized N, unpolarized SF, and FF phases as well as the vacuum (vac) without fermions. The polarized N and SF (FF) phases are separated by the first-order (second-order) quantum phase transition with the phase boundary h_c in Eq. (2.20) [$h_{\rm FF}$ in Eq. (2.22)]. Two boundaries, h_c and $h_{\rm FF}$, meet at $\mu = 5\epsilon_b/4$, and therefore, for $\mu > 5\epsilon_b/4$, the phase boundary h_c, derived as the first-order phase transition between the N and SF phases, becomes the first-order phase transition between the SF and FF phases. Since the thermodynamic potential for the FF state is slightly lower than that for the N state, the true h_c for $\mu > 5\epsilon_b/4$ will be slightly lower than that depicted in Fig. 2.1.

2.2 Bose-Hubbard model

Ultracold Bose gases on an optical lattice are well described by the Bose-Hubbard model [1], which was introduced by Fisher *et al.* [92] to investigate the superfluid-insulator transition. In 1989, Jaksch *et al.* proposed a way to implement the Bose-Hubbard model in ultracold atom experiments [93]. Motivated by this proposal, the quantum phase transition from a superfluid to a Mott insulator was observed in 3D by Greiner *et al.* [94], in 1D by Stöferle *at al.* [95], and in 2D by Spielman *et al.* [96, 97]. In this section, we review the mean-field phase diagram of the Bose-Hubbard model at zero temperature. We follow Refs. [1, 98, 99].

2.2.1 Ground-state phase diagram

The Bose-Hubbard model is defined by the following Hamiltonian:

$$\hat{H} = -J \sum_{\langle j,k \rangle} \left(\hat{b}_j^\dagger \hat{b}_k + \hat{b}_k^\dagger \hat{b}_j \right) + \frac{U}{2} \sum_j \hat{n}_j (\hat{n}_j - 1) - \mu \sum_j \hat{n}_j, \tag{2.24}$$

where $\langle j, k \rangle$ denotes the set of nearest-neighbor sites and $\hat{n}_j \equiv \hat{b}_j^\dagger \hat{b}_j$ represents the number operator at site j with bosonic creation and annihilation operators, $\hat{b}_j^\dagger$ and $\hat{b}_j$, respectively. Here, $J > 0$ is the hopping amplitude between nearest-neighbor sites, $U > 0$ is the on-site repulsive interaction, and μ is the chemical potential. We now consider the 2D square lattice with N_L lattice sites.

The ground state of the Bose-Hubbard model is determined by the competition between the hopping amplitude J and the on-site interaction U. In the limit $J/U \gg 1$, the interaction U can be negligible compared to the hopping J and the ground state is an ideal BEC where all N bosons occupy the lowest Bloch state. The many-body wave function of this ground state can be written as

$$|\Psi_N\rangle_{U=0} \propto \left(\sum_{j=1}^{N_L} \hat{b}_j^\dagger \right)^N |0\rangle \tag{2.25}$$

with the vacuum state $|0\rangle$. On the other hand, in the limit $J/U \ll 1$, the hopping J can be negligible compared to the interaction U. Considering $\nu \equiv N/N_L = 0, 1, \ldots$, the ground state is a Mott insulator, which consists of ν localized bosons per site. The many-body wave function of this ground state can be written as

$$|\Psi_N\rangle_{J=0} \propto \prod_{j=1}^{N_L} \left(\hat{b}_j^\dagger \right)^\nu |0\rangle \,. \tag{2.26}$$

Therefore, by increasing the ratio J/U, we expect the quantum phase transition from a Mott insulator phase to a superfluid phase.

To investigate this quantum phase transition, we perform the mean-field approximation with $\psi_B = \langle \hat{b}_j^\dagger \rangle = \langle \hat{b}_j \rangle$, which leads to

$$\hat{H} = \sum_j \left[4J\psi_B^2 + \frac{U}{2}\hat{n}_j(\hat{n}_j - 1) - \mu\hat{n}_j - 4J\psi_B(\hat{b}_j^\dagger + \hat{b}_j) \right] \equiv \sum_j \hat{H}_{\mathrm{MF},j}. \tag{2.27}$$

Therefore, one can see that it is sufficient to minimize the Hamiltonian $\hat{H}_{\mathrm{MF},j}$ per site. We drop the subscript j for brevity and write $\hat{H}_{\mathrm{MF}} = \hat{H}_0 + \hat{V}$ with

$$\hat{H}_0 = 4J\psi_B^2 + \frac{U}{2}\hat{n}(\hat{n} - 1) - \mu\hat{n}, \tag{2.28}$$

$$\hat{V} = -4J\psi_B(\hat{b}^\dagger + \hat{b}). \tag{2.29}$$

When we choose eigenstates $|\nu\rangle$ of the number operator $\hat{n}$ as unperturbed states, the Hamiltonian $\hat{H}_0$ can be diagonalized in the basis $\{|\nu\rangle\}$ and its unperturbed ground-state energy is found to be

$$\langle \nu|\hat{H}_0|\nu\rangle = 4J\psi_B^2 + \frac{U}{2}\nu(\nu - 1) - \mu\nu \equiv 4J\psi_B^2 + E_0, \tag{2.30}$$

where we have used $\hat{n}\,|\nu\rangle = \nu\,|\nu\rangle$ $(\nu = 0, 1, 2, \ldots)$. The order parameter ψ_B is determined so as to minimize the energy $E_{\mathrm{MF}} \equiv \langle \nu|\hat{H}_{\mathrm{MF}}|\nu\rangle$. By performing the usual perturbation theory up to the fourth order in ψ_B assumed to be small, the energy E_{MF} is given by

$$E_{\mathrm{MF}} = E_0 + E_2\psi_B^2 + E_4\psi_B^4 + \mathcal{O}\left(\psi_B^6\right) \tag{2.31}$$

with

$$E_0 = \frac{U}{2}\nu(\nu - 1) - \mu\nu, \tag{2.32a}$$

$$E_2 = 4J\left[1 - 4J\left(\frac{\nu}{U(\nu - 1) - \mu} + \frac{\nu + 1}{\mu - U\nu}\right)\right], \tag{2.32b}$$

$$E_4 = (4J)^4\left[\frac{\nu(\nu - 1)}{(U(\nu - 1) - \mu)^2(U(2\nu - 3) - 2\mu)} + \frac{(\nu + 1)(\nu + 2)}{(\mu - U\nu)^2(2\mu - U(2\nu + 1))} - \left(\frac{\nu}{U(\nu - 1) - \mu} + \frac{\nu + 1}{\mu - U\nu}\right)\left(\frac{\nu}{(U(\nu - 1) - \mu)^2} + \frac{\nu + 1}{(\mu - U\nu)^2}\right)\right]. \tag{2.32c}$$

According to Ref. [98], the coefficient E_4 is positive, and therefore, the quantum phase transition between an insulator phase with $\psi_B = 0$ and a superfluid phase

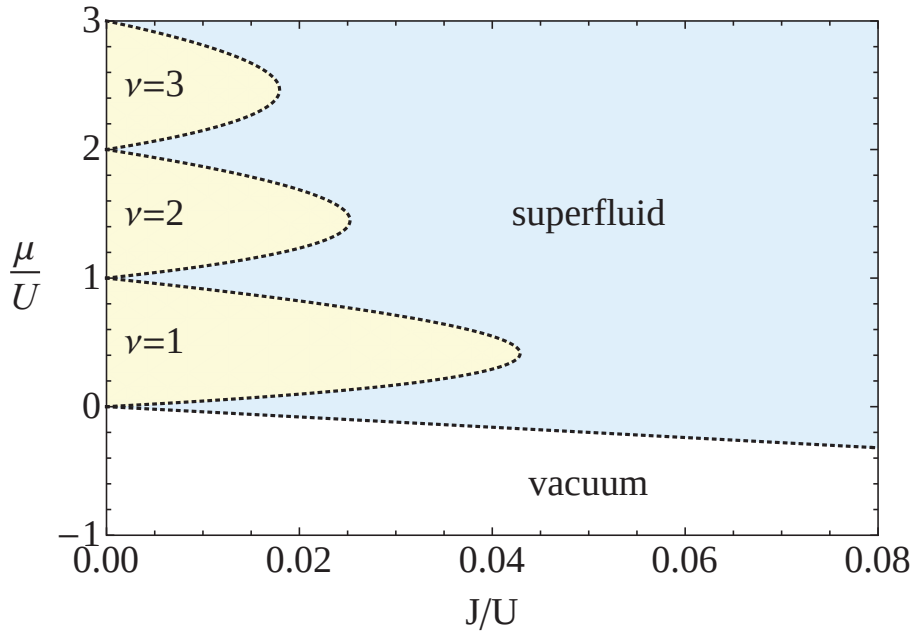

Figure 2.2: Mean-field ground-state phase diagram in the plane of the chemical potential μ and the hopping amplitude J in units of the on-site interaction U. The phase diagram consists of three phases corresponding to the vacuum, superfluid, and Mott insulator labeled by the filling factor $\nu = 1, 2, \ldots$. They are separated by the second-order quantum phase transition located at Eq. (2.33).

with $\psi_B \neq 0$ is of the second order. Its phase boundary is determined by solving $E_2 = 0$, which leads to the critical chemical potential

$$\mu_\pm = \frac{1}{2}(U(2\nu - 1) - 4J) \pm \frac{1}{2}\sqrt{U^2 - 8JU(2\nu + 1) + (4J)^2}, \tag{2.33}$$

where the subscripts $\pm$ represent the upper and lower halves of the phase boundary.

The ground-state phase diagram of the Bose-Hubbard model is depicted in Fig. 2.2. The insulator phase with $\psi_B = 0$ is divided into different phases by the filling factor $\nu = 0, 1, 2 \ldots$. Since the filling factor represents how many bosons occupy per site, the phase with $\nu = 0$ corresponds to the vacuum without bosons. On the other hand, the phase with $\nu = 1, 2, \ldots$ corresponds to a Mott insulator. This state is incompressible because its density does not change when the chemical potential is varied. The tip of each Mott lobe is located at

$$\left(\frac{J_c}{U}, \frac{\mu_c}{U}\right) = \left(\frac{2\nu + 1 - 2\sqrt{\nu^2 + \nu}}{4}, \sqrt{\nu^2 + \nu} - 1\right), \tag{2.34}$$

which is obtained by solving $\mu_+ = \mu_-$. The rest of the phase diagram is occupied by the superfluid with $\psi_B \neq 0$.

The nature of the continuous phase transition between the Mott insulator and superfluid phases is captured by considering the effective theory for the complex bosonic parameter. In Ref. [92], Fisher *et al.* showed that at the tips of the Mott lobes, the effective theory becomes that of the XY model, that is, the quantum phase transition is in the universality class of the XY model. In this phase transition, the density remains unchanged from that in the Mott insulator. On the other hand, away from the tips of the Mott lobes, Fisher *et al.* showed that the quantum phase transition always involves a change in the density and is in the universality class of the dilute Bose gas.

2.3 Magnetic catalysis

In Section 2.3.1, we review free Dirac fermions in a magnetic field in (2+1) D and show that a magnetic field induces the condensation of fermion-antifermion pairs. Then, we review interacting Dirac fermions in a magnetic field in (2+1) D and show that a magnetic field induces the dynamical fermion mass in Section 2.3.2. We follow Refs. [63, 64].

2.3.1 Free Dirac fermions in a magnetic field

To understand the dimensional reduction, we firstly consider charged Dirac fermions subjected to a magnetic field with its magnitude $B > 0$ in (2+1) D, which are described by the following Lagrangian density:

$$\mathcal{L} = \bar{\Psi}(i\gamma^\mu D_\mu - m)\Psi, \tag{2.35}$$

where m is the mass of Dirac fermions. The covariant derivative $D_\mu \equiv \partial_\mu - ieA_\mu$ with the fermion charge $e > 0$ depends on the external gauge field A_μ. Without loss of generality, we choose the vector potential as $A_\mu = (0, -\boldsymbol{A})$ with $\boldsymbol{A} = (-By, 0)$. Here, we use the four-dimensional representation of the Dirac matrices γ^μ:

$$\gamma^0 = \begin{pmatrix} \sigma_3 & 0 \\ 0 & -\sigma_3 \end{pmatrix}, \quad \gamma^1 = \begin{pmatrix} i\sigma_1 & 0 \\ 0 & -i\sigma_1 \end{pmatrix}, \quad \gamma^2 = \begin{pmatrix} i\sigma_2 & 0 \\ 0 & -i\sigma_2 \end{pmatrix}, \tag{2.36}$$

where σ_i $(i = 1, 2, 3)$ are the Pauli matrices. We note that in the massless limit $m \to 0$, the Lagrangian density in Eq. (2.35) is invariant under the global $U(2)$ transformations with the generators $T_0 = I$, $T_1 = \gamma^5$, $T_2 = -i\gamma^3$, and $T_3 = \gamma^3\gamma^5$, where

$$\gamma^3 = i \begin{pmatrix} 0 & I \\ I & 0 \end{pmatrix}, \quad \gamma^5 = i \begin{pmatrix} 0 & I \\ -I & 0 \end{pmatrix}. \tag{2.37}$$

The mass term breaks the $U(2)$ symmetry down to the $U(1) \times U(1)$ symmetry with the generators T_0 and T_3. By solving the Dirac equation of motion, the energy spectrum E_n ($n = 0, 1, 2, \ldots$) is given by

$$E_{n=0} = \pm m, \tag{2.38a}$$

$$E_{n\geq 1} = \pm\sqrt{m^2 + eBn}. \tag{2.38b}$$

The density of state for the lowest Landau level with $n = 0$ is $eB/(2\pi)$, whereas that for higher landau level with $n \geq 1$ is eB/π.

In the massless limit $m \to 0$, the spontaneous $U(2)$ symmetry breaking takes place already in the free theory. The condensate $\langle 0|\bar{\Psi}(x)\Psi(x)|0\rangle$ can be expressed as

$$\langle 0|\bar{\Psi}(x)\Psi(x)|0\rangle = -\lim_{y\to x} \mathrm{Tr}[S(x,y)], \tag{2.39}$$

where $x^\mu = (t, \boldsymbol{r})$ denotes the space-time coordinate. The fermion propagator $S(x,y) = \langle 0|T[\Psi(x)\bar{\Psi}(y)]|0\rangle$ can be calculated by using the Schwinger proper-time approach [100]. In the limit $m \to 0$, the condensate is given by

$$\begin{aligned}
&\langle 0|\bar{\Psi}(x)\Psi(x)|0\rangle \\
&= -\lim_{\Lambda\to\infty}\lim_{m\to 0} \frac{m}{2\pi^3} \int d^3k \int_{1/\Lambda^2}^{\infty} ds\, \exp\left[-s\left(m^2 + \boldsymbol{k}^2 \frac{\tanh(eBs)}{eBs} + k_3^2\right)\right] \\
&= -\lim_{\Lambda\to\infty}\lim_{m\to 0} \frac{m}{2\pi^{3/2}} \int_{1/\Lambda^2}^{\infty} \frac{ds}{\sqrt{s}} \mathrm{e}^{-sm^2} eB\coth(eBs) \\
&= -\lim_{\Lambda\to\infty}\lim_{m\to 0} \frac{m}{2\pi^{3/2}} \left[2\Lambda + \sqrt{\pi}\frac{eB}{|m|} + \mathcal{O}\left(m, \sqrt{eB}, \frac{m^2}{\Lambda}\right)\right] \\
&= -\frac{eB}{2\pi}\mathrm{sign}(m),
\end{aligned} \tag{2.40}$$

where we have introduced an ultraviolet cutoff Λ in the intermediate calculation. This is a specific phenomenon in (2+1) D because the corresponding result in (3+1) D is given by $\langle 0|\bar{\Psi}(x)\Psi(x)|0\rangle \sim eBm\log(m)$, which goes to zero in the limit $m \to 0$. To understand the physical origin of this phenomenon, we note that the singular $1/m$ behavior in the parentheses of Eq. (2.40) comes from the infrared region ($s \to \infty$) of the integral over s. At $s \to \infty$, the function $eB\coth(eBs)/\sqrt{s}$ approaches $eB/s^{1/2}$ for $B \neq 0$ and $1/s^{3/2}$ for $B \to 0$. Since the $1/s^{d/2}$ behavior originates in the d-dimensional Gaussian integral over k, a magnetic field is found to reduce the (2+1)-dimensional dynamics to the (0+1)-dimensional dynamics, which is the dimensional reduction.

2.3.2 Interacting Dirac fermions in a magnetic field

We next consider the Nambu-Jona-Lasinio (NJL) model in (2+1) D, which is useful to see that a magnetic field induces the dynamical fermion mass. The NJL model invariant under the $U(2)$ transformations is described by the following Lagrangian density:

$$\mathcal{L} = \bar{\Psi} i\gamma^\mu D_\mu \Psi + \frac{G}{2}\left[(\bar{\Psi}\Psi)^2 + (\bar{\Psi}\gamma^3\Psi)^2 + (\bar{\Psi} i\gamma^5\Psi)^2\right], \tag{2.41}$$

where G is the coupling constant and the fermionic fields carry an additional color index $\alpha = 1, 2, \ldots, N$. By performing the Hubbard-Stratonovich transformation, the Lagrangian density becomes

$$\mathcal{L} = \bar{\Psi} i\gamma^\mu D_\mu \Psi - \bar{\Psi}(\sigma + \gamma^3\tau + i\gamma^5)\Psi - \frac{1}{2G}(\sigma^2 + \tau^2 + \lambda^2). \tag{2.42}$$

The equation of motion for the auxiliary fields σ, τ, and λ is given by $\sigma = -G(\bar{\Psi}\Psi)$, $\tau = -G(\bar{\Psi}\gamma^3\Psi)$, and $\lambda = -G(\bar{\Psi} i\gamma^5\Psi)$, respectively. The effective action can then be written as

$$\Gamma(\sigma, \tau, \lambda) = -\frac{1}{2G}\int d^3x\,(\sigma^2 + \tau^2 + \lambda^2) - i\log\det\left[i\gamma^\mu D_\mu - (\sigma + \gamma^3\tau + i\gamma^5\lambda)\right]. \tag{2.43}$$

To obtain the effective potential $V(\sigma, \tau, \lambda)$, we perform the derivative expansion of the effective action in the auxiliary fields. Because of the $U(2)$ symmetry, the effective potential $V(\sigma, \tau, \lambda)$ depends on σ, τ, and λ via $\rho^2 \equiv \sigma^2 + \tau^2 + \lambda^2$, so that it is sufficient to consider $\tau = \lambda = 0$. We also assume σ to be independent of the space-time coordinates. By using the Schwinger proper-time approach [100], the effective potential is given by

$$V(\sigma) = \frac{N}{\pi}\left[\frac{\Lambda}{2}\left(\frac{1}{g} - \frac{1}{\sqrt{\pi}}\right)\sigma^2 - \sqrt{2}(eB)^{3/2}\zeta\left(-\frac{1}{2}, 1 + \frac{\sigma^2}{2eB}\right) - \sigma\frac{eB}{2}\right] + \mathcal{O}\left(\frac{1}{\Lambda}\right), \tag{2.44}$$

where $g = NG\Lambda/\pi$ is the dimensionless coupling constant and ζ is the generalized Riemann zeta function [101]. The auxiliary field σ minimizing the effective potential $V(\sigma)$ is determined by solving the gap equation $\partial V(\sigma)/\partial\sigma = 0$,

$$\Lambda\left(\frac{1}{g} - \frac{1}{\sqrt{\pi}}\right)\sigma = \frac{eB}{2} + \sigma\sqrt{\frac{eB}{2}}\zeta\left(\frac{1}{2}, 1 + \frac{\sigma^2}{2eB}\right) + \mathcal{O}\left(\frac{1}{\Lambda}\right). \tag{2.45}$$

By comparing Eqs. (2.35) and (2.42), the solution of the gap equation is found to be the fermion dynamical mass $m_{\rm dyn}$.

In the limit $B \to 0$, the gap equation reduces to

$$\sigma^2 = \sigma\Lambda\left(\frac{1}{\sqrt{\pi}} - \frac{1}{g}\right), \tag{2.46}$$

which leads to the fermion dynamical mass

$$m_{\rm dyn}^{B=0} = \begin{cases} \Lambda\dfrac{(g-\sqrt{\pi})}{\sqrt{\pi}g} & (g > \sqrt{\pi}), \\ 0 & (g < \sqrt{\pi}). \end{cases} \tag{2.47}$$

Therefore, it is found that no fermion dynamical mass exists in the weak-coupling limit $g \to 0$. On the other hand, for $B \neq 0$, we obtain the approximate solution in the weak-coupling limit $g \to 0$,

$$m_{\rm dyn}^{B\neq 0} = GN\frac{eB}{2\pi}. \tag{2.48}$$

In Ref. [66], it was also shown that the dynamical mass takes a finite value at any strength of the coupling constant when a magnetic field is nonzero. This dynamical generation of a fermion mass by a magnetic field is an important consequence of magnetic catalysis.

2.4 Summary

In this chapter, we reviewed topics related to our study of an attractive Fermi gas in antiparallel magnetic fields. In Section 2.1, we introduced the BCS-BEC crossover in 2D. We discussed the scattering problem in 2D and derived the relation between the coupling constant and the two-body binding energy. Under the ansatz of the FF state, it was found in Fig. 2.1 that the mean-field phase diagram of a 2D spin-imbalanced Fermi gas at zero temperature consists of the polarized normal, unpolarized superfluid, and FF phases as well as the vacuum without fermions. In Section 2.2, we introduced the Bose-Hubbard model in 2D and it was found in Fig. 2.2 that the mean-field phase diagram at zero temperature consists of three phases corresponding to the vacuum, Mott insulator, and superfluid phases. In Section 2.3, we reviewed the magnetic catalysis. We introduced the Lagrangian density for free Dirac fermions in (2+1) D and a magnetic field proved to induce the spontaneous symmetry breaking already in the massless free theory. We also introduced the NJL model to describe interacting Dirac fermions in (2+1) D and a magnetic field was found to enhance the dynamical generation of a fermion mass.

Chapter 3

Ground-state properties of a two-dimensional spin-balanced Fermi gas

In this chapter, we study the ground-state properties of a two-dimensional (2D) spin-balanced Fermi gas with an attractive interaction subjected to antiparallel magnetic fields in the mean-field approximation. Firstly, we introduce the action of our system and derive the zero-temperature thermodynamic potential by using the functional integral method in Section 3.1. By minimizing the thermodynamic potential, the zero-temperature phase diagram of the system is investigated in Section 3.2. To elucidate ground-state properties in the superfluid state, we calculate some physical quantities such as pairing gap, chemical potential, condensate density, sound velocity, superfluid density, binding energy, and effective mass in Section 3.3. We derive the Ginzburg-Landau action to discuss the universality class of the quantum phase transition in Section 3.4 and we finally summarize this chapter in Section 3.5.

In this and next chapters, and appendixes, we use shorthand notations, $(x) \equiv (\tau, \boldsymbol{x})$, $\int dx \equiv \int_0^\beta d\tau \iint_0^L d^2\boldsymbol{x}$, $\delta(x-x') \equiv \delta(\tau-\tau')\delta^2(\boldsymbol{x}-\boldsymbol{x}')$, where τ is the imaginary time and $\boldsymbol{x}$ is the 2D spatial coordinates, $(k) \equiv (i\omega_n, k_x, l)$, $\sum_k \equiv \sum_{i\omega_n} \sum_{k_x} \sum_{l=0}^\infty$, and $\delta_{k,k'} \equiv \delta_{\omega_n,\omega_{n'}} \delta_{k_x,k_x'} \delta_{l,l'}$, where $\omega_n = (2n+1)\pi/\beta$ is the fermionic Matsubara frequency with $n \in \mathbb{Z}$, $k_x = 2\pi n_x/L$ is the wave number in the x direction with $n_x = 0, \pm 1, \ldots, \pm m\omega_B L^2/(4\pi)$, and $l = 0, 1, \ldots$ labels Landau levels. Whereas the inverse temperature β and the linear size of the system L are kept finite in the intermediate calculations, we take the zero-temperature and the thermodynamic limits $\beta, L \to \infty$ at the end.

3.1 Zero-temperature thermodynamic potential

3.1.1 Model

In this chapter, we consider 2D attractive fermions with two spin components of atoms in antiparallel magnetic fields, which are described by the following imaginary-time action:

$$S = \sum_{\sigma=\uparrow,\downarrow} \int dx\, \phi_\sigma^*(x) \left(\partial_\tau - \frac{[\boldsymbol{\nabla} + i\boldsymbol{A}_\sigma(\boldsymbol{x})]^2}{2m} - \mu \right) \phi_\sigma(x) - g \int dx\, \phi_\uparrow^*(x) \phi_\downarrow^*(x) \phi_\downarrow(x) \phi_\uparrow(x). \tag{3.1}$$

Here, m and μ are the mass and chemical potential of fermions, and $g > 0$ is the coupling constant. In this action, fermions with two spin components are described by the Grassmann fields $\phi_\sigma^*, \phi_\sigma$ with $\sigma = (\uparrow, \downarrow)$. We choose the spin-dependent vector potentials as

$$\boldsymbol{A}_\uparrow(\boldsymbol{x}) = -\boldsymbol{A}_\downarrow(\boldsymbol{x}) = -By\hat{\boldsymbol{x}}, \tag{3.2}$$

so that fermions with different spin components experience antiparallel magnetic fields with its magnitude $B > 0$; $\boldsymbol{\nabla} \times \boldsymbol{A}_\uparrow(\boldsymbol{x}) = -\boldsymbol{\nabla} \times \boldsymbol{A}_\downarrow(\boldsymbol{x}) = B\hat{\boldsymbol{z}}$. By employing the usual Hubbard-Stratonovich transformation [102], we can decouple the interaction term in the action (3.1) by introducing a complex pair field $\Delta(x)$, which leads to

$$S' = \int dx\, \frac{|\Delta(x)|^2}{g} - \int dx\, \Phi^*(x) \begin{bmatrix} -\partial_\tau + \frac{[\boldsymbol{\nabla} + i\boldsymbol{A}_\uparrow(\boldsymbol{x})]^2}{2m} + \mu & \Delta(x) \\ \Delta^*(x) & -\partial_\tau - \frac{[\boldsymbol{\nabla} - i\boldsymbol{A}_\downarrow(\boldsymbol{x})]^2}{2m} - \mu \end{bmatrix} \Phi(x) \tag{3.3}$$

with the Nambu-Gor'kov spinor $\Phi(x) \equiv [\phi_\uparrow(x), \phi_\downarrow^*(x)]^{\mathrm{T}}$.

Here, we expand the Nambu-Gor'kov spinor over the eigenfunctions of the single-particle Hamiltonian. The eigenfunction in the Landau gauge is given by

$$\chi_k(x) = \sum_k \frac{\mathrm{e}^{-i\omega_n \tau + ik_x x}}{\sqrt{\beta L}} F_l(y - k_x \ell_B^2) \tag{3.4}$$

with

$$F_l(y) = \frac{\mathrm{e}^{-(y/\ell_B)^2/2}}{\sqrt{2^l l! \sqrt{\pi} \ell_B}} H_l\left(\frac{y}{\ell_B}\right) \tag{3.5}$$

being the l-th eigenfunction of the harmonic oscillator with the Hermite polynomial $H_n(z)$, which solves the Schrödinger equation

$$-\frac{[\boldsymbol{\nabla} - iBy\hat{\boldsymbol{x}}]^2}{2m}\chi_k(x) = \epsilon_l \chi_k(x) \tag{3.6}$$

with the single-particle energy provided by $\epsilon_l \equiv \omega_B(l+1/2)$ [103]. Here, $\ell_B \equiv 1/\sqrt{B}$ and $\omega_B \equiv B/m$ denote the magnetic length and cyclotron frequency, respectively. The eigenfunction also satisfies the orthogonality relation

$$\int dx\, \chi_k^*(x)\chi_{k'}(x) = \delta_{k,k'} \tag{3.7}$$

and the completeness relation

$$\sum_k \chi_k^*(x)\chi_k(x') = \delta(x'-x). \tag{3.8}$$

By substituting $\Phi(x) = \sum_k \chi_k(x)\widetilde{\Phi}(k)$ with $\widetilde{\Phi}(k) \equiv [\widetilde{\phi}_\uparrow(k), \widetilde{\phi}_\downarrow^*(k)]^{\mathrm{T}}$ into the action in Eq. (3.3), we obtain

$$S' = \int dx\, \frac{|\Delta(x)|^2}{g} - \sum_k \sum_{k'} \widetilde{\Phi}^*(k) G^{-1}(k,k') \widetilde{\Phi}(k'), \tag{3.9}$$

where the inverse Nambu-Gor'kov propagator is defined by

$$G^{-1}(k,k') = \begin{bmatrix} (i\omega_n - \xi_l)\delta_{k,k'} & \widetilde{\Delta}(k,k') \\ \widetilde{\Delta}^*(k',k) & (i\omega_n + \xi_l)\delta_{k,k'} \end{bmatrix} \tag{3.10}$$

with $\xi_l \equiv \epsilon_l - \mu$ and $\widetilde{\Delta}(k,k') \equiv \int dx\, \chi_k^*(x)\Delta(x)\chi_{k'}(x)$. By integrating out the fermionic fields $\widetilde{\phi}_\sigma^*(k)$ and $\widetilde{\phi}_\sigma(k)$, we obtain the effective action written in terms of the pair fields:

$$S_{\text{eff}} = \int dx\, \frac{|\Delta(x)|^2}{g} - \mathrm{Tr}\ln G^{-1}(k,k'). \tag{3.11}$$

While this effective action is formally exact with the understanding of the renormalization procedure discussed below, we need some approximation to proceed with our theoretical analysis.

3.1.2 Mean-field approximation

Let us employ the mean-field approximation by setting $\Delta(x) = \Delta_0 \geq 0$, which leads to

$$\widetilde{\Delta}(k, k') = \Delta_0 \int dx\, \chi_k^*(x)\chi_{k'}(x) = \Delta_0 \delta_{k,k'}. \tag{3.12}$$

Therefore, we obtain the thermodynamic potential $\Omega_{\mathrm{MF}} \equiv S_{\mathrm{eff}}|_{\Delta(x)=\Delta_0}/(\beta L^2)$ in the mean-field approximation:

$$\Omega_{\mathrm{MF}} = \frac{\Delta_0^2}{g} - \frac{1}{\beta L^2} \sum_k \ln\det G_0^{-1}(k) \tag{3.13}$$

with

$$G_0^{-1}(k) = \begin{bmatrix} (G_0^{-1})_{11}(k) & (G_0^{-1})_{12}(k) \\ (G_0^{-1})_{21}(k) & (G_0^{-1})_{22}(k) \end{bmatrix} = \begin{bmatrix} i\omega_n - \xi_l & \Delta_0 \\ \Delta_0 & i\omega_n + \xi_l \end{bmatrix}. \tag{3.14}$$

By performing the fermionic Matsubara summation and taking the limits $\beta, L \to \infty$, the zero-temperature thermodynamic potential is found to be

$$\Omega_{\mathrm{MF}} = \frac{\Delta_0^2}{g} - \frac{m\omega_B}{2\pi} \sum_{l=0}^{\infty} (E_l - \xi_l)\theta(\Lambda - \epsilon_l), \tag{3.15}$$

where $E_l \equiv \sqrt{\xi_l^2 + \Delta_0^2}$ is the quasiparticle energy. The detail of the Matsubara summation is shown in Appendix A. We introduce an energy cutoff Λ because the second term in Eq. (3.15) is logarithmically divergent. This logarithmic divergence should be removed by the same form of divergence hidden in the coupling constant [104]:

$$\frac{1}{g} = \frac{m}{2\pi} \int_0^{\Lambda} d\epsilon\, \frac{1}{2\epsilon + \epsilon_b} = \frac{m}{4\pi} \ln\left(\frac{2\Lambda}{\epsilon_b}\right), \tag{3.16}$$

where $\epsilon_b = 2\Lambda \mathrm{e}^{-4\pi/(mg)} > 0$ is the binding energy of a two-body bound state in the vacuum without magnetic fields. This binding energy always exists for $g > 0$ in 2D, and thus, can be used to parameterize the attractive interaction [8, 9].

By separating the divergent part from the second term, combining the first term

in Eq. (3.15), and taking the limit $\Lambda \to \infty$, we obtain

$$\begin{aligned}\Omega_{\rm MF} &= \frac{m\Delta_0^2}{4\pi}\lim_{\Lambda\to\infty}\left[\ln\left(\frac{2\Lambda}{\epsilon_b}\right) - \omega_B\sum_{l=0}^{\infty}\frac{\theta(\Lambda-\epsilon_l)}{\xi_l}\right] - \frac{m\omega_B}{2\pi}\sum_{l=0}^{\infty}\left(E_l - \xi_l - \frac{\Delta_0^2}{2\xi_l}\right) \\ &= \frac{m\Delta_0^2}{4\pi}\lim_{\Lambda\to\infty}\left[\ln\left(\frac{2\Lambda}{\epsilon_b}\right) - \psi\left(\frac{\Lambda}{\omega_B}+1-\frac{\mu}{\omega_B}\right) + \psi\left(\frac{1}{2}-\frac{\mu}{\omega_B}\right)\right] \\ &\quad - \frac{m\omega_B}{2\pi}\sum_{l=0}^{\infty}\left(E_l - \xi_l - \frac{\Delta_0^2}{2\xi_l}\right) \\ &= \frac{m\Delta_0^2}{4\pi}\left[\ln\left(\frac{2\omega_B}{\epsilon_b}\right) + \psi\left(\frac{1}{2}-\frac{\mu}{\omega_B}\right)\right] - \frac{m\omega_B}{2\pi}\sum_{l=0}^{\infty}\left(E_l - \xi_l - \frac{\Delta_0^2}{2\xi_l}\right), \end{aligned} \tag{3.17}$$

where $\psi(z) \equiv d\ln[\Gamma(z)]/dz$ is the digamma function defined as the logarithmic derivative of the gamma function $\Gamma(z)$. Here, we have used the relation [101],

$$\psi(z+1) - \psi(z) = \frac{1}{z}, \tag{3.18}$$

and the asymptotic expansion of the digamma function,

$$\psi(z) = \ln(z) - \frac{1}{2z} + \mathcal{O}\left(\frac{1}{z^2}\right). \tag{3.19}$$

3.2 Ground-state phase diagram

In this section, we investigate the ground-state phase diagram of the system. The pairing gap Δ_0 is determined so as to minimize the thermodynamic potential (3.17). Let us consider the case when the chemical potential μ does not match any Landau level (i.e. $\xi_l \neq 0$ for all $l \in \mathbb{N}_0$). To clarify a quantum phase transition, we expand the thermodynamic potential up to the quartic order in Δ_0 assumed to be small:

$$\Omega_{\rm MF} = C_0 + C_2\Delta_0^2 + C_4\Delta_0^4 + \mathcal{O}(\Delta_0^6), \tag{3.20}$$

where the coefficients C_i $(i = 0, 2, 4)$ are given by

$$C_0 = -\frac{m\omega_B}{2\pi}\sum_{l=0}^{\infty}(|\xi_l| - \xi_l) = \frac{m\omega_B^2}{2\pi}\nu\left[\nu - \frac{2\mu}{\omega_B}\right] \tag{3.21a}$$

$$\begin{aligned} C_2 &= \frac{m}{4\pi}\left[\ln\left(\frac{2\omega_B}{\epsilon_b}\right) + \psi\left(\frac{1}{2}-\frac{\mu}{\omega_B}\right) - \omega_B\sum_{l=0}^{\infty}\left(\frac{1}{|\xi_l|} - \frac{1}{\xi_l}\right)\right] \\ &= \frac{m}{4\pi}\left[\ln\left(\frac{2\omega_B}{\epsilon_b}\right) - \psi\left(\frac{1}{2}-\frac{\mu}{\omega_B}\right) + 2\psi\left(\frac{1}{2}-\frac{\mu}{\omega_B}+\nu\right)\right] \end{aligned} \tag{3.21b}$$

$$C_4 = \frac{m\omega_B}{16\pi}\sum_{l=0}^{\infty}\frac{1}{|\xi_l|^3}$$
$$= \frac{m}{32\pi\omega_B^2}\left[\psi''\left(\frac{1}{2}-\frac{\mu}{\omega_B}\right) - 2\psi''\left(\frac{1}{2}-\frac{\mu}{\omega_B}+\nu\right)\right] \tag{3.21c}$$

with $\nu = \lfloor 1/2 + \mu/\omega_B \rfloor \theta(\mu)$ being the filling factor per spin. The coefficient C_0 coincides with the thermodynamic potential in the normal state. Because C_4 is positive, we find a second-order quantum phase transition from a normal state with $\Delta_0 = 0$ to a superfluid state with $\Delta_0 > 0$ by increasing the two-body binding energy ϵ_b. The boundary of this phase transition is determined by solving $C_2 = 0$, which leads to

$$\frac{\epsilon_b}{\omega_B} = 2\exp\left[-\psi\left(\frac{1}{2}-\frac{\mu}{\omega_B}\right) + 2\psi\left(\frac{1}{2}-\frac{\mu}{\omega_B}+\nu\right)\right]. \tag{3.22}$$

The mean-field phase diagram at zero temperature is depicted in Fig 3.1. The normal state with $\Delta_0 = 0$ is separated into different phases by the filling factors $\nu = 0, 1, \ldots$. The normal density therein is given by

$$n = -\frac{\partial C_0}{\partial \mu} = \frac{m\omega_B}{\pi}\nu, \tag{3.23}$$

so that the phase with $\nu = 0$ corresponds to the vacuum, where no particles are present. On the other hand, for $\nu > 0$, fermions with each spin component fill the ν-th Landau level. Therefore, the phase with $\nu > 0$ corresponds to a quantum spin Hall (QSH) insulator consisting of two quantum Hall states with opposite chiralities for different spin components [59, 60, 61]. The rest of the phase diagram is occupied by the pair superfluid state with $\Delta_0 > 0$. In particular, only when the chemical potential lies right at a Landau level (i.e. $\xi_l = 0$ for all $l \in \mathbb{N}_0$), we find that the superfluid state persists down to the weak-coupling limit $\epsilon_b \to 0$. We note that the phase diagram obtained here has a similar structure to that of the Bose-Hubbard model which consists of superfluid and Mott insulator phases [92].

3.3 Physical quantities in the superfluid state

3.3.1 Pairing gap and chemical potential

The BCS-BEC crossover in the superfluid state is described by the number density equation,

$$n = -\frac{\partial \Omega_{\mathrm{MF}}}{\partial \mu} = \frac{m\omega_B}{2\pi}\sum_{l=0}^{\infty}\left(1 - \frac{\xi_l}{E_l}\right), \tag{3.24}$$

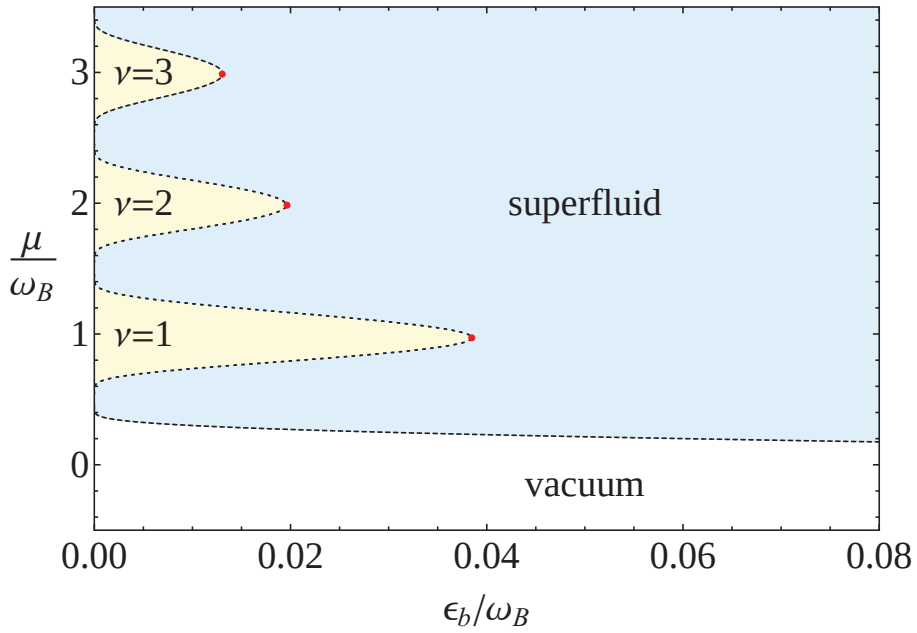

Figure 3.1: Mean-field ground-state phase diagram in the plane of the chemical potential μ and the two-body binding energy ϵ_b in units of the cyclotron frequency ω_B. The phase diagram is composed of three phases corresponding to the vacuum, the superfluid, and the QSH insulator labeled by the filling factor $\nu = 1, 2, \ldots$. They are divided by the second-order quantum phase transition located at Eq. (3.22). The tips of the QSH insulators are indicated by the dots.

together with the gap equation, $\partial\Omega_{\rm MF}/\partial\Delta_0 = 0$:

$$\ln\left(\frac{2\omega_B}{\epsilon_b}\right) + \psi\left(\frac{1}{2} - \frac{\mu}{\omega_B}\right) - \omega_B \sum_{l=0}^{\infty}\left(\frac{1}{E_l} - \frac{1}{\xi_l}\right) = 0. \tag{3.25}$$

Firstly, we consider the strong-coupling limit $\epsilon_b \to \infty$. By using $\mu < 0, |\mu| \gg \Delta_0$, the number density equation reads

$$n \simeq \frac{m\omega_B}{4\pi}\sum_{l=0}^{\infty}\frac{\Delta_0^2}{\xi_l^2} = \frac{m\Delta_0^2}{4\pi\omega_B}\psi'\left(\frac{1}{2} - \frac{\mu}{\omega_B}\right) \simeq \frac{m\Delta_0^2}{4\pi(-\mu)}, \tag{3.26}$$

while the gap equation becomes

$$\begin{aligned} 0 &\simeq \ln\left(\frac{-2\mu}{\epsilon_b}\right) + \omega_B \sum_{l=0}^{\infty}\frac{\Delta_0^2}{2\xi_l^3} \\ &= \ln\left(\frac{-2\mu}{\epsilon_b}\right) - \frac{\Delta_0^2}{4\omega_B^2}\psi''\left(\frac{1}{2} - \frac{\mu}{\omega_B}\right) \end{aligned}$$

$$\simeq \ln\left(\frac{-2\mu}{\epsilon_b}\right) + \left(\frac{\Delta_0}{2\mu}\right)^2. \tag{3.27}$$

By combining Eqs. (3.26) and (3.27), we obtain

$$\frac{\epsilon_b}{2\epsilon_F} = \exp\left[\ln\left(\frac{-\mu}{\epsilon_F}\right) + \frac{\epsilon_F}{-\mu}\right] \simeq -\frac{\mu}{\epsilon_F} + 1 \tag{3.28}$$

with $\epsilon_F \equiv \pi n/m$ being the Fermi energy. Therefore, the pairing gap and chemical potential are given by

$$\frac{\Delta_0}{\epsilon_F} \to \sqrt{\frac{2\epsilon_b}{\epsilon_F}}, \tag{3.29}$$

$$\frac{\mu}{\epsilon_F} \to 1 - \frac{\epsilon_b}{2\epsilon_F}, \tag{3.30}$$

which correspond to the results obtained in the context of the BCS-BEC crossover without magnetic fields [7, 8, 9]. One can understand this fact because, in the strong-coupling limit, the pairs of fermions with different spin components become tightly bound spin-singlet molecules, for which antiparallel magnetic fields cancel out.

Next, we consider the weak-coupling limit $\epsilon_b \to 0$ and $\omega_B/\epsilon_F = 2/(2l_0+1)$. The chemical potential then approaches the (l_0+1)-th Landau level ($l_0 \in \mathbb{N}_0$), so that we set $\mu = \omega_B(l_0+1/2)+\delta\mu$ ($|\delta\mu| \ll \omega_B$). In this case, the number density equation reduces to

$$\begin{aligned}
2\frac{\epsilon_F}{\omega_B} &= 1 + \frac{\delta\mu}{\sqrt{\delta\mu^2+\Delta_0^2}} + \sum_{l\neq l_0}\left[1 - \frac{\xi_l}{E_l}\right] \\
&\simeq 1 + \frac{\delta\mu}{\sqrt{\delta\mu^2+\Delta_0^2}} + \sum_{l=1}^{l_0}\left[1 + \frac{l}{\sqrt{l^2+(\Delta_0/\omega_B)^2}}\right] + \sum_{l=1}^{\infty}\left[1 - \frac{l}{\sqrt{l^2+(\Delta_0/\omega_B)^2}}\right] \\
&\simeq 2l_0 + 1 + \frac{\delta\mu}{\sqrt{\delta\mu^2+\Delta_0^2}} + \frac{1}{2}\left(\frac{\Delta_0}{\omega_B}\right)^2\left[-\sum_{l=1}^{l_0}\frac{1}{l^2} + \sum_{l=1}^{\infty}\frac{1}{l^2}\right] \\
&\simeq 2l_0 + 1 + \frac{\delta\mu}{\sqrt{\delta\mu^2+\Delta_0^2}} + \frac{1}{2}\psi'(l_0+1)\left(\frac{\Delta_0}{\omega_B}\right)^2,
\end{aligned} \tag{3.31}$$

which leads to

$$\frac{\mu}{\omega_B} \to l_0 + \frac{1}{2} - \frac{1}{2}\psi'(l_0+1)\left(\frac{\Delta_0}{\omega_B}\right)^3. \tag{3.32}$$

Therefore, we find that the chemical potential measured from the (l_0+1)-th Landau level decreases with the third power of a pairing gap. On the other hand, the gap

equation becomes

$$\begin{aligned} 0 &\simeq \ln\left(\frac{2\omega_B}{\epsilon_b}\right) + \psi(1) - \sum_{l=1}^{l_0} \frac{1}{l} - \frac{\omega_B}{\Delta_0} \\ &= \ln\left(\frac{2\omega_B}{\epsilon_b}\right) + 2\psi(1) - \psi(l_0+1) - \frac{\omega_B}{\Delta_0}, \end{aligned} \tag{3.33}$$

which leads to

$$\frac{\Delta_0}{\omega_B} \to \frac{1}{\ln(2\omega_B/\epsilon_b) - 2\gamma - \psi(l_0+1)} \tag{3.34}$$

with $\gamma = -\psi(1) = 0.577\ldots$ being the Euler-Mascheroni constant. Therefore, we find that the pairing gap in terms of the small coupling constant (3.16) is expressed as

$$\frac{\Delta_0}{\omega_B} \to \frac{mg}{4\pi}, \tag{3.35}$$

which is consistent with the result obtained in Ref. [78]. The behavior of the pairing gap exhibits the remarkable linear dependence in contrast to the usual exponential dependence without magnetic fields [8, 9],

$$\frac{\Delta_0}{\omega_B} \to \exp\left(-\frac{4\pi}{mg}\right). \tag{3.36}$$

This results from the divergent density of states at Landau levels and such an enhancement of dynamical symmetry breaking by magnetic fields is generally referred to as "magnetic catalysis" [63, 64].

Finally, we calculate the pairing gap and chemical potential for any strength of the two-body binding energy. To compare with the results obtained without magnetic fields, we simultaneously solve the number density equation (3.24) and the gap equation (3.25) in units of the Fermi energy. The pairing gap and chemical potential with $\omega_B/\epsilon_F = 2$ is plotted in Figs. 3.2 and 3.3, respectively. In particular, one can see that the pairing gap is indeed enhanced remarkably by antiparallel magnetic fields.

3.3.2 Condensate density

Next, we compute a condensate density n_c, which is related to the condensation of Cooper pairs and provided by [105, 106, 107]

$$n_c \equiv \frac{1}{L^2} \int d\boldsymbol{x} \int d\boldsymbol{x}' \, |\Psi(\boldsymbol{x}, \boldsymbol{x}')|^2, \tag{3.37}$$

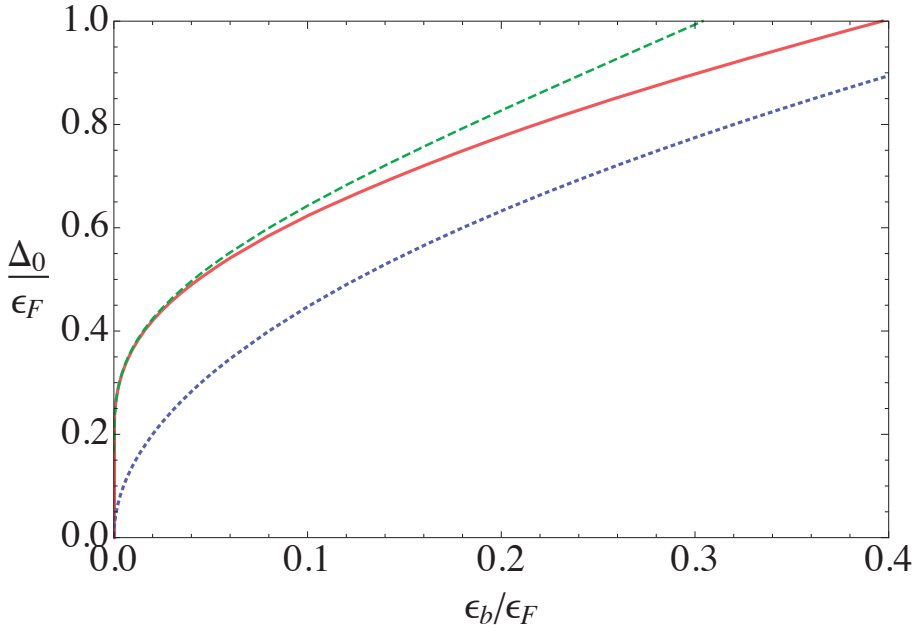

Figure 3.2: Pairing gap Δ_0 as a function of the two-body binding energy ϵ_b in units of the Fermi energy ϵ_F. The solid curve shows the result in the presence of antiparallel magnetic fields with $\omega_B/\epsilon_F = 2$, while the dotted curve shows $\Delta_0 = \sqrt{2\epsilon_F\epsilon_b}$ without magnetic fields. The asymptotic behavior of the pairing gap in the weak-coupling limit [Eq. (3.34)] is also indicated by the dashed curve.

where $\Psi(\boldsymbol{x},\boldsymbol{x}') \equiv \langle\phi_\downarrow(0,\boldsymbol{x})\phi_\uparrow(0,\boldsymbol{x}')\rangle$ is the wave function of Cooper pairs. In the mean-field approximation, we have

$$\begin{aligned}\Psi(\boldsymbol{x},\boldsymbol{x}') &= (G_0)_{12}(0,\boldsymbol{x};0,\boldsymbol{x}') \\ &= \sum_k (G_0)_{12}(k)\chi_k(0,\boldsymbol{x})\chi_k(0,\boldsymbol{x}') \\ &= \frac{1}{L}\sum_{k_x}\sum_{l=0}^{\infty}\frac{\Delta_0}{2E_l}\tanh\left(\frac{\beta E_l}{2}\right)\mathrm{e}^{ik_x(x-x')}F_l(y-k_x\ell_B^2)F_l(y'-k_x\ell_B^2),\end{aligned}$$

where we have performed the following Matsubara summation:

$$\frac{1}{\beta}\sum_{i\omega_n}(G_0)_{12}(k) = -\frac{1}{\beta}\sum_{i\omega_n}\frac{\Delta_0}{(i\omega_n - E_l)(i\omega_n + E_l)} = \frac{\Delta_0}{2E_l}\tanh\left(\frac{\beta E_l}{2}\right). \tag{3.38}$$

Therefore, the condensate density at zero temperature is found to be

$$n_c = \frac{m\omega_B}{8\pi}\sum_{l=0}^{\infty}\frac{\Delta_0^2}{E_l^2}. \tag{3.39}$$

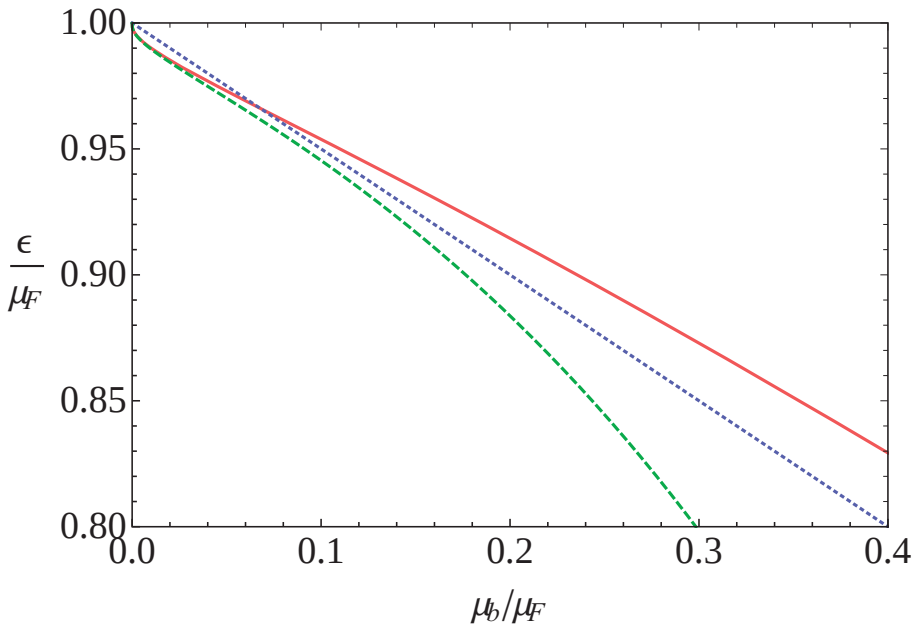

Figure 3.3: Chemical potential μ as a function of the two-body binding energy ϵ_b in units of the Fermi energy ϵ_F. The solid curve shows the result in the presence of antiparallel magnetic fields with $\omega_B/\epsilon_F = 2$, while the dotted curve shows $\mu = \epsilon_F - \epsilon_b/2$ without magnetic fields. The asymptotic behavior of the chemical potential in the weak-coupling limit [Eq. (3.32) with Eq. (3.34)] is also indicated by the dashed curve.

In the strong-coupling limit $\epsilon_b \to \infty$, we obtain

$$\frac{2n_c}{n} \simeq \frac{\omega_B \Delta_0^2}{4\epsilon_F} \sum_{l=0}^{\infty} \frac{1}{\xi_l^2} = \frac{\Delta_0^2}{4\epsilon_F \omega_B} \psi' \left(\frac{1}{2} - \frac{\mu}{\omega_B} \right) \simeq \frac{\Delta_0^2}{4\epsilon_F(-\mu)},$$

which leads to

$$\frac{2n_c}{n} \to 1 \tag{3.40}$$

with the pairing gap and chemical potential in the strong-coupling limit [see Eqs. (3.29) and (3.30)]. This is understandable because all $n/2$ fermion pairs contribute to the condensation.

In the weak-coupling limit $\epsilon_b \to 0$ with $\omega_B/\epsilon_F = 2/(2l_0+1)$, we obtain

$$\frac{2n_c}{n} \simeq \frac{\omega_B \Delta_0^2}{4\epsilon_F} \left[\left(\frac{\omega_B}{\Delta_0} \right)^2 + \sum_{l \neq l_0} \frac{1}{(l-l_0)^2} \right]$$

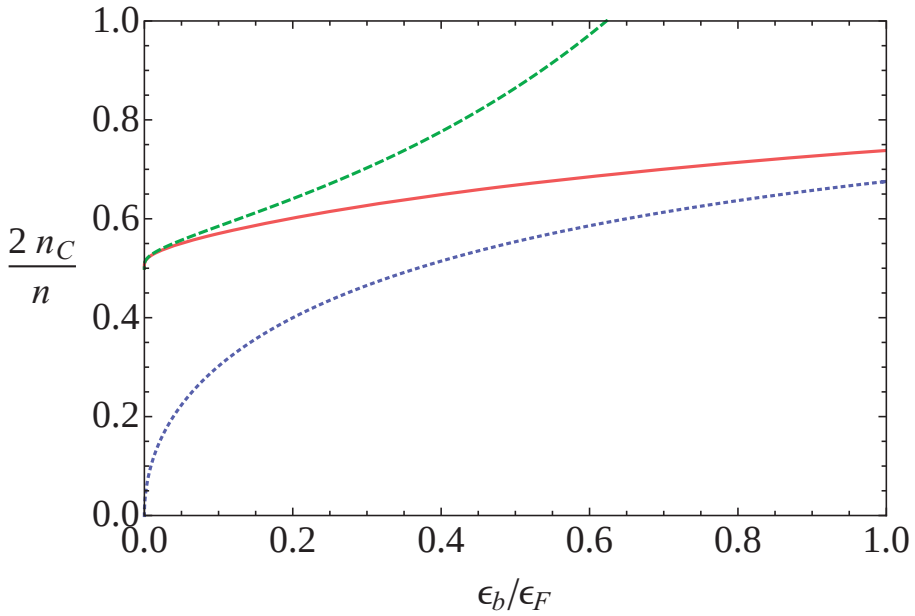

Figure 3.4: Scaled condensate density $2n_c/n$ as a function of the two-body binding energy ϵ_b in a unit of the Fermi energy ϵ_F. The solid curve shows the result in the presence of antiparallel magnetic fields with $\omega_B/\epsilon_F = 2$, while the dotted curve shows the result in their absence [Eq. (3.42)]. The asymptotic behavior of the condensate density in the weak-coupling limit [Eq. (3.41)] is also indicated by the dashed curve.

$$\begin{aligned} &\simeq \frac{\omega_B}{4\epsilon_F}\left[1+\left(\frac{\Delta_0}{\omega_B}\right)^2\left(\sum_{l=1}^{l_0}\frac{1}{l^2}+\sum_{l=1}^{\infty}\frac{1}{l^2}\right)\right] \\ &= \frac{\omega_B}{4\epsilon_F}\left[1+(2\psi'(1)-\psi'(l_0+1))\left(\frac{\Delta_0}{\omega_B}\right)^2\right]. \end{aligned} \tag{3.41}$$

Therefore, we find that the condensate density increases with the second power of a pairing gap. Moreover, for $\omega_B/\epsilon_F = 2$, this result shows that at least 50% fermion pairs condense as soon as an attractive interaction is switched on.

The condensate density beyond the weak-coupling limit is plotted in Fig. 3.4. We also plot the condensate density obtained without magnetic fields [107]:

$$\frac{2n_c}{n} = \frac{1}{2}\sqrt{\frac{\epsilon_b}{2\epsilon_F}}\left[\frac{\pi}{2}+\arctan\left(\sqrt{\frac{\epsilon_F}{2\epsilon_b}}\left(1-\frac{\epsilon_b}{2\epsilon_F}\right)\right)\right]. \tag{3.42}$$

One can see that the condensate density is also enhanced by antiparallel magnetic fields as with the pairing gap.

3.3.3 Sound velocity

We now calculate a sound velocity c_s, which is related to the Nambu-Goldstone mode due to the broken symmetry. The sound velocity is derived from zeros of the determinant of the inverse fluctuation propagator $M(p)$ in the low-energy limit $\omega, \boldsymbol{p} \to 0$ with the analytic continuation $ip_n \to \omega + 0^+$ [104, 108]. The inverse fluctuation propagator $M(p)$ is a 2×2 matrix and its elements at zero temperature are given by

$$\begin{aligned} M_{11}(p) &= M_{22}(-p) \\ &= \frac{m}{4\pi}\left[\log\left(\frac{2\omega_B}{\epsilon_b}\right) + \psi\left(\frac{1}{2} - \frac{\mu}{\omega_B}\right)\right] \\ &\quad + \frac{m\omega_B}{2\pi}\sum_{l=0}^{\infty}\left[\sum_{l'=0}^{\infty}|I_{l,l'}(\boldsymbol{p})|^2\left(\frac{u_l^2 u_{l'}^2}{ip_n - E_l - E_{l'}} - \frac{v_l^2 v_{l'}^2}{ip_n + E_l + E_{l'}}\right) + \frac{1}{2\xi_l}\right], \end{aligned} \tag{3.43a}$$

$$\begin{aligned} M_{12}(p) &= M_{21}(p) \\ &= \frac{m\omega_B}{2\pi}\sum_{l=0}^{\infty}\sum_{l'=0}^{\infty}|I_{l,l'}(\boldsymbol{p})|^2\left(\frac{u_l v_l u_{l'} v_{l'}}{ip_n + E_l + E_{l'}} - \frac{u_l v_l u_{l'} v_{l'}}{ip_n - E_l - E_{l'}}\right), \end{aligned} \tag{3.43b}$$

where we have defined the functions u_l, v_l as

$$u_l^2 = 1 - v_l^2 \equiv \frac{1}{2}\left(1 + \frac{\xi_l}{E_l}\right), \tag{3.44}$$

and have used a shorthand notation $(p) \equiv (ip_n, \boldsymbol{p})$ with the bosonic Matsubara frequency $p_n = 2\pi n/\beta$ $(n \in \mathbb{Z})$. In Appendix B, we calculate the effective action in the Gaussian approximation and derive the inverse fluctuation propagator in detail. Expanding the elements $M_{11}(p)$ and $M_{12}(p)$ up to the quadratic order in $\omega, \boldsymbol{p}$ yields

$$M_{11}(p) \simeq a_0 + a_1\omega + a_2\omega^2 + b_2\boldsymbol{p}^2, \tag{3.45a}$$

$$M_{12}(p) \simeq a_0 + a_2'\omega^2 + b_2'\boldsymbol{p}^2, \tag{3.45b}$$

where the coefficients are provided in Eqs. (B.32). By using this expansion, we obtain

$$\begin{aligned} 0 &= \det M(p) \\ &= M_{11}(p)M_{11}(-p) - [M_{12}(p)]^2 \\ &\simeq [2a_0(a_2 - a_2') - a_1^2]\omega^2 + 2a_0(b_2 - b_2')\boldsymbol{p}^2, \end{aligned} \tag{3.46}$$

which vanishes for $\omega = c_s|\boldsymbol{p}|$, and therefore, the sound velocity is found to be

$$c_s = \sqrt{\frac{2a_0(b_2 - b_2')}{a_1^2 + 2a_0(a_2' - a_2)}} \tag{3.47}$$

with

$$a_0 = \frac{m\omega_B}{8\pi} \sum_{l=0}^{\infty} \frac{\Delta_0^2}{E_l^3}, \tag{3.48a}$$

$$a_1 = -\frac{m\omega_B}{8\pi} \sum_{l=0}^{\infty} \frac{\xi_l}{E_l^3}, \tag{3.48b}$$

$$a_2' - a_2 = \frac{m\omega_B}{16\pi} \sum_{l=0}^{\infty} \frac{1}{E_l^3}, \tag{3.48c}$$

$$b_2 - b_2' = \frac{1}{4\pi} \sum_{l=0}^{\infty} \left[\left(l + \frac{1}{2} \right) \frac{1}{E_l} - l \frac{(u_l u_{l-1} + v_l v_{l-1})^2}{E_l + E_{l-1}} - (l+1) \frac{(u_l u_{l+1} + v_l v_{l+1})^2}{E_l + E_{l+1}} \right]. \tag{3.48d}$$

In the strong-coupling limit $\epsilon_b \to \infty$, we have

$$a_0 \simeq -\frac{m\Delta_0^2}{16\pi\omega_B^2} \psi'' \left(\frac{1}{2} - \frac{\mu}{\omega_B} \right) \simeq \frac{m}{16\pi} \left(\frac{\Delta_0}{\mu} \right)^2, \tag{3.49a}$$

$$a_1 \simeq -\frac{m}{8\pi\omega_B} \psi' \left(\frac{1}{2} - \frac{\mu}{\omega_B} \right) \simeq \frac{m}{8\pi\mu}, \tag{3.49b}$$

$$a_2' - a_2 \simeq -\frac{m}{32\pi\omega_B^2} \psi'' \left(\frac{1}{2} - \frac{\mu}{\omega_B} \right) \simeq \frac{m}{32\pi\mu^2}, \tag{3.49c}$$

$$\begin{aligned} b_2 - b_2' &\simeq -\frac{\mu}{8\pi\omega_B^2} \left[2\psi \left(\frac{1}{2} - \frac{\mu}{\omega_B} \right) - \psi \left(-\frac{\mu}{\omega_B} \right) - \psi \left(1 - \frac{\mu}{\omega_B} \right) \right] \\ &\simeq -\frac{1}{32\pi\mu}, \end{aligned} \tag{3.49d}$$

which lead to

$$\frac{c_s}{v_F} \simeq \sqrt{\frac{2a_0(b_2 - b_2')}{a_1^2}} \simeq \frac{\Delta_0}{2\sqrt{2\epsilon_F(-\mu)}} \to \frac{1}{\sqrt{2}} \tag{3.50}$$

with the Fermi velocity $v_F = \sqrt{2\epsilon_F/m}$. This result corresponds to the exact result obtained without magnetic fields [104].

In the weak-coupling limit $\epsilon_b \to 0$ with $\omega_B/\epsilon_F = 2/(2l_0+1)$, we have

$$a_0 \simeq \frac{m\omega_B}{8\pi\Delta_0}, \tag{3.51a}$$

$$a_1 \simeq -\frac{3m}{16\pi\omega_B}\psi'(l_0+1), \tag{3.51b}$$

$$a_2' - a_2 \simeq \frac{m}{16\pi\omega_B^2}\left(\frac{\omega_B}{\Delta_0}\right)^3, \tag{3.51c}$$

$$b_2 - b_2' \simeq \frac{\omega_B}{4\pi\epsilon_F\Delta_0}, \tag{3.51d}$$

which lead to

$$\frac{c_s}{v_F} \simeq \sqrt{\frac{b_2-b_2'}{a_2'-a_2}} \to \sqrt{2}\frac{\Delta_0}{\omega_B}. \tag{3.52}$$

Therefore, we find that the sound velocity increases in proportion to a pairing gap.

The sound velocity is plotted in Fig. 3.5. One can see that the sound velocity in the presence of antiparallel magnetic fields is always lower than $c_s = v_F/\sqrt{2}$ in their absence [104] unlike the pairing gap and condensate density.

3.3.4 Superfluid density

Now, we calculate a superfluid density n_s, which refers to the number density of fermions involved in the superfluid motion [106]. The superfluid density is determined as the coefficients of the spatial derivative of phase fluctuations $\theta(x)$ in the effective action S_{eff}:

$$\frac{1}{2}\int dx\, \frac{1}{4m} n_s |\boldsymbol{\nabla}\theta(x)|^2 = \beta L^2 \sum_p \left(\frac{n_s}{8m}\right)\boldsymbol{p}^2 |\widetilde{\theta}(p)|^2, \tag{3.53}$$

where we have performed the Fourier transformation,

$$\theta(x) = \sum_p \mathrm{e}^{-ip_n\tau + i\boldsymbol{p}\cdot\boldsymbol{x}}\widetilde{\theta}(p) \tag{3.54}$$

with a shorthand notation $\sum_p = \sum_{ip_n}\sum_{\boldsymbol{p}}$. In our analysis, the phase fluctuation is introduced by $\Delta(x) = \Delta_0 \mathrm{e}^{i\theta(x)} \simeq \Delta_0 + i\Delta_0\theta(x) \equiv \Delta_0 + \eta(x)$, and thus, we set $\eta(x) = i\Delta_0\theta(x)$. By substituting this into the Gaussian part S_{G} of the effective action [see Eq. (B.19)],

$$S_{\text{G}} = \beta L^2 \sum_p \left[M_{11}(p)|\widetilde{\eta}(p)|^2 + \frac{1}{2}M_{12}(p)(\widetilde{\eta}(p)\widetilde{\eta}(-p) + \widetilde{\eta}^*(-p)\widetilde{\eta}^*(p))\right], \tag{3.55}$$

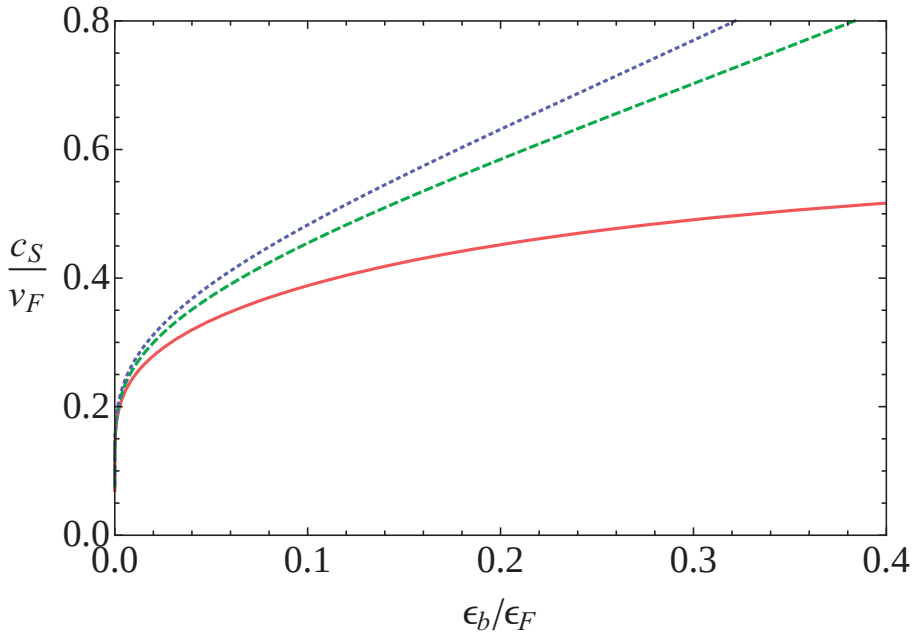

Figure 3.5: Sound velocity c_s/v_F scaled with the Fermi velocity $v_F = \sqrt{2\epsilon_F/m}$ as a function of the two-body binding energy ϵ_b in a unit of the Fermi energy ϵ_F. The solid curve shows the result in the presence of antiparallel magnetic fields with $\omega_B/\epsilon_F = 2$, while the dotted line shows $c_s/v_F = 1/\sqrt{2}$ without magnetic fields [104]. The asymptotic behavior of the sound velocity in the weak-coupling limit [Eq. (3.52)] is also indicated by the dashed curve.

we obtain

$$S_{\rm G} = \beta L^2 \sum_p \Delta_0^2 [M_{11}(p) - M_{12}(p)] |\widetilde{\theta}(p)|^2. \tag{3.56}$$

By using the inverse fluctuation propagator in the low energy limit $\omega, \boldsymbol{p} \to 0$ with the analytic continuation $ip_n \to \omega + 0^+$, we obtain

$$\Delta_0^2 [M_{11}(p) - M_{12}(p)] \simeq \Delta_0^2 [a_1\omega + (a_2 - a_2')\omega^2 + (b_2 - b_2')\boldsymbol{p}^2], \tag{3.57}$$

and therefore, the superfluid density reads

$$n_s = 8m\Delta_0^2(b_2 - b_2'). \tag{3.58}$$

In the strong coupling limit $\epsilon_b \to \infty$, we have

$$\frac{n_s}{n} \simeq \frac{\Delta_0^2}{4\epsilon_F(-\mu)} \to 1, \tag{3.59}$$

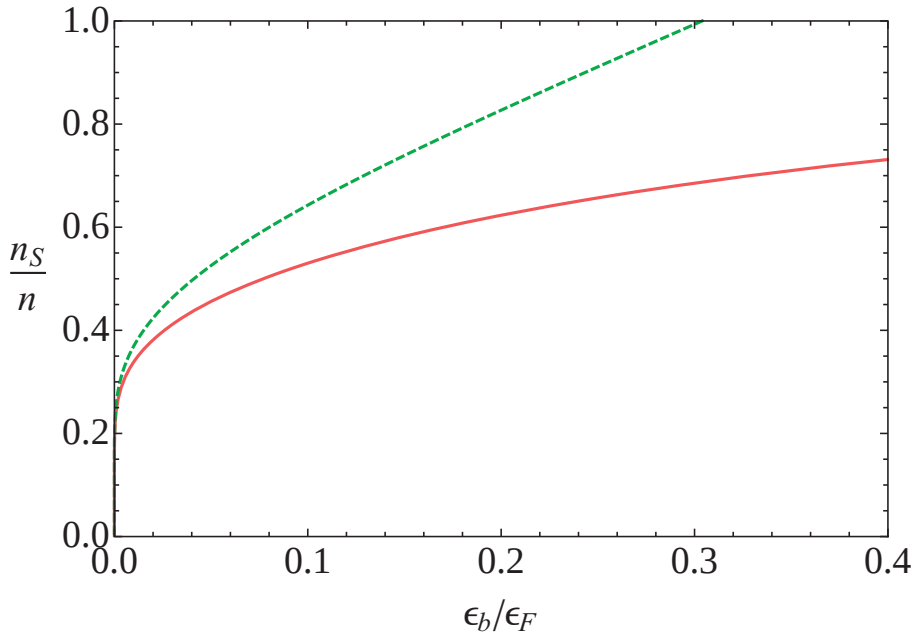

Figure 3.6: Scaled superfluid density n_s/n as a function of the two-body binding energy ϵ_b in a unit of the Fermi energy ϵ_F. The solid line shows the result in the presence of antiparallel magnetic fields with $\omega_B/\epsilon_F = 2$, while the dashed line shows the asymptotic behavior of the superfluid density in the weak-coupling limit [Eq. (3.60)].

where we have used the pairing gap and chemical potential in the strong-coupling limit [see Eqs. (3.29) and (3.30)]. This coincides with the result obtained without magnetic fields and means that all fermions participate in the superfluid motion as tightly bound molecules.

In the weak-coupling limit $\epsilon_b \to 0$ with $\omega_B/\epsilon_F = 2/(2l_0+1)$, we have

$$\frac{n_s}{n} \simeq 2\frac{\Delta_0}{\omega_B}. \tag{3.60}$$

Therefore, we find that the superfluid density increases in proportion to a pairing gap as with the sound velocity [see Eq. (3.52)]. This result is consistent with the result obtained in Ref. [78].

The superfluid density is plotted in Fig. 3.6. At zero temperature, it is known that the superfluid density without magnetic fields is $n_s/n = 1$ [106]. Therefore, the superfluid density is suppressed by antiparallel magnetic fields compared to that without magnetic fields. This results from the fact that fermions forming a pair cannot easily move because of their cyclotron motion. Actually, in the next section, we see that an effective mass of a two-body bound state is divergent in the weak-

coupling limit.

3.3.5 Two-body physics

At the end of this section, we discuss the two-body problem. To this end, we consider the Green function $\Gamma^{-1}(p)$ given by taking the limits $\Delta_0, \mu \to 0$ in the inverse fluctuation propagator $M(p)$ at zero temperature. Performing the analytical continuation $ip_n \to \omega + i0^+$ yields

$$\Gamma^{-1}(\omega, \boldsymbol{p}) = \frac{m}{4\pi}\left[\log\left(\frac{2\omega_B}{\epsilon_b}\right) + \psi\left(\frac{1}{2}\right)\right] + \frac{m}{2\pi}\sum_{l=0}^{\infty}\left[\sum_{l'=0}^{\infty}|I_{l,l'}(\boldsymbol{p})|^2\frac{\omega_B}{\omega - \omega_B(l+l'+1)} + \frac{1}{2l+1}\right]. \quad (3.61)$$

Binding energy

A binding energy E_b in antiparallel magnetic fields is determined by solving the equation $\Gamma^{-1}(\omega = \omega_B - E_b, \boldsymbol{p} = 0) = 0$, which leads to

$$\begin{aligned} 0 &= \log\left(\frac{2\omega_B}{\epsilon_b}\right) + \psi\left(\frac{1}{2}\right) - \sum_{l=0}^{\infty}\left[\frac{\omega_B}{\omega_B l + E_b/2} - \frac{1}{l+1/2}\right] \\ &= \log\left(\frac{2\omega_B}{\epsilon_b}\right) + \psi\left(\frac{E_b}{2\omega_B}\right). \end{aligned} \quad (3.62)$$

Therefore, we obtain

$$\frac{\epsilon_b}{\omega_B} = 2\exp\left[\psi\left(\frac{E_b}{2\omega_B}\right)\right], \quad (3.63)$$

which corresponds to the boundary of the quantum phase transition from the vacuum to the superfluid phase with $\Delta_0 > 0$ [see Eq. (3.22)]. The binding energy E_b in antiparallel magnetic fields is plotted in Fig. 3.7.

In the strong-coupling limit $\epsilon_b \to \infty$, we obtain

$$\frac{\epsilon_b}{\omega_B} \simeq \frac{E_b}{\omega_B}\exp\left[-\frac{\omega_B}{E_b}\right] \simeq \frac{E_b}{\omega_B} - 1 \quad (3.64)$$

with the asymptotic behavior of $\psi(z)$ [see Eq. (3.19)]. Therefore, the binding energy E_b is given by

$$E_b \to \epsilon_b + \omega_B. \quad (3.65)$$

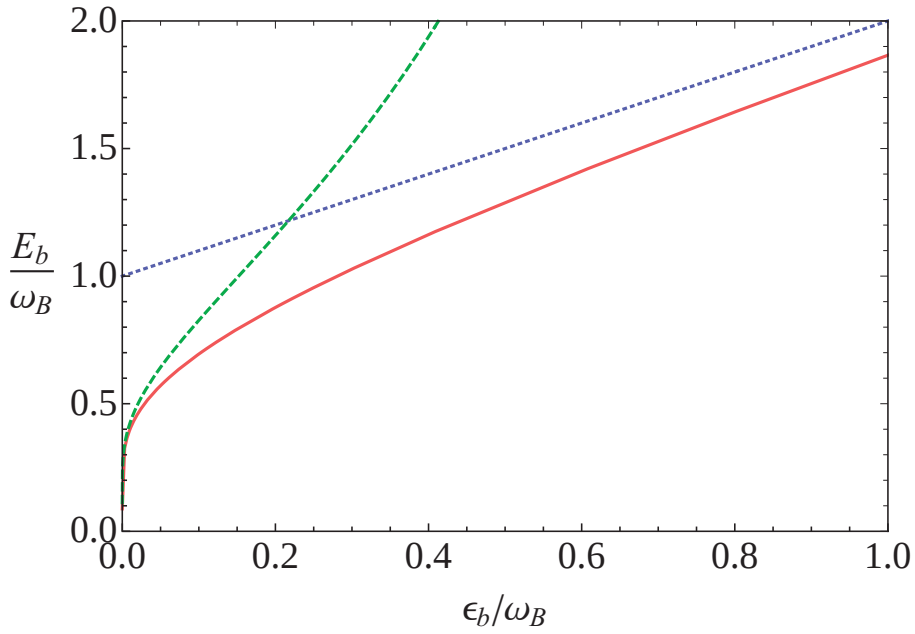

Figure 3.7: Binding energy E_b in antiparallel magnetic fields as a function of the two-body binding energy ϵ_b in their absence in units of the cyclotron frequency ω_B. The solid curve shows the result, while the dotted line shows $E_b = \epsilon_b + \omega_B$, which is the asymptotic behavior of the binding energy in the strong-coupling limit [Eq. (3.65)]. We also show the asymptotic behavior of the binding energy E_b in the weak-coupling limit [Eq. (3.66)] by the dashed curve.

This is understandable because tightly bound molecules composed of fermions with different spin components are insensitive to antiparallel magnetic fields. The cyclotron frequency ω_B on the right-hand side of Eq. (3.65) means that two fermions occupy the lowest Landau level whose energy is $\omega_B/2$.

In the weak-coupling limit $\epsilon_b \to 0$, we obtain

$$E_b \to \frac{2\omega_B}{\log(2\omega_B/\epsilon_b) - \gamma}, \tag{3.66}$$

where we use the series expansion of $\psi(z)$ for $z \neq 0, -1, -2, \ldots$ [101],

$$\psi(z) = -\gamma + \sum_{l=0}^{\infty} \left(\frac{1}{l+1} - \frac{1}{l+z} \right). \tag{3.67}$$

One can see that the binding energy E_b in antiparallel magnetic fields has the same dependence of the two-body binding energy ϵ_b in their absence as the behavior of the pairing gap. [see Eq. (3.34)].

Effective mass

We can investigate an effective mass m^* by considering the momentum dependence of zeros of $\Gamma^{-1}(\omega, \boldsymbol{p})$ with $\omega = \omega_B - E_b + \boldsymbol{p}^2/(2m^*)$. By expanding the Green function $\Gamma^{-1}(\omega, \boldsymbol{p})$ up to the quadratic order in $\boldsymbol{p}$, we obtain

$$\begin{aligned}
&\Gamma^{-1}\left(\omega = \omega_B - E_b + \frac{\boldsymbol{p}^2}{2m^*}, \boldsymbol{p} \neq 0\right) \\
&\quad = \frac{m}{4\pi}\left[\log\left(\frac{2\omega_B}{\epsilon_b}\right) + \psi\left(\frac{E_b}{2\omega_B}\right)\right] \\
&\qquad + \frac{\boldsymbol{p}^2}{8\pi\omega_B}\sum_{l=0}^{\infty}\left[2\frac{l+1/2}{l+E_b/(2\omega_B)} - \frac{l}{l-1/2+E_b/(2\omega_B)}\right. \\
&\qquad\qquad \left. - \frac{l+1}{l+1/2+E_b/(2\omega_B)} - \frac{m}{2m^*}\frac{1}{(l+E_b/(2\omega_B))^2}\right] \\
&\quad = \frac{\boldsymbol{p}^2}{8\pi\omega_B}\left[-\frac{m}{2m^*}\psi'\left(\frac{E_b}{2\omega_B}\right)\right. \\
&\qquad \left. + \left(\frac{E_b}{2\omega_B} - \frac{1}{2}\right)\left\{2\psi\left(\frac{E_b}{2\omega_B}\right) - \psi\left(-\frac{1}{2}+\frac{E_b}{2\omega_B}\right) - \psi\left(\frac{1}{2}+\frac{E_b}{2\omega_B}\right)\right\}\right].
\end{aligned} \tag{3.68}$$

Solving $\Gamma^{-1}(\omega, \boldsymbol{p}) = 0$ with $\omega = \omega_B - E_b + \boldsymbol{p}^2/(2m^*)$ yields

$$\frac{m^*}{2m} = \psi'\left(\frac{E_b}{2\omega_B}\right)\left[2\left(\frac{E_b}{\omega_B} - 1\right)\left\{2\psi\left(\frac{E_b}{2\omega_B}\right) - \psi\left(-\frac{1}{2}+\frac{E_b}{2\omega_B}\right) - \psi\left(\frac{1}{2}+\frac{E_b}{2\omega_B}\right)\right\}\right]^{-1}. \tag{3.69}$$

The effective mass is plotted in Fig. 3.8. In the strong-coupling limit $\epsilon_b \to \infty$ with Eq. (3.65), we have

$$\psi'\left(\frac{E_b}{2\omega_B}\right) \simeq \frac{2\omega_B}{E_b}, \tag{3.70a}$$

$$2\psi\left(\frac{E_b}{2\omega_B}\right) - \psi\left(-\frac{1}{2}+\frac{E_b}{2\omega_B}\right) - \psi\left(\frac{1}{2}+\frac{E_b}{2\omega_B}\right) \simeq \left(\frac{\omega_B}{E_b}\right)^2, \tag{3.70b}$$

which lead to

$$m^* \to 2m \tag{3.71}$$

as expected from the tightly bound molecules. On the other hand, the effective mass is divergent in the weak-coupling limit $\epsilon_b \to 0$, which results from the fact that fermions forming a pair cannot easily move because of their cyclotron motion.

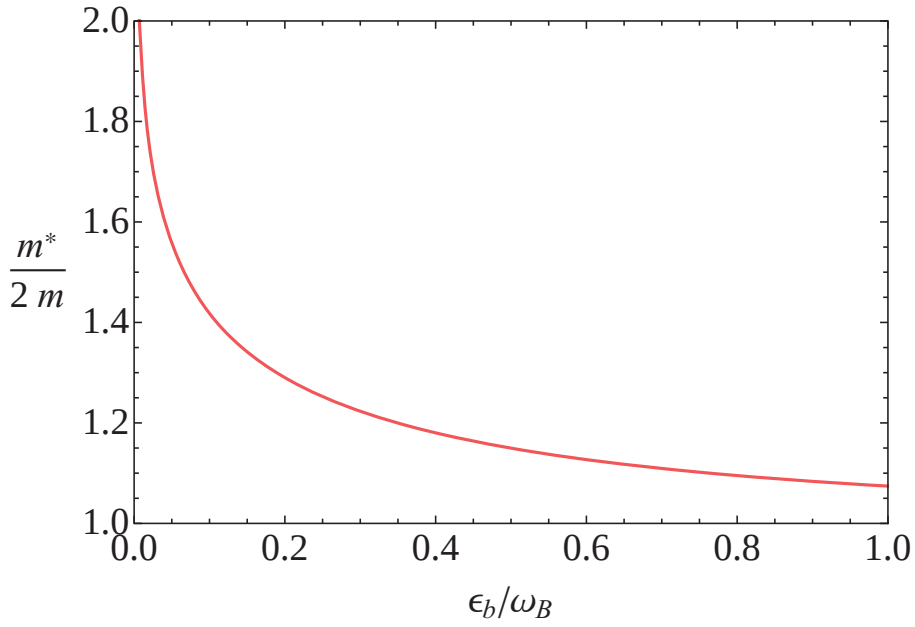

Figure 3.8: Scaled effective mass $m^*/(2m)$ as a function of the two-body binding energy ϵ_b in a unit of the cyclotron frequency ω_B.

3.4 Universality class of the quantum phase transition

We found that the phase diagram obtained in Section 3.2 closely resembles that of the Bose-Hubbard model which is composed of superfluid and Mott insulator phases [92]. Here, it was revealed that the quantum phase transition between them is classified into the universality class of the dilute Bose gas or XY model. This fact and the mutual resemblance motivate us to elucidate the universality class of the quantum phase transition in our system.

Let us derive the Ginzburg-Landau action in the vicinity of the quantum phase transition. To this end, we need to expand the effective action $S_{\rm eff}$ (3.11) up to the quadratic order in the pair field $\Delta(x)$ assumed to be small and smooth. Actually, we can determine the Ginzburg-Landau action by comparing it with the effective action within the Gaussian approximation, which is already obtained in Eqs. (3.17) and (B.19). Now, we write the Ginzburg-Landau action as follows:

$$S_{\rm GL} = C_0 + \int dx \Big[A_1 \Delta^*(x) \partial_\tau \Delta(x) + A_2 |\partial_\tau \Delta(x)|^2 + B_2 |\nabla \Delta(x)|^2 + C_2 |\Delta(x)|^2 + C_4 |\Delta(x)|^4 \Big]. \tag{3.72}$$

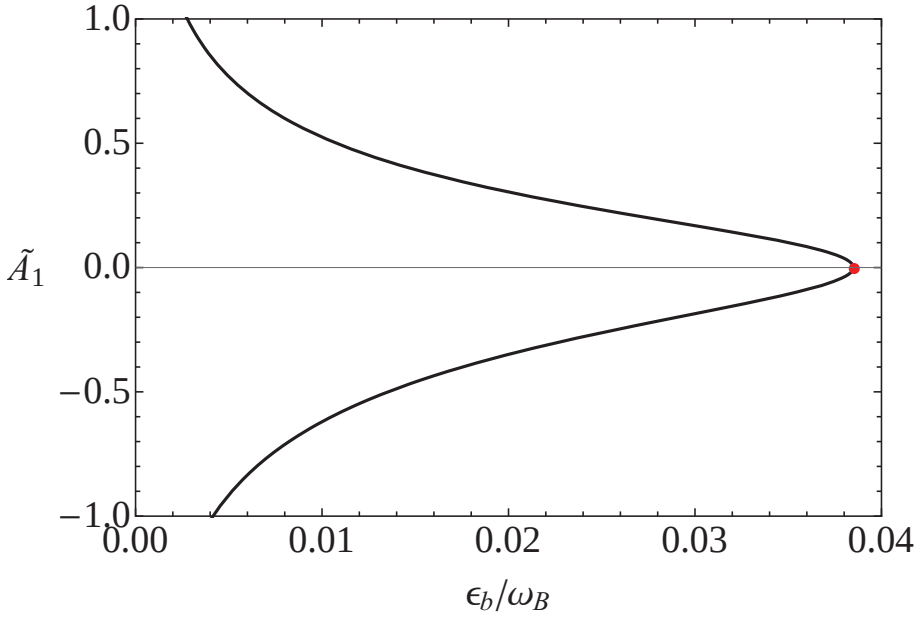

Figure 3.9: Scaled coefficient $\widetilde{A}_1 \equiv \omega_B A_1/m$ along the phase boundary of the quantum phase transition with $\nu = 1$. The dot indicates the tip of the QSH insulator.

When we set $\Delta(x) = \Delta_0$, the above action reduces to the mean-field action $S_{\rm MF}$ (3.17), so that the coefficients C_i $(i = 0, 2, 4)$ are provided by Eqs. (3.21). On the other hand, the coefficients A_1, A_2, B_2 are obtained by replacing $\Delta_0 \to 0, \eta(x) \to \Delta(x)$ in the Gaussian part of the effective action $S_{\rm G}$ (B.19):

$$\begin{aligned} S_{\rm G}|_{\Delta_0\to 0,\eta(x)\to\Delta(x)} &= \beta L^2 \sum_p M_{11}(p)\big|_{\Delta_0\to 0}|\widetilde{\Delta}(p)|^2 \\ &\simeq \beta L^2 \sum_p \left[a_1(ip_n) + a_2(ip_n)^2 + b_2\boldsymbol{p}^2\right]\big|_{\Delta_0\to 0}|\widetilde{\Delta}(p)|^2 \\ &= \int dx \left[\left(-a_1\big|_{\Delta_0\to 0}\right)\Delta^*(x)\partial_\tau\Delta(x) \right. \\ &\qquad \left. + \left(-a_2\big|_{\Delta_0\to 0}\right)|\partial_\tau\Delta(x)|^2 + \left(b_2\big|_{\Delta_0\to 0}\right)|\nabla\Delta(x)|^2\right], \end{aligned} \tag{3.73}$$

where we have performed the low-energy expansion of the inverse fluctuation propagator (B.31). Therefore, we obtain

$$A_1 = \frac{m\omega_B}{8\pi}\sum_{l=0}^{\infty}\frac{\xi_l}{|\xi_l|^3} = \frac{m}{8\pi\omega_B}\left[2\psi'\left(\frac{1}{2} - \frac{\mu}{\omega_B} + \nu\right) - \psi'\left(\frac{1}{2} - \frac{\mu}{\omega_B}\right)\right], \tag{3.74a}$$

$$A_2 = C_4 = \frac{m}{32\pi\omega_B^2}\left[\psi''\left(\frac{1}{2} - \frac{\mu}{\omega_B}\right) - 2\psi''\left(\frac{1}{2} - \frac{\mu}{\omega_B} + \nu\right)\right], \tag{3.74b}$$

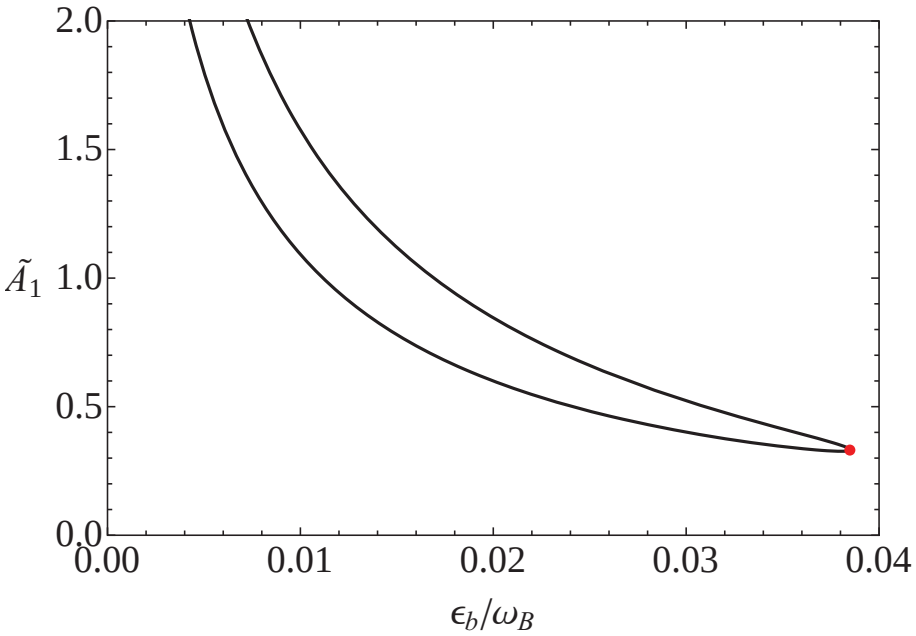

Figure 3.10: Scaled coefficient $\widetilde{A}_2 \equiv \omega_B^2 A_2/m$ along the phase boundary of the quantum phase transition with $\nu = 1$. The dot indicates the tip of the QSH insulator.

$$
\begin{aligned}
B_2 = \frac{1}{4\pi}\sum_{l=0}^{\infty}\Bigg[\left(l+\frac{1}{2}\right)\frac{1}{|\xi_l|} - l\frac{\theta(\xi_l)\theta(\xi_{l-1})+\theta(-\xi_l)\theta(-\xi_{l-1})}{|\xi_l|+|\xi_{l-1}|} \\
- (l+1)\frac{\theta(\xi_l)\theta(\xi_{l+1})+\theta(-\xi_l)\theta(-\xi_{l+1})}{|\xi_l|+|\xi_{l+1}|}\Bigg] \\
= \frac{\mu}{8\pi\omega_B^2}\Bigg[2\psi\left(\frac{1}{2}-\frac{\mu}{\omega_B}\right) - \psi\left(-\frac{\mu}{\omega_B}\right) - \psi\left(1-\frac{\mu}{\omega_B}\right) \\
- 4\psi\left(\frac{1}{2}-\frac{\mu}{\omega_B}+\nu\right) + 2\psi\left(-\frac{\mu}{\omega_B}+\nu\right) + 2\psi\left(1-\frac{\mu}{\omega_B}+\nu\right)\Bigg]. \qquad (3.74c)
\end{aligned}
$$

We plot the coefficients A_1, A_2, and B_2 along the phase boundary (3.22) in Figs. 3.9, 3.10, and 3.11. While A_2, C_4 and B_2 are always positive, C_2 changes its sign when the phase boundary located at Eq. (3.10) is crossed. Moreover, we find that A_1 is related to C_2,

$$A_1 = -\frac{1}{2}\frac{\partial C_2}{\partial \mu}, \qquad (3.75)$$

and therefore, A_1 vanishes at $\partial C_2/\partial\mu = 0$ corresponding to the tip of each QSH insulator labeled by a filling factor ν. In Fig. 3.1, we indicate the tip of each QSH insulator by the dots.

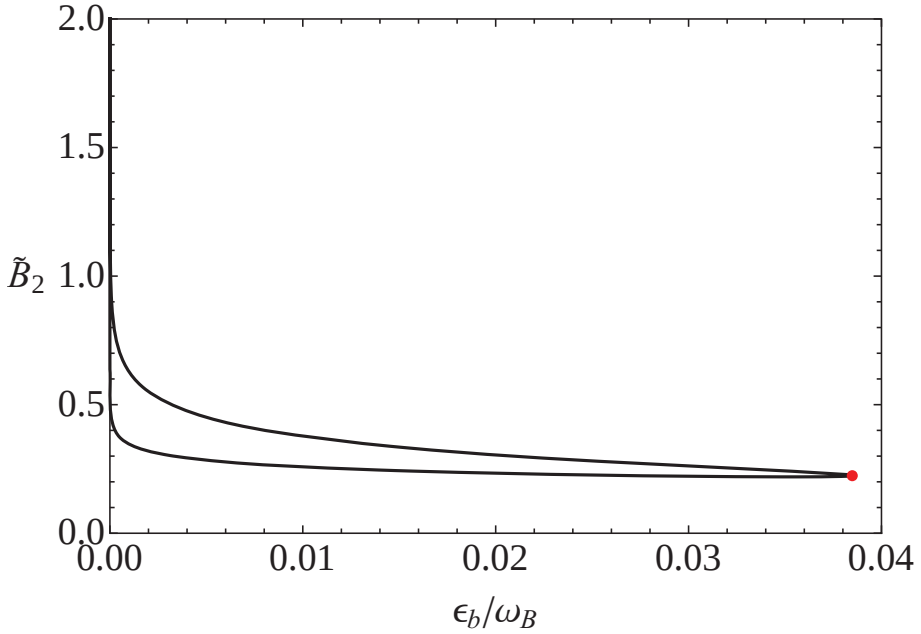

Figure 3.11: Scaled coefficient $\widetilde{B}_2 \equiv \omega_B^2 B_2$ along the phase boundary of the quantum phase transition with $\nu = 1$. The dot indicates the tip of the QSH insulator.

When $A_1 = 0$, the Ginzburg-Landau action is invariant under the exchange of $\Delta^*(x) \leftrightarrow \Delta(x)$, which signals the particle-hole symmetry emergent in the low-energy limit. The equation of motion obeyed by the pair field is given by $\delta S_{\rm GL}/\delta\Delta^*(x) = 0$:

$$-A_1\partial_\tau\Delta(x) + A_2\partial_\tau^2\Delta(x) = \left[-B_2\boldsymbol{\nabla}^2 + C_2 + 2C_4|\Delta(x)|^2\right]\Delta(x). \tag{3.76}$$

Therefore, the equation of motion becomes the non-linear Klein-Gordon equation, which is relativistic and Lorentz invariant. The quantum phase transition turns out to be in the universality class of the XY model [99]. On the other hand, away from the tip of each QSH insulator, A_2 term in the action is negligible compared to the non-vanishing A_1 term. In this case, the equation of motion becomes the usual Gross-Pitaevskii equation, and therefore, the quantum phase transition turns out to be in the universality class of the dilute Bose gas [99].

3.5 Summary

In this chapter, we considered a 2D spin-balanced Fermi gas with an attractive interaction in antiparallel magnetic fields and investigated the ground-state properties within the mean-field approximation. We determined the zero-temperature phase diagram by minimizing the mean-field thermodynamic potential for a pairing gap.

When the chemical potential does not match any Landau levels, we found that a superfluid phase changes into a QSH phase by decreasing the attractive interaction and two phases are separated by a second-order quantum phase transition. Its universality class of the quantum phase transition turns out to be that of the XY model at the tip of each QSH insulator and that of the dilute Bose gas elsewhere, which closely resembles the phase diagram of the Bose-Hubbard model.

On the other hand, we found that a superfluid state persists down to the weak-coupling limit when the chemical potential matches some Landau level. We calculated physical quantities to clarify ground-state properties in the superfluid state. We found that in the strong-coupling limit, the results in the presence of antiparallel magnetic fields correspond to that in their absence, although the significant difference between them appears in the weak-coupling limit. In particular, we found that a pairing gap exhibits the linear dependence of the small coupling contrast, which is remarkably different from the usual exponential dependence. Interestingly, a pairing gap and condensate density are enhanced by antiparallel magnetic fields as a consequence of magnetic catalysis. On the other hand, we found that a sound velocity and superfluid density are suppressed by antiparallel magnetic fields compared to that without magnetic fields. This results from the fact that fermions forming a pair cannot easily move because of their cyclotron motion.

Chapter 4

Ground-state phase diagram of a two-dimensional spin-imbalanced Fermi gas

In the previous chapter, we found that the zero-temperature phase diagram of a spin-balanced Fermi gas consists of superfluid and QSH insulator phases, which are separated by a second-order quantum phase transition (see Fig. 3.1). Our purpose in this chapter is to extend our previous analysis on the zero-temperature phase diagram to the population-imbalanced system with particular attention on the possible Fulde-Ferrell (FF) and Larkin-Ovchinnikov (LO) phases, which has been discussed in the context of ultracold atoms [39, 40, 41, 42].

The FF state is an anisotropic superfluid state where the order parameter has a spatially varying phase with a constant magnitude, $\Delta(x) = \Delta_0 e^{i\boldsymbol{p}\cdot\boldsymbol{x}}$, so that the Cooper pairing takes place with nonzero momentum [43]. On the other hand, the LO state is an inhomogeneous superfluid state where the order parameter is periodically modulated in its magnitude, such as $\Delta(x) = \Delta_0 \cos(\boldsymbol{p}\cdot\boldsymbol{x})$ [44]. Although the FF state is assumed by an ansatz because of its ease to handle theoretically, the LO state has been known to be energetically favored in the familiar population imbalance systems such as ultracold Fermi gas [42, 110, 111] and electric superconductor [112, 113]. In contrast, when the antiparallel magnetic fields are applied, we will find below that the FF state is energetically favored over the LO state at least in the weak-coupling limit where the mean-field approximation is employed. In Section 4.1, we clarify the zero-temperature phase diagram in the space of attractive interaction and two chemical potentials analytically at weak coupling as well as numerically beyond it in Section 4.2. Finally, we summarize this chapter in Section 4.3.

By repeating the same procedure performed in Section 3.1, the action for a spin-

imbalanced case is given by

$$S' = \int dx \, \frac{|\Delta(x)|^2}{g} - \int dx \, \Phi^*(x) \begin{bmatrix} -\partial_\tau + \frac{[\boldsymbol{\nabla} + i\boldsymbol{A}_\uparrow(\boldsymbol{x})]^2}{2m} + \mu_\uparrow & \Delta(x) \\ \Delta^*(x) & -\partial_\tau - \frac{[\boldsymbol{\nabla} - i\boldsymbol{A}_\downarrow(\boldsymbol{x})]^2}{2m} - \mu_\downarrow \end{bmatrix} \Phi(x), \quad (4.1)$$

where μ_σ is the chemical potential for each spin component.

4.1 Weak-coupling limit

4.1.1 FF state versus LO state

To discuss the Cooper pairing with an infinitesimal coupling $g \to 0$, we assume that the chemical potential for each spin component matches some Landau level, i.e., $\mu_\sigma = \epsilon_{l_\sigma} (l_\sigma \in \mathbb{N})$, because we showed in the previous chapter that the system is otherwise insulating. In this case, we can expand the fermionic fields over the eigenfunctions in Eq. (3.4) restricted to the $(l_\sigma+1)$-th Landau level, whose energy is provided by $\epsilon_{l_\sigma} = \omega_B(l_\sigma + 1/2)$, because the mixing with the other Landau levels is negligible in the weak-coupling limit. By substituting $\phi_\uparrow(x) = \sum_{i\omega_n} \sum_{k_x} \chi_{i\omega_n,k_x,l_\uparrow}(x) \widetilde{\phi}_\uparrow(i\omega_n, k_x, l_\uparrow)$ and $\phi_\downarrow(x) = \sum_{i\omega_n} \sum_{k_x} \chi^*_{i\omega_n,k_x,l_\downarrow}(x) \widetilde{\phi}_\downarrow(i\omega_n, k_x, l_\downarrow)$ into Eq. (4.1), the action reads

$$S' = \int dx \, \frac{|\Delta(x)|^2}{g} - \sum_{i\omega_n, i\omega_{n'}} \sum_{k_x, k'_x} \widetilde{\Phi}^*(k) \begin{bmatrix} i\omega_n \delta_{i\omega_n, i\omega_{n'}} \delta_{k_x,k'_x} & \widetilde{\Delta}(k,k') \\ \widetilde{\Delta}^*(k',k) & i\omega_n \delta_{i\omega_n, i\omega_{n'}} \delta_{k_x,k'_x} \end{bmatrix} \widetilde{\Phi}(k') \quad (4.2)$$

with $\widetilde{\Phi}(k) \equiv [\widetilde{\phi}_\uparrow(i\omega_n, k_x, l_\uparrow), \widetilde{\phi}^*_\uparrow(i\omega_n, k_x, l_\downarrow)]^{\mathrm{T}}$ and

$$\widetilde{\Delta}(k,k') = \int dx \, \chi^*_{i\omega_n,k_x,l_\uparrow}(x) \Delta(x) \chi_{i\omega_{n'},k'_x,l_\downarrow}(x) \quad (4.3)$$

measuring the overlap of two fermion wave functions with the pair field $\Delta(x)$. This action allows us to evaluate and compute the mean-field thermodynamic potentials for the FF and LO states analytically.

FF state

Because of the rotational invariance, the pair field in the FF ansatz can be chosen to be $\Delta(x) = \Delta_0 e^{iQy}$ with $\Delta_0 \geq 0$, for which we obtain

$$\begin{aligned}\widetilde{\Delta}(k,k') &= \Delta_0 \int dx\, e^{iQy} \chi^*_{i\omega_n,k_x,l_\uparrow}(x)\chi_{i\omega_{n'},k'_x,l_\downarrow}(x) \\ &= \Delta_0 e^{ik_xQ\ell_B^2}\delta_{i\omega_n,i\omega_{n'}}\delta_{k_x,k'_x}\int dy\, e^{iQy}F_{l_\uparrow}(y)F_{l_\downarrow}(y) \\ &\equiv \delta_{i\omega_n,i\omega_{n'}}\delta_{k_x,k'_x}e^{ik_xQ\ell_B^2}f_Q\Delta_0. \end{aligned} \tag{4.4}$$

Here the overlap is

$$f_Q \equiv I_{l_\uparrow,l_\downarrow}(0,Q) = \sqrt{\frac{l_\downarrow!}{l_\uparrow!}}e^{-Q^2\ell_B^2/4}\left(\frac{iQ\ell_B}{\sqrt{2}}\right)^{l_\uparrow-l_\downarrow} L_{l_\downarrow}^{l_\uparrow-l_\downarrow}\left(\frac{Q^2\ell_B^2}{2}\right), \tag{4.5}$$

where the function $I_{l,l'}(\boldsymbol{p})$ is obtained in Appendix B.2 [see Eqs. (B.27) and (B.28)]. The action can then be written as

$$S' = \beta L^2\frac{\Delta_0^2}{g} - \sum_{i\omega_n}\sum_{k_x}\widetilde{\Phi}^*(k)\begin{bmatrix} i\omega_n & e^{+ik_xQ\ell_B^2}f_Q\Delta_0 \\ e^{-ik_xQ\ell_B^2}f_Q^*\Delta_0 & i\omega_n\end{bmatrix}\widetilde{\Phi}(k). \tag{4.6}$$

By integrating out the fermionic fields and taking the limits $\beta, L \to \infty$, we obtain the zero-temperature thermodynamic potential in the mean-field approximation,

$$\begin{aligned}\Omega_{\rm FF} &= \frac{\Delta_0^2}{g} - \frac{m\omega_B}{2\pi}|f_Q|\Delta_0 \\ &= \frac{1}{g}\left(\Delta_0 - g\frac{m\omega_B}{4\pi}|f_Q|\right)^2 - g\left(\frac{m\omega_B}{4\pi}|f_Q|\right)^2. \end{aligned} \tag{4.7}$$

Its minimization with respect to Δ_0 and Q leads to

$$\min\Omega_{\rm FF} = -g\left(\frac{m\omega_B}{4\pi}|f_{Q_0}|\right)^2, \tag{4.8}$$

where $\Delta_0 = gm\omega_B|f_{Q_0}|/(4\pi)$ with Q_0 maximizing $|f_Q|$. Although $Q_0 = 0$ for $l_\uparrow = l_\downarrow$ without population imbalance corresponding to the unpolarized superfluid state as expected from the previous chapter, we find $Q_0 \neq 0$ for $l_\uparrow \neq l_\downarrow$ with population imbalance corresponding to the FF state. As examples, $Q_0/\ell_B = \sqrt{2}, 2$, and $\sqrt{5-\sqrt{17}}$ are found for $(l_\uparrow, l_\downarrow) = (1,0), (2,0)$, and $(2,1)$, respectively.

LO state

The same analysis can be repeated in the LO ansatz, $\Delta(x) = \Delta_0 \cos(Qy)$ with $\Delta_0 \geq 0$, for which we obtain

$$\begin{aligned}\widetilde{\Delta}(k,k') &= \frac{\Delta_0}{2}\int dx\, \left(\mathrm{e}^{iQy}+\mathrm{e}^{-iQy}\right)\chi^*_{i\omega_n,k_x,l_\uparrow}(x)\chi_{i\omega_{n'},k'_x,l_\downarrow}(x)\\ &= \delta_{i\omega_n,i\omega_{n'}}\delta_{k_x,k'_x}\frac{\mathrm{e}^{ik_xQ\ell_B^2}+(-1)^{l_\uparrow-l_\downarrow}\mathrm{e}^{-ik_xQ\ell_B^2}}{2}f_Q\Delta_0\\ &= \delta_{i\omega_n,i\omega_{n'}}\delta_{k_x,k'_x}\mathrm{e}^{-i\varphi}\cos(k_xQ\ell_B^2+\varphi)f_Q\Delta_0 \end{aligned} \tag{4.9}$$

with $\varphi = \pi(l_\uparrow - l_\downarrow)/2$. The action can then be written as

$$\begin{aligned}S' &= \beta L^2\frac{\Delta_0^2}{2g}\\ &\quad -\sum_{i\omega_n}\sum_{k_x}\widetilde{\Phi}^*(k)\begin{bmatrix} i\omega_n & \mathrm{e}^{-i\varphi}\cos(k_xQ\ell_B^2+\varphi)f_Q\Delta_0\\ \mathrm{e}^{+i\varphi}\cos(k_xQ\ell_B^2+\varphi)f_Q^*\Delta_0 & i\omega_n\end{bmatrix}\widetilde{\Phi}(k).\end{aligned} \tag{4.10}$$

By integrating out the fermionic fields and taking the limits $\beta, L \to \infty$, we obtain the zero-temperature thermodynamic potential in the mean-field approximation,

$$\begin{aligned}\Omega_{\mathrm{LO}} &= \frac{\Delta_0^2}{2g} - \frac{m\omega_B}{\pi^2}|f_Q|\Delta_0\\ &= \frac{1}{2g}\left(\Delta_0 - g\frac{m\omega_B}{\pi^2}|f_Q|\right)^2 - \frac{8g}{\pi^2}\left(\frac{m\omega_B}{4\pi}|f_Q|\right)^2,\end{aligned} \tag{4.11}$$

where we have performed the following calculations:

$$\frac{1}{\beta L^2}\int dx\,\frac{|\Delta(x)|^2}{g} = \frac{\Delta_0^2}{gL}\int_{-L/2}^{L/2}dy\,\cos^2(Qy) \xrightarrow{L\to\infty} \frac{\Delta_0^2}{2g}, \tag{4.12}$$

$$\frac{1}{L^2}\sum_{k_x}|\cos(k_xQ\ell_B^2+\varphi)| = \frac{m\omega_B}{2\pi L}\int_{-L/2}^{L/2}dk_x\,|\cos(k_xQ+\varphi)| \xrightarrow{L\to\infty} \frac{m\omega_B}{\pi^2}. \tag{4.13}$$

Its minimization with respect to Δ_0 and Q leads to

$$\min\Omega_{\mathrm{LO}} = -\frac{8g}{\pi^2}\left(\frac{m\omega_B}{4\pi}|f_{Q_0}|\right)^2, \tag{4.14}$$

where $\Delta_0 = gm\omega_B|f_{Q_0}|/\pi^2$ with the same Q_0 maximizing $|f_Q|$.

By comparing Eqs. (4.8) and (4.14), we find

$$\min\Omega_{\mathrm{FF}} = \frac{\pi^2}{8}\min\Omega_{\mathrm{LO}} < \min\Omega_{\mathrm{LO}}, \tag{4.15}$$

and therefore, the FF state proves to be energetically favored over the LO state.

4.1.2 Phase diagram at weak coupling

Now that the FF state is energetically favored in the weak-coupling limit, we set $\Delta(x) = \Delta_0 e^{iQy}$ with $\Delta_0 \geq 0$ and investigate the ground-state phase diagram at weak coupling. To this end, we assume that the chemical potential for each spin component lies slightly off some Landau level, i.e., $\mu_\sigma = \epsilon_{l_\sigma} + \delta\mu_\sigma$ with $|\delta\mu_\sigma| \ll \omega_B$, so that the mixing with the other Landau levels is still negligible. By denoting $\delta\mu_\uparrow = \delta\mu + \delta h$ and $\delta\mu_\downarrow = \delta\mu - \delta h$, the action in Eq. (4.2) with the use of Eq. (4.4) is modified into

$$S' = \beta L^2 \frac{\Delta_0^2}{g} - \sum_{i\omega_n} \sum_{k_x} \widetilde{\Phi}^*(k) \begin{bmatrix} i\omega_n + \delta\mu + \delta h & e^{+ik_x Q\ell_B^2} f_Q \Delta_0 \\ e^{-ik_x Q\ell_B^2} f_Q^* \Delta_0 & i\omega_n - \delta\mu + \delta h \end{bmatrix} \widetilde{\Phi}(k). \tag{4.16}$$

By integrating out the fermionic fields and taking the limits $\beta, L \to \infty$, the zero-temperature thermodynamic potential in the mean-field approximation is found to be

$$\Omega_{\rm MF} = \frac{\Delta_0^2}{g} - \frac{m\omega_B}{2\pi} \left(\sqrt{\delta\mu^2 + |f_Q \Delta_0|^2} + \delta\mu \right) - \frac{m\omega_B}{2\pi} \left(|\delta h| - \sqrt{\delta\mu^2 + |f_Q \Delta_0|^2} \right)_>, \tag{4.17}$$

where $(z)_> \equiv z\theta(z)$ for brevity.

The resulting phases are determined by finding the pairing gap Δ_0 and momentum Q minimizing the thermodynamic potential $\Omega_{\rm MF}$. It is minimized by Q always at $Q = Q_0$ maximizing $|f_Q|$. A phase with $\Delta_0 > 0$ then corresponds to the unpolarized superfluid (SF) or FF state depending on $l_\uparrow = l_\downarrow$ ($Q_0 = 0$) or $l_\uparrow \neq l_\downarrow$ ($Q_0 \neq 0$). On the other hand, a phase with $\Delta_0 = 0$ corresponds to the normal state where the system is composed of two quantum Hall insulators (QHIs) with filling factors of $(\nu_\uparrow, \nu_\downarrow) = (l_\uparrow + \theta(\delta\mu_\uparrow), l_\downarrow + \theta(\delta\mu_\downarrow))$ for different spin components. In particular, when $\nu_\uparrow = \nu_\downarrow > 0$, the system without population imbalance is the QSH insulator without time-reversal invariance [59, 60, 61].

It is an elementary analysis to minimize the thermodynamic potential in Eq. (4.17) with respect to Δ_0 and the obtained phase diagram at zero temperature is depicted in Fig. 4.1. When $|\delta\mu| > |\delta h|$, the thermodynamic potential in Eq. (4.17) reduces to

$$\Omega_{\rm MF} = \frac{\Delta_0^2}{g} - \frac{m\omega_B}{2\pi} \left(\sqrt{\delta\mu^2 + |f_{Q_0} \Delta_0|^2} + \delta\mu \right), \tag{4.18}$$

which is independent of $|\delta h|$. To elucidate a quantum phase transition, we expand the above thermodynamic potential up to the quartic order in Δ_0 assumed to be small:

$$\Omega_{\rm MF} = -\frac{m\omega_B}{2\pi} (|\delta\mu| + \delta\mu) + \left[\frac{1}{g} - \frac{m\omega_B}{4\pi} \frac{|f_{Q_0}|^2}{|\delta\mu|} \right] \Delta_0^2 + \frac{m\omega_B}{16\pi} \frac{|f_{Q_0}|^4}{|\delta\mu|^3} \Delta_0^4 + \mathcal{O}\left(\Delta_0^6\right). \tag{4.19}$$

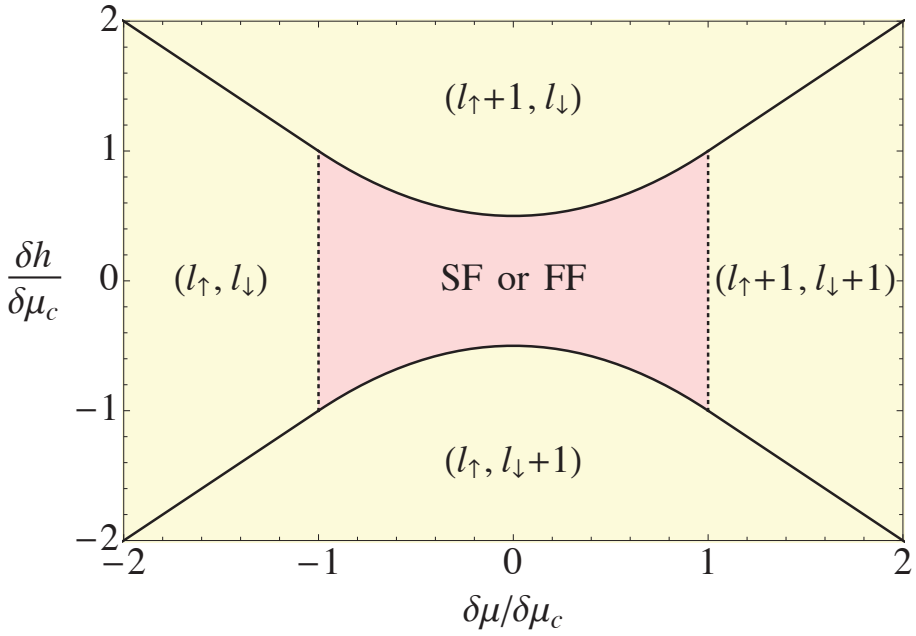

Figure 4.1: Zero-temperature phase diagram at weak coupling in the plane of $\delta\mu$ and δh for $\mu_\sigma \simeq \epsilon_{l_\sigma}$ in units of $\delta\mu_c$. The unpolarized SF or FF phase is located at the center depending on $l_\uparrow = l_\downarrow$ or $l_\uparrow \neq l_\downarrow$, and the other four phases are QHIs whose filling factors $(\nu_\uparrow, \nu_\downarrow)$ are indicated. The quantum phase transitions denoted by the dotted lines at $|\delta\mu| = \delta\mu_c$ are of the second order, whereas those denoted by the solid lines at $|\delta h| = (\delta\mu_c^2 + \delta\mu^2)/(2\delta\mu_c) < \delta\mu_c$ and $|\delta h| = |\delta\mu| > \delta\mu_c$ are of the first order.

Because the fourth-order coefficient of the pairing gap is always positive, we find a second-order quantum phase transition from a pairing state with $\Delta_0 > 0$ to a normal state with $\Delta_0 = 0$ by increasing $|\delta\mu|$. The boundary of this phase transition is given by

$$|\delta\mu| = \delta\mu_c \equiv g\frac{m\omega_B}{4\pi}|f_{Q_0}|^2. \tag{4.20}$$

The pairing gap Δ_0 in the pairing state ($|\delta\mu| < \delta\mu_c$) is determined by solving the gap equation $\partial\Omega_{\rm MF}/\partial\Delta_0 = 0$, which leads to

$$\Delta_0 = \frac{\sqrt{\delta\mu_c^2 - \delta\mu^2}}{|f_{Q_0}|}. \tag{4.21}$$

On the other hand, when $|\delta h| > |\delta\mu|$ and $|\delta h| > \delta\mu_c$, the thermodynamic potential in Eq. (4.17) becomes

$$\Omega_{\rm MF} = \frac{\Delta_0^2}{g} - \frac{m\omega_B}{2\pi}(|\delta h| + \delta\mu). \tag{4.22}$$

Therefore, the system is in the normal state with $\Delta_0 = 0$, where the thermodynamic potential is given by

$$\Omega_{\rm N} \equiv -\frac{m\omega_B}{2\pi}(|\delta h| + \delta\mu). \tag{4.23}$$

When $\delta\mu_c > |\delta h| > |\delta\mu|$, we find that the thermodynamic potential in Eq. (4.17) has two local minima. One is $\Omega_{\rm N}$ in Eq. (4.23), and the other is $\Omega_{\rm Pair}$ in the pairing state, which is given by substituting Eq. (4.21) into Eq. (4.18):

$$\Omega_{\rm Pair} \equiv -\frac{m\omega_B}{2\pi}\left[\frac{\delta\mu_c^2 + \delta\mu^2}{2\delta\mu_c} + \delta\mu\right]. \tag{4.24}$$

The normal and pairing states are separated by a first-order quantum phase transition and its phase boundary is determined by solving $\Omega_{\rm N} = \Omega_{\rm Pair}$, which leads to

$$|\delta h| = \delta h_c \equiv \frac{\delta\mu_c^2 + \delta\mu^2}{2\delta\mu_c}. \tag{4.25}$$

This phase transition continues into another first-order quantum phase transition at $|\delta h| = |\delta\mu| > \delta\mu_c$ separating the two QHI phases with different filling factors. The quasiparticle energy in the SF or FF phase is found to be

$$\sqrt{\delta\mu + |f_{Q_0}\Delta_0|^2} = \delta\mu_c \tag{4.26}$$

independent of $\delta\mu$ and the ratio

$$\frac{\delta h_c}{\delta\mu_c} = \frac{1}{2}\left[1 + \left(\frac{\delta\mu}{\delta\mu_c}\right)^2\right] \tag{4.27}$$

varies from 1/2 to 1 for $0 \le \delta\mu \le \delta\mu_c$.

The zero-temperature phase diagram in Fig. 4.1 is valid in the vicinity of $\mu_\sigma \simeq \epsilon_{l_\sigma}$ for every $l_\sigma = 0, 1, 2, \ldots$, which all together leads to the global phase diagram in the plane of the average chemical potential $\mu \equiv (\mu_\uparrow + \mu_\downarrow)/2$ and Zeeman field $h \equiv (\mu_\uparrow - \mu_\downarrow)/2$ as depicted in Fig. 4.2. It consists of the QHIs, SF, and FF phases as well as the vacuum (vac) with $\nu_\uparrow = \nu_\downarrow = 0$ and is symmetric under $h \leftrightarrow -h$ with $\nu_\uparrow \leftrightarrow \nu_\downarrow$. The SF or FF, and QHI phases are separated by the second-order (first-order) quantum phase transition along the direction of μ (h), whereas the two QHI phases with different filling factors $(\nu_\uparrow, \nu_\downarrow)$ are separated by the first-order quantum phase transition. We note that a large value of $mg = 2.5$ is artificially chosen for Fig. 4.2 in order to make the FF phases visible.

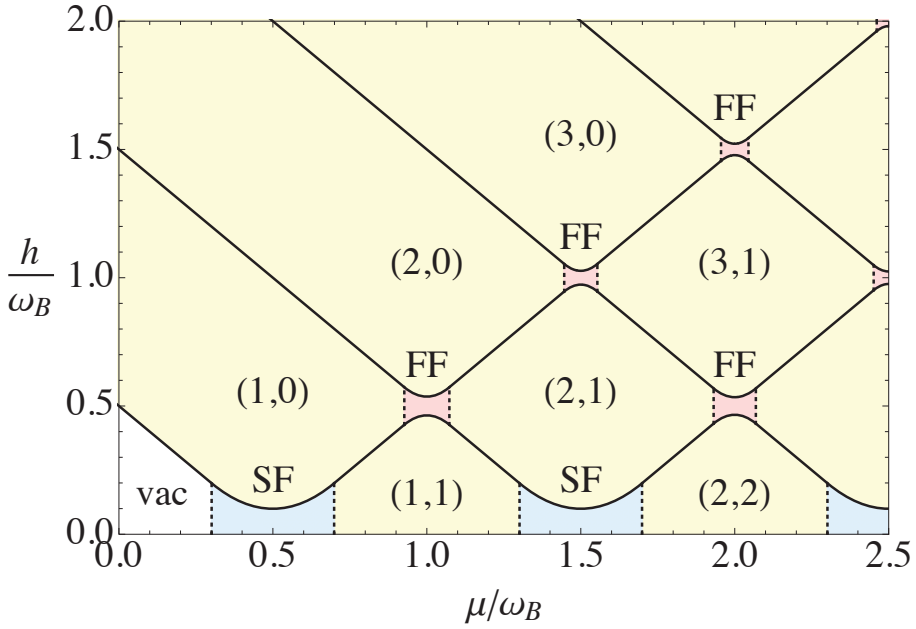

Figure 4.2: Zero-temperature phase diagram in the plane of the average chemical potential $\mu = (\mu_\uparrow + \mu_\downarrow)/2$ and Zeeman field $h = (\mu_\uparrow - \mu_\downarrow)/2$ in units of the cyclotron frequency ω_B deduced from Fig. 4.1 for $mg = 2.5$. See the caption in Fig. 4.1 for the other details.

4.2 Phase diagram beyond weak coupling

Because the FF phases occupy only the tiny portions of the phase diagram in the weak-coupling limit, it is important to elucidate how they extend beyond the weak coupling. To this end, we go back to the action in Eq. (4.1) and expand the fermionic fields over all the eigenfunctions in Eq. (3.4) so as to allow for the mixing of the Landau levels. By assuming the FF ansatz, $\Delta(x) = \Delta_0 \mathrm{e}^{iQy}$ with $\Delta_0 \geq 0$, making the gauge transformation, $\phi_\sigma(x) \to \mathrm{e}^{iQy/2}\phi_\sigma(x)$, and then substituting $\phi_\uparrow(x) = \sum_k \chi_k(x)\widetilde{\phi}_\uparrow(k)$ and $\phi_\downarrow(x) = \sum_k \chi_k^*(x)\widetilde{\phi}_\downarrow(k)$ into Eq. (4.1), the action reads

$$S' = \beta L^2 \frac{\Delta_0^2}{g} - \sum_k \sum_{k'} \widetilde{\Phi}^*(k) G^{-1}(k,k') \widetilde{\Phi}(k') \tag{4.28}$$

with $\widetilde{\Phi}(k) \equiv [\widetilde{\phi}_\uparrow(k), \widetilde{\phi}_\downarrow^*(k)]^{\mathrm{T}}$ and

$$G^{-1}(k,k') = \begin{bmatrix} i\omega_n - \epsilon_l - \frac{Q^2}{8m} + \mu + h & \Delta_0 \\ \Delta_0 & i\omega_n + \epsilon_l + \frac{Q^2}{8m} - \mu + h \end{bmatrix} \delta_{k,k'}$$

$$- \frac{iQ}{2m\ell_B} \begin{pmatrix} 1 & 0 \\ 0 & 1 \end{pmatrix} \left[\sqrt{\frac{l}{2}} \delta_{l-1,l'} - \sqrt{\frac{l+1}{2}} \delta_{l+1,l'} \right] \delta_{i\omega_n, i\omega_{n'}} \delta_{k_x, k'_x}. \quad (4.29)$$

Here, we have employed the following relation,

$$\ell_B \frac{\partial}{\partial z} F_l(z) = \sqrt{\frac{l}{2}} F_{l-1}(z) - \sqrt{\frac{l+1}{2}} F_{l+1}(z), \quad (4.30)$$

and the orthogonality relation in Eq. (3.7). The eigenvalues of the inverse Green function $G^{-1}(k, k')$ are provided in the form of $\pm E_l - (h + i\omega_n)$ ($E_l > 0, l = 0, 1, 2, \ldots, n \in \mathbb{Z}$) for every k_x, and therefore, by integrating out the fermionic fields and taking the limits $\beta, L \to \infty$, the zero-temperature thermodynamic potential in the mean-field approximation is given by

$$\Omega_{\rm MF} = \frac{\Delta_0^2}{g} - \frac{m\omega_B}{2\pi} \sum_{l=0}^{\infty} (E_l - \epsilon_l + \mu) \theta(\Lambda - \epsilon_l) - \frac{m\omega_B}{2\pi} \sum_{l=0}^{\infty} (|h| - E_l)_>. \quad (4.31)$$

The quasiparticle energy E_l depends on μ, Δ_0, and Q and is confirmed to have the asymptotic form of $\lim_{l\to\infty} E_l = \sqrt{(\epsilon_l - \mu)^2 + \Delta_0^2}$. Therefore, the second term on the right-hand side of Eq. (4.31) is logarithmically divergent and is regularized by introducing an energy cutoff Λ. By performing the same renormalization procedure used to evaluate the thermodynamic potential for a spin-balanced Fermi gas [see from Eq. (3.15) to Eq. (3.17)], we obtain

$$\begin{aligned} \Omega_{\rm MF} = {} & \frac{m\Delta_0^2}{4\pi} \left[\ln \left(\frac{2\omega_B}{\epsilon_b} \right) + \psi \left(\frac{1}{2} - \frac{\mu}{\omega_B} \right) \right] \\ & - \frac{m\omega_B}{2\pi} \sum_{l=0}^{\infty} \left[E_l - \epsilon_l + \mu - \frac{\Delta_0^2}{2(\epsilon_l - \mu)} + (|h| - E_l)_> \right]. \end{aligned} \quad (4.32)$$

We minimize the resulting thermodynamic potential numerically to find Δ_0 and Q by employing up to $l_{\rm max} = 500$ quasiparticle energies, which are confirmed to be enough for convergence of the summation over l. The obtained phase diagrams are depicted in Fig. 4.3 in the planes of the two-body binding energy ϵ_b and the average chemical potential μ at (a) $h/\omega_B = 0.0$, (b) 0.5, and (c) 1.0 and in the planes of ϵ_b and the Zeeman field h at (d) $\mu/\omega_B = 0.5$, (e) 1.0, and (f) 1.5 in units of the cyclotron frequency ω_B. They are composed of the QHI ($\Delta_0 = 0$), the unpolarized SF ($\Delta_0 \neq 0, Q = 0$), and FF ($\Delta_0 \neq 0, Q \neq 0$) phases and are consistent with the phase diagram at weak coupling elucidated in the previous section (see Fig. 4.3). In particular, we find that each FF phase appearing at $\mu = (\epsilon_{l_\uparrow} + \epsilon_{l_\downarrow})/2$ and $h = (\epsilon_{l_\uparrow} - \epsilon_{l_\downarrow})/2$ with $l_\uparrow \neq l_\downarrow$ in the weak-coupling limit extends well by increasing the attractive interaction and is eventually replaced by the SF phase with the first-order quantum phase transition. We also find that the QHI phase is replaced by the

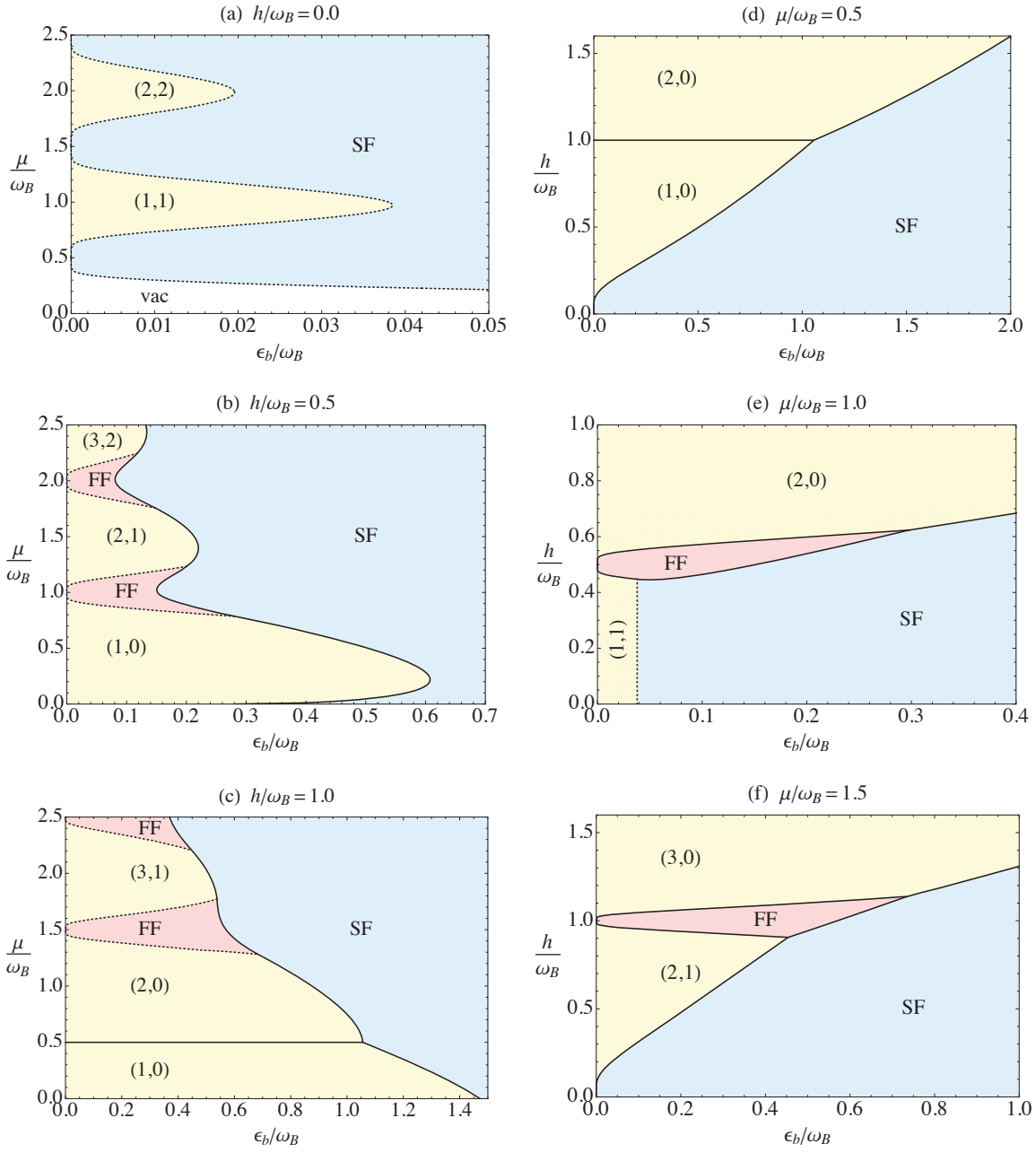

Figure 4.3: Zero-temperature phase diagrams in the planes of the two-body binding energy ϵ_b and average chemical potential μ at (a) $h/\omega_B = 0.0$, (b) 0.5, and (c) 1.0 and in the planes of ϵ_b and the Zeeman field h at (d) $\mu/\omega_B = 0.5$, (e) 1.0, and (f) 1.5 in units of the cyclotron frequency ω_B. There appear the unpolarized SF and FF phases as well as QHIs with their filling factors $(\nu_\uparrow, \nu_\downarrow)$ indicated. They are separated by the various second-order (dotted curves) and first-order (solid curves) quantum phase transitions.

SF phase with the second-order (first-order) quantum phase transition for $\nu_\uparrow = \nu_\downarrow$ ($\nu_\uparrow \neq \nu_\downarrow$) by increasing the attractive interaction. Because the FF phases are found to occupy the reasonable portions of the phase diagram, they may, in principle, be realized by ultracold atom experiments.

4.3 Summary

In this chapter, we considered a 2D spin-imbalanced Fermi gas with an attractive interaction in antiparallel magnetic fields and investigated the ground-state phase diagram within the mean-field approximation.

By evaluating the mean-field thermodynamic potentials for the FF and LO states analytically, we showed that the FF state is energetically favored over the LO state in the weak-coupling limit. We then clarified the ground-state phase diagram in the space of the attractive interaction, average chemical potential μ, and Zeeman field h analytically at weak coupling (see Fig. 4.2) as well as numerically beyond it (see Fig. 4.3). It was found to show the rich structures consisting of the QHI, unpolarized SF, and FF phases, where

(i) the SF or FF, and QHI phases are separated by the second-order (first-order) quantum phase transition along the direction of μ (h),

(ii) the two QHI phases with different filling factors $(\nu_\uparrow, \nu_\downarrow)$ are separated by the first-order quantum phase transition,

(iii) the FF phase is replaced by the SF phase with the first-order quantum phase transition by increasing the attractive interaction,

(iv) the QHI phase is replaced by the SF phase with the second-order (first-order) quantum phase transition for $\nu_\uparrow = \nu_\downarrow$ ($\nu_\uparrow \neq \nu_\downarrow$) by increasing the attractive interaction.

In particular, the FF phases were found to occupy the reasonable portions of the phase diagram, so that they may, in principle, be realized by ultracold atom experiments.

Chapter 5

Ground-state phase diagram of a three-dimensional spin-imbalanced Fermi gas

In the previous chapter, we investigated the ground-state phase diagram of a 2D spin-imbalanced Fermi gas subjected to antiparallel magnetic fields. We now extend this previous analysis on the ground-state phase diagram to the 3D case and consider the FF state to make theoretical treatment easier. In Section 5.1, we clarify the ground-state phase diagram at weak coupling under the condition that fermions only occupy the lowest Landau level. We also comment on the case where fermions occupy higher Landau levels. We discuss the stability of the superfluid state by calculating the collective excitation spectrum in Section 5.2 and summarize this chapter in Section 5.3. In this chapter, we use shorthand notation, $(x) \equiv (\tau, \boldsymbol{x})$, $\int dx \equiv \int_0^\beta d\tau \iiint_0^L d^3\boldsymbol{x}$, $\delta(x-x') \equiv \delta(\tau-\tau')\delta^3(\boldsymbol{x}-\boldsymbol{x}')$, where τ is the imaginary time and $\boldsymbol{x}$ is the 3D spatial coordinates, $(k) \equiv (i\omega_n, k_x, l, k_z)$, $\sum_k \equiv \sum_{i\omega_n}\sum_{k_x}\sum_{l=0}^\infty\sum_{k_z}$, and $\delta_{k,k'} \equiv \delta_{\omega_n,\omega_{n'}}\delta_{k_x,k_x'}\delta_{l,l'}\delta_{k_z,k_z'}$, where $\omega_n = (2n+1)\pi/\beta$ is the fermionic Matsubara frequency with $n \in \mathbb{Z}$, $k_x = 2\pi n_x/L$ ($k_z = 2\pi n_z/L$) is the wave number in the x (z) direction with $n_x = 0, \pm 1, \ldots, \pm m\omega_B L^2/(4\pi)$ ($n_z \in \mathbb{Z}$), and $l = 0, 1, \ldots$ labels Landau levels.

By repeating the same procedure performed in Section 3.1, the action for a 3D spin-imbalanced Fermi gas is given by

$$S' = \int dx \, \frac{|\Delta(x)|^2}{g_{3\mathrm{D}}} - \int dx \, \Phi^*(x) \begin{bmatrix} -\partial_\tau + \frac{[\boldsymbol{\nabla} - iBy\hat{\boldsymbol{x}}]^2}{2m} + \mu_\uparrow & \Delta(x) \\ \Delta^*(x) & -\partial_\tau - \frac{[\boldsymbol{\nabla} - iBy\hat{\boldsymbol{x}}]^2}{2m} - \mu_\downarrow \end{bmatrix} \Phi(x) \tag{5.1}$$

with the coupling constant $g_{3\mathrm{D}} > 0$ in 3D, which is related to the 3D scattering

length $a_{3\mathrm{D}}$ by the following expression [114]:

$$\frac{m}{4\pi a_{3\mathrm{D}}} = -\frac{1}{g_{3\mathrm{D}}} + \frac{1}{L^3}\sum_{\boldsymbol{k}}^{\Lambda}\frac{m}{\boldsymbol{k}^2} \tag{5.2}$$

with an energy cutoff Λ. We use this equation to remove the ultraviolet divergence from our theory as with Eq. (3.16) in 2D.

Here, we employ the mean-field approximation and assume the FF state. Because of the rotational invariance about the axis parallel to the magnetic fields, the pair field $\Delta(x)$ can be chosen to be $\Delta(x) = \Delta_0 \mathrm{e}^{iQ_\perp y + iQ_z z}$. By making the gauge transformation, $\phi_\sigma \to \mathrm{e}^{iQ_z z/2}\phi_\sigma$, and expanding the Nambu-Gor'kov spinor over the eigenfunctions of the single-particle Hamiltonian, we obtain

$$S' = \beta L^3 \frac{\Delta_0^2}{g} - \sum_k \sum_{k'} \widetilde{\Phi}(k) G_{3\mathrm{D}}^{-1}(k,k') \widetilde{\Phi}(k')$$

with the inverse propagator $G_{3\mathrm{D}}^{-1}(k,k')$,

$$\begin{aligned} &G_{3\mathrm{D}}^{-1}(k,k') \\ &= \begin{bmatrix} [i\omega_n - \frac{(k_z+Q_z/2)^2}{2m} - \omega_B(l+\frac{1}{2}) + \mu_\uparrow]\delta_{l,l'} & \mathrm{e}^{+ik_x Q_\perp \ell_B^2} f_{l,l'}(Q_\perp)\Delta_0 \\ \mathrm{e}^{-ik_x Q_\perp \ell_B^2} f_{l,l'}^*(Q_\perp)\Delta_0 & [i\omega_n + \frac{(k_z-Q_z/2)^2}{2m} + \omega_B(l+\frac{1}{2}) - \mu_\downarrow]\delta_{l,l'} \end{bmatrix} \\ &\quad \times \delta_{i\omega_n, i\omega_{n'}} \delta_{k_x,k_x'} \delta_{k_z,k_z'}. \end{aligned} \tag{5.3}$$

5.1 Phase diagram at weak coupling

5.1.1 Lowest Landau level

We consider that each chemical potential slightly lies off the lowest Landau level, i.e., $\mu_\sigma = \omega_B/2 + \delta\mu_\sigma$ with $|\delta\mu_\sigma| \ll \omega_B$, so that the mixing with the higher Landau levels is negligible. The inverse propagator then reads

$$G_{3\mathrm{D}}^{-1}(k,k') = \begin{bmatrix} i\omega_n - \frac{(k_z+Q_z/2)^2}{2m} + \delta\mu_\uparrow & \mathrm{e}^{+ik_x Q_\perp \ell_B^2} f_{00}(Q_\perp)\Delta_0 \\ \mathrm{e}^{-ik_x Q_\perp \ell_B^2} f_{00}^*(Q_\perp)\Delta_0 & i\omega_n + \frac{(k_z-Q_z/2)^2}{2m} - \delta\mu_\downarrow \end{bmatrix} \delta_{i\omega_n, i\omega_{n'}} \delta_{k_x,k_x'} \delta_{k_z,k_z'}. \tag{5.4}$$

By integrating out the fermionic fields and taking the limits $\beta, L \to \infty$, the zero-temperature thermodynamic potential is given by

$$\Omega_{\mathrm{MF}} = \frac{\Delta_0^2}{g_{3\mathrm{D}}} - \frac{m\omega_B}{4\pi}\int_{-\infty}^{\infty} dk_z \left[E_{k_z} - \xi_{k_z}\right] + \frac{m\omega_B}{4\pi^2}\sum_{\alpha=\pm}\int_{-\infty}^{\infty} dk_z\, E_{k_z\alpha}\theta\left(-E_{k_z\alpha}\right), \tag{5.5}$$

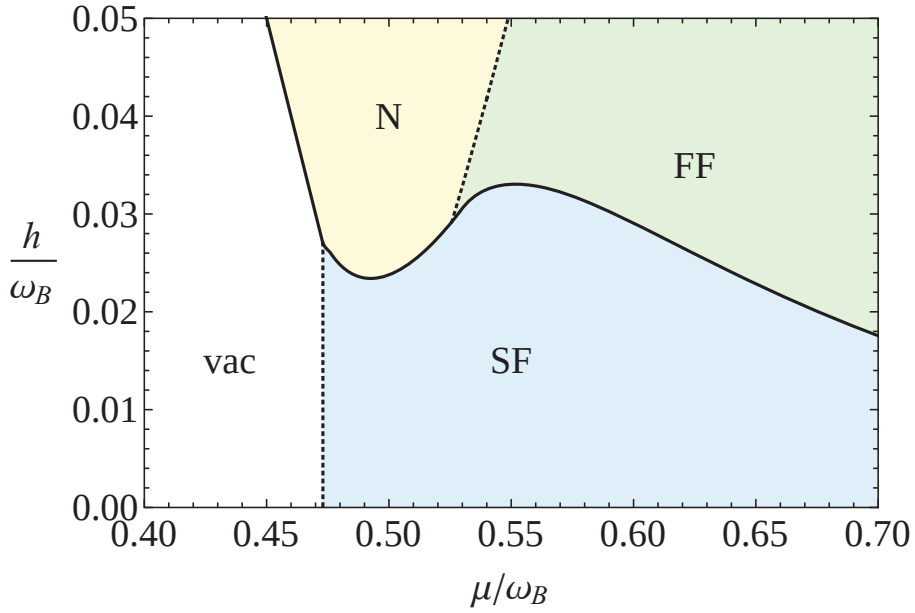

Figure 5.1: Mean-field phase diagram in the plane of the chemical potential $\mu = (\mu_\uparrow + \mu_\downarrow)/2$ and Zeeman field $h = (\mu_\uparrow - \mu_\downarrow)/2$ around $(\mu, h) = (\omega_B/2, 0)$ in units of the cyclotron frequency ω_B for $mg/\ell_B = 3.0$. The quantum phase transitions denoted by the dotted curves are of the second order, whereas that denoted by the solid curve is of the first order.

which has the same form as the thermodynamic potential for an attractive 1D Fermi gas without the magnetic fields in the mean-field approximation. Here, we have defined

$$E_{k_z\pm} = E_{k_z} \pm \left(\delta h - \frac{k_z Q_z}{2m}\right), \tag{5.6a}$$

$$E_{k_z} = \sqrt{\xi_{k_z}^2 + |f_{00}(Q_\perp)\Delta_0|^2}, \tag{5.6b}$$

$$\xi_{k_z} = \frac{k_z^2 + Q_z^2/4}{2m} - \delta\mu \tag{5.6c}$$

with $\delta\mu = (\delta\mu_\uparrow + \delta\mu_\downarrow)/2$ and $\delta h = (\delta\mu_\uparrow - \delta\mu_\downarrow)/2$.

We numerically minimize the thermodynamic potential in Eq. (5.5) to find the pairing gap Δ_0 and momentum $\boldsymbol{Q} = (0, Q_\perp, Q_z)$. In particular, it is minimized at $Q_\perp = 0$ maximizing $|f_{00}(Q_\perp)|$. The obtained phase diagram consists of the fully polarized normal (N), the unpolarized superfluid (SF), and the FF phases as well as the vacuum (vac) and is depicted in Fig. 5.1. We find that the N or FF and SF phases are separated by the first-order quantum phase transition, whereas the N and FF phases are separated by the second-order quantum phase transition. Moreover,

the partially polarized N does not appear because the thermodynamic potential for the FF phase is slightly lower than that for the partially polarized N phase. We note that to determine the phase diagram easily, a large value of $mg/\ell_B = 3.0$ is artificially chosen and the solid curve in Fig. 5.1 is actually the boundary between the N and SF phases, and therefore, the true boundary between the SF and FF phases is slightly lower than the solid curve in Fig. 5.1.

5.1.2 Higher Landau levels

Let us consider that each chemical potential slightly lies off the $(l_\sigma + 1)$-th Landau level, i.e., $\mu_\sigma = \omega_B(l_\sigma + 1/2) + \delta\mu_\sigma$ with $0 < |\delta\mu_\sigma| < \omega_B/2$. Since fermions can move in the direction parallel to the magnetic fields, fermions in Landau levels below the chemical potentials contribute to the pairing. In this case, we can expect different types of FF states, such as the Cooper pairing with nonzero momentum parallel to the magnetic fields, perpendicular to the magnetic fields, and both of them. To determine the phase diagram at weak coupling, we need to include the $l_\uparrow \times l_\downarrow$ combinations of possible pairings when we evaluate the thermodynamic potential.

5.2 Collective excitation spectrum

In the previous section, we showed that when we only consider the lowest Landau level, the thermodynamic potential for a 3D Fermi gas in the magnetic fields corresponds to that for a 1D Fermi gas in their absence at weak coupling. It is an important question whether the long-range order exists in the weak-coupling limit. To answer this question, we now investigate the sound velocity for a 3D Fermi gas in the magnetic fields.

As we saw in Section 3.3.3, the sound velocity for $h = 0$ can be obtained from zeros of the determinant of the inverse fluctuation propagator in the low-energy limit $\omega, \boldsymbol{p} \to 0$ with the analytic continuation $ip_n \to \omega + 0^+$ [104, 108]. The inverse fluctuation propagator $M^{(3D)}$ is a 2×2 matrix and its elements at zero temperature are given as follows:

$$\begin{aligned} M_{11}^{(3D)}(p) &= M_{22}^{(3D)}(p) \\ &= -\frac{m}{4\pi a_{3\mathrm{D}}} - \frac{m\sqrt{m\omega_B}}{4\sqrt{2}}\zeta\left(\frac{1}{2}, \frac{1}{2} - \frac{\mu}{\omega_B}\right) \\ &\quad + \frac{m\omega_B}{4\pi}\int_{-\infty}^{\infty} dk_z \sum_{l=0}^{\infty}\left[\frac{1}{2\xi_{l,k_z}} + \sum_{l'=0}^{\infty}|I_{l,l'}(\boldsymbol{p}_\perp)|^2\right. \\ &\quad \left.\times\left(\frac{u_{l,k_z}^2 u_{l',k_z+p_z}^2}{ip_n - E_{l,k_z} - E_{l',k_z+p_z}} - \frac{v_{l,k_z}^2 v_{l',k_z+p_z}^2}{ip_n + E_{l,k_z} + E_{l',k_z+p_z}}\right)\right], \end{aligned} \tag{5.7a}$$

$$M_{12}^{(3D)}(p) = M_{21}^{(3D)}(p)$$
$$= \frac{m\omega_B}{4\pi}\int_{-\infty}^{\infty}dk_z\sum_{l=0}^{\infty}\sum_{l'=0}^{\infty}|I_{l,l'}(\boldsymbol{p}_\perp)|^2$$
$$\times\left(\frac{u_{l,k_z}v_{l,k_z}u_{l',k_z+p_z}v_{l',k_z+p_z}}{ip_n+E_{l,k_z}+E_{l',k_z+p_z}}-\frac{u_{l,k_z}v_{l,k_z}u_{l',k_z+p_z}v_{l',k_z+p_z}}{ip_n-E_{l,k_z}-E_{l',k_z+p_z}}\right), \quad (5.7b)$$

where we have used shorthand notations $(p)\equiv(ip_n,\boldsymbol{p}_\perp,p_z)$, where $\boldsymbol{p}_\perp$ is the momentum in the direction perpendicular to the magnetic fields, and have defined

$$u_{l,k_z}^2 = 1-v_{l,k_z}^2 = \frac{1}{2}\left(1+\frac{\xi_{l,k_z}}{E_{l,k_z}}\right), \quad (5.8)$$
$$E_{l,k_z} = \sqrt{\xi_{l,k_z}^2+\Delta_0^2}, \quad (5.9)$$
$$\xi_{l,k_z} = \omega_B\left(l+\frac{1}{2}\right)+\frac{k_z^2}{2m}-\mu. \quad (5.10)$$

Expanding the elements $M_{11}^{(3D)}(p)$ and $M_{12}^{(3D)}(p)$ up to the quadratic order in $\omega,\boldsymbol{p}$ yields

$$M_{11}^{(3D)}(p) = a_0+a_1\omega+a_2\omega^2+b_\perp\boldsymbol{p}_\perp^2+b_\parallel p_z^2, \quad (5.11a)$$
$$M_{12}^{(3D)}(p) = a_0+a_2'\omega^2+b_\perp'\boldsymbol{p}_\perp^2+b_\parallel' p_z^2 \quad (5.11b)$$

with

$$a_0 = \frac{m\omega_B}{16\pi^2}\int_{-\infty}^{\infty}dk_z\sum_{l=0}^{\infty}\frac{\Delta_0^2}{E_{l,k_z}^3}, \quad (5.12a)$$
$$a_1 = -\frac{m\omega_B}{16\pi^2}\int_{-\infty}^{\infty}dk_z\sum_{l=0}^{\infty}\frac{\xi_{l,k_z}}{E_{l,k_z}^3}, \quad (5.12b)$$
$$a_2 = -\frac{m\omega_B}{64\pi^2}\int_{-\infty}^{\infty}dk_z\sum_{l=0}^{\infty}\frac{2\xi_{l,k_z}^2+\Delta_0^2}{E_{l,k_z}^5}, \quad (5.12c)$$
$$a_2' = \frac{m\omega_B}{64\pi^2}\int_{-\infty}^{\infty}dk_z\sum_{l=0}^{\infty}\frac{\Delta_0^2}{E_{l,k_z}^5}, \quad (5.12d)$$
$$b_\perp = \frac{1}{8\pi^2}\int_{-\infty}^{\infty}dk_z\sum_{l=0}^{\infty}\left[\left(l+\frac{1}{2}\right)\frac{2\xi_{l,k_z}^2+\Delta_0^2}{2E_{l,k_z}^3}\right.$$
$$\left.-l\frac{u_{l,k_z}^2u_{l-1,k_z}^2+v_{l,k_z}^2v_{l-1,k_z}^2}{E_{l,k_z}+E_{l-1,k_z}}-(l+1)\frac{u_{l,k_z}^2u_{l+1,k_z}^2+v_{l,k_z}^2v_{l+1,k_z}^2}{E_{l,k_z}+E_{l+1,k_z}}\right], \quad (5.12e)$$
$$b_\perp' = -\frac{1}{8\pi^2}\int_{-\infty}^{\infty}dk_z\sum_{l=0}^{\infty}\left[\left(l+\frac{1}{2}\right)\frac{\Delta_0^2}{2E_{l,k_z}^3}\right.$$

$$-2l\frac{u_{l,k_z}v_{l,k_z}u_{l-1,k_z}v_{l-1,k_z}}{E_{l,k_z}+E_{l-1,k_z}}-2(l+1)\frac{u_{l,k_z}v_{l,k_z}u_{l+1,k_z}v_{l+1,k_z}}{E_{l,k_z}+E_{l+1,k_z}}\Bigg], \tag{5.12f}$$

$$b_\parallel=\frac{\omega_B}{128\pi^2}\int_{-\infty}^{\infty}dk_z\sum_{l=0}^{\infty}\left[\frac{\xi_{l,k_z}(2\xi_{l,k_z}^2-\Delta_0^2)}{E_{l,k_z}^5}-\frac{k_z^2}{m}\frac{\Delta_0^2(8\xi_{l,k_z}^2+3\Delta_0^2)}{E_{l,k_z}^7}\right], \tag{5.12g}$$

$$b'_\parallel=\frac{\omega_B}{128\pi^2}\int_{-\infty}^{\infty}dk_z\sum_{l=0}^{\infty}\left[-\frac{3\Delta_0^2}{E_{l,k_z}^5}+\frac{k_z^2}{m}\frac{\Delta_0^2(2\xi_{l,k_z}^2-3\Delta_0^2)}{E_{l,k_z}^7}\right]. \tag{5.12h}$$

By using this expansion, we obtain

$$\begin{aligned}0&=\det M^{(3D)}(p)\\&=M_{11}^{(3D)}(p)M_{11}^{(3D)}(-p)-[M_{12}^{(3D)}(p)]^2\\&\simeq[2a_0(a_2-a_2')-a_1^2]\omega^2+2a_0(b_\perp-b'_\perp)\boldsymbol{p}_\perp^2+2a_0(b_\parallel-b'_\parallel)p_z^2.\end{aligned} \tag{5.13}$$

Therefore, the collective excitation spectrum for $\boldsymbol{p}\to 0$ is found to be

$$\omega=\sqrt{c_\perp^2\boldsymbol{p}_\perp^2+c_\parallel^2p_z^2} \tag{5.14}$$

with

$$c_\perp=\sqrt{\frac{2a_0(b_\perp-b'_\perp)}{2a_0(a_2'-a_2)+a_1^2}}, \tag{5.15a}$$

$$c_\parallel=\sqrt{\frac{2a_0(b_\parallel-b'_\parallel)}{2a_0(a_2'-a_2)+a_1^2}}, \tag{5.15b}$$

where $c_\perp$ and $c_\parallel$ are sound velocities in the direction perpendicular and parallel to the magnetic fields, respectively. From Eqs. (5.12), we obtain

$$a_2'-a_2=\frac{m\omega_B}{32\pi^2}\int_{-\infty}^{\infty}dk_z\sum_{l=0}^{\infty}\frac{1}{E_{l,k_z}^3}, \tag{5.16a}$$

$$\begin{aligned}b_\perp-b'_\perp=\frac{1}{8\pi^2}\int_{-\infty}^{\infty}dk_z\sum_{l=0}^{\infty}\Bigg[&\left(l+\frac{1}{2}\right)\frac{1}{E_{l,k_z}}\\&-l\frac{(u_{l,k_z}u_{l-1,k_z}+v_{l,k_z}v_{l-1,k_z})^2}{E_{l,k_z}+E_{l-1,k_z}}-(l+1)\frac{(u_{l,k_z}u_{l+1,k_z}+v_{l,k_z}v_{l+1,k_z})^2}{E_{l,k_z}+E_{l+1,k_z}}\Bigg],\end{aligned} \tag{5.16b}$$

$$b_\parallel-b'_\parallel=\frac{\omega_B}{64\pi^2}\int_{-\infty}^{\infty}dk_z\sum_{l=0}^{\infty}\left[\frac{\xi_{l,k_z}}{E_{l,k_z}^3}+\frac{k_z^2}{m}\frac{3\Delta_0^2}{E_{l,k_z}^5}\right]. \tag{5.16c}$$

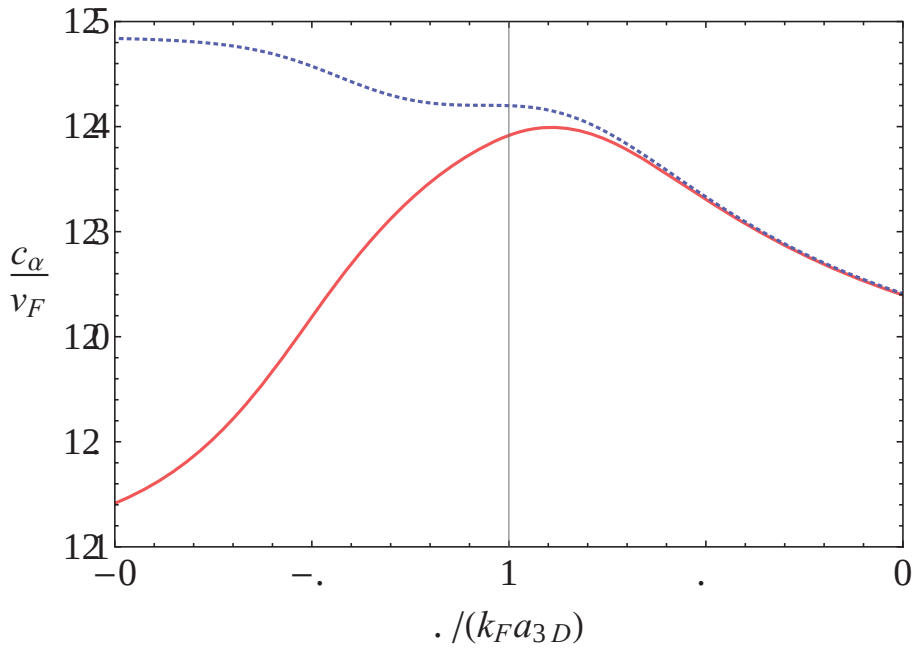

Figure 5.2: Sound velocity c_α/v_F ($\alpha = \perp, \parallel$) scaled with the Fermi velocity $v_F = \sqrt{2\epsilon_F/m}$ as a function of the dimensionless coupling $1/(k_F a_{3D})$ for $\omega_B/\epsilon_F = 1$. The solid (dotted) curve denotes the sound velocity $c_\perp/v_F$ ($c_\parallel/v_F$) in the direction perpendicular (parallel) to the magnetic fields.

To calculate the sound velocities, we use the pairing gap Δ_0 and chemical potential μ obtained by solving the gap and number equations simultaneously:

$$-\frac{m}{4\pi a_{3D}} = \frac{m\sqrt{m\omega_B}}{4\sqrt{2}}\zeta\left(\frac{1}{2}, \frac{1}{2} - \frac{\mu}{\omega_B}\right) + \frac{m\omega_B}{8\pi^2}\int_{-\infty}^{\infty} dk_z \sum_{l=0}^{\infty}\left[\frac{1}{E_{l,k_z}} - \frac{1}{\xi_{l,k_z}}\right], \tag{5.17}$$

$$n = \frac{m\omega_B}{4\pi^2}\int_{-\infty}^{\infty} dk_z \sum_{l=0}^{\infty}\left[1 - \frac{\xi_{l,k_z}}{E_{l,k_z}}\right]. \tag{5.18}$$

The sound velocities $c_\perp$ and $c_\parallel$ in Eqs. (5.15) are plotted in Fig. 5.2. Both $c_\perp$ and $c_\parallel$ are found to be always positive across the BCS-BEC crossover, which indicates that the long-range order exists in the weak-coupling limit. One can see that $c_\perp$ ($c_\parallel$) decreases (increases) with decrease in the dimensionless coupling $1/(k_F a_{3D})$. Therefore, at weak coupling, the magnetic fields effectively make our system one-dimensional, which results from magnetic catalysis. On the other hand, we also find that $c_\perp = c_\parallel$ at strong coupling, which leads to the isotropic collective excitation $\omega = c_\perp|\boldsymbol{p}|$. This is because, in the strong coupling limit, the pairs of fermions with different spin components become tightly bound spin-singlet molecules, for which antiparallel magnetic fields cancel out.

5.3 Summary

In this chapter, we firstly investigated the ground-state phase diagram of a 3D spin-imbalanced Fermi gas in antiparallel magnetic fields. Under the condition that fermions only occupy the lowest Landau level, we found that the phase diagram is composed of the fully polarized N, unpolarized SF, and FF phases as well as the vacuum (see Fig. 5.1). We mentioned that different types of FF states, such as the Cooper pairing with nonzero momentum parallel to the magnetic fields, perpendicular to the magnetic fields, and both of them, are expected when fermions occupy higher Landau levels. Next, we calculated the sound velocities, $c_\perp$ and $c_\parallel$, in the direction perpendicular and parallel to the magnetic fields. Both sound velocities were found to be positive across the BCS-BEC crossover, which indicates that the SF phase is stable in the weak-coupling limit, where our system is effectively described by a 1D spin-imbalanced Fermi gas without the magnetic fields. From the behavior of the sound velocities at weak coupling (see Fig. 5.2), we found that the magnetic fields reduce the 3D dynamics to the 1D dynamics effectively, which results from magnetic catalysis.

Chapter 6

Summary and outlook

We studied the ground-state properties of an attractive Fermi gas subjected to antiparallel magnetic fields in the mean-field approximation to deeply understand how the Cooper pairing and antiparallel magnetic fields compete or cooperate to give rise to interesting physics.

In Chapter 2, we reviewed topics on 2D quantum systems related to our study. Under the ansatz of the FF state, we showed that the ground-state phase diagram of a 2D spin-imbalanced Fermi gas without the magnetic fields consists of polarized normal, unpolarized superfluid, and FF phases (see Fig. 2.1). We also showed that the ground-state phase diagram of the Bose-Hubbard model consists of Mott insulator and superfluid phases (see Fig. 2.2). By introducing free and interacting Dirac fermions subjected to a magnetic field in $(2 + 1)$ D, a magnetic field was found to play an important role in generating the condensation and dynamical fermion mass, which results from magnetic catalysis.

In Chapter 3, we investigated a 2D spin-balanced Fermi gas in antiparallel magnetic fields. By employing the mean-field approximation, the ground-state phase diagram was found to consist of quantum spin Hall insulator and superfluid phases and to closely resemble that of the Bose-Hubbard model (see Fig.3.1). When the chemical potential does not match any Landau levels, we found that the antiparallel magnetic fields compete with the Cooper pairing, i.e., a superfluid phase changes into a quantum spin Hall phase by decreasing the attractive interaction. We showed that two phases are separated by a second-order quantum phase transition classified into the universality class of either the dilute Bose gas or XY model. On the other hand, when the chemical potential matches some Landau level, we found that the antiparallel magnetic fields cooperate with the Cooper pairing i.e., our system is a superfluid down to the weak-coupling limit. We showed that the pairing gap and the condensate density are enhanced by antiparallel magnetic fields as a consequence of magnetic catalysis, although the sound velocity and superfluid density are suppressed by antiparallel magnetic fields.

In Chapter 4, we investigated a 2D spin-imbalanced Fermi gas in antiparallel magnetic fields. By calculating the thermodynamic potential for FF and LO states, we found that the FF state is energetically favored over the LO state in the weak-coupling limit. We showed that the ground-state phase diagrams at weak coupling (see Fig. 4.2) and beyond it (see Fig. 4.3) consist of quantum Hall insulator, unpolarized superfluid, and FF phases. They are separated by various first-order and second-order quantum phase transitions. When the chemical potential for each spin component matches some Landau level, we found that the FF phases appear in the weak-coupling limit. We also clarified that the FF phases occupy the reasonable portions of the phase diagram.

In Chapter 5, we investigated a 3D spin-imbalanced Fermi gas in antiparallel magnetic fields under the ansatz of the FF state. When fermions only occupy the lowest Landau level, we showed that the thermodynamic potential for a 3D spin-imbalanced Fermi gas in the magnetic fields has the same form as that for a 1D Fermi gas without the magnetic fields, and the ground-state phase diagram consists of polarized normal, unpolarized superfluid, and FF phases at weak coupling (see Fig. 5.1). We calculated the collective excitation spectrum and showed that both sound velocities in the direction perpendicular and parallel to the magnetic fields are always positive across the BCS-BEC crossover, so that the long-range order exists in the weak-coupling limit, where our system is effectively described by a 1D spin-imbalanced Fermi gas without the magnetic fields.

As for future works, it is an interesting problem to determine the ground-state phase diagram of a 3D spin-imbalanced Fermi gas in antiparallel magnetic fields at weak coupling under the condition that fermions occupy higher Landau levels. As mentioned in Section 5.1.2, we then need to consider the $l_\uparrow \times l_\downarrow$ combinations of possible pairings when each chemical potential slightly lies off the $(l_\sigma+1)$-th Landau level, i.e., $\mu_\sigma = \omega_B(l_\sigma+1/2)+\delta\mu_\sigma$ with $0 < |\delta\mu_\sigma| < \omega_B/2$. In this case, we can expect different types of FF states, such as the Cooper pairing with nonzero momentum parallel to the magnetic fields, perpendicular to the magnetic fields, and both of them. To elucidate how much area in the ground-state phase diagram is occupied by the FF states is also of interest.

In the 3D spin-imbalanced case, we assumed the FF state to make theoretical treatment easier. In the 2D spin-imbalanced case, we determined the ground-state phase diagram with particular attention on the FF and LO states. In general, we can write the order parameter as $\Delta(\boldsymbol{x}) = \sum_{\boldsymbol{Q}} \Delta_{\boldsymbol{Q}} \mathrm{e}^{i\boldsymbol{Q}\cdot\boldsymbol{x}}$, which is referred to as the FFLO state [42]. It is also a future work to investigate which of possible FFLO states are favored in the ground-state phase diagram.

When we extend our study to finite temperature case, fluctuations beyond the mean-field approximation need to be taken into consideration. For example, the effect of antiparallel magnetic fields on the critical superfluid temperature was discussed by including fluctuations in Ref. [72]. It is an important problem to elucidate

whether antiparallel magnetic fields increase or decrease the critical BKT transition temperature compared to that without the magnetic fields.

In this thesis, we elucidated the various ground-state properties of an attractive Fermi gas in antiparallel magnetic fields. For example, the FF phases were found to occupy the reasonable portions of the phase diagram of a 2D spin-imbalanced Fermi gas. For trapped systems, the chemical potential μ is replaced by $\mu(\boldsymbol{x}) = \mu_0 - U(\boldsymbol{x})$ within the local-density approximation, whereas the Zeeman field h remains constant [1]. By realizing a sufficiently large μ_0 with $|h| \simeq \mathbb{N}_+\omega_B/2$, a series of FF phases separated by quantum Hall insulators may appear along the path from the trap center $\mu(\boldsymbol{0}) = \mu_0$ towards the edge $\mu(|\boldsymbol{x}| \to \infty) \to -\infty$. We expect that our studies will stimulate the further development of FFLO physics with ultracold atoms.

So far, the interaction and dimensionality can be arbitrarily tuned, which leads to the observation of the quasi-condensation of Cooper pairs in 2D [28]. On the other hand, the antiparallel magnetic fields may be implemented for a two-component Fermi gas according to the proposal in Ref. [56]. Therefore, by combining experimental techniques to control the interaction, dimensionality, and magnetic fields, an attractively interacting Fermi gas in antiparallel magnetic fields may, in principle, be realized in ultracold atom experiments. To observe a pairing gap in antiparallel magnetic fields, the thermal energy scale k_BT, cyclotron frequency ω_B, and pairing gap Δ_0 must satisfy $k_BT < \hbar\omega_B, \Delta_0$. According to Ref. [56], the cyclotron frequency is $\omega_B \simeq 2\pi \times 200\,\mathrm{Hz}$ for realistic system sizes of $10\,\mu\mathrm{m}$. For $\epsilon_b/\epsilon_F = 0.4$ and $\epsilon_F/\hbar\omega_B = 0.5$, a pairing gap is given by $\Delta_0 \simeq \hbar\omega_B/2$ (see Fig. 3.2), and therefore, we obtain $T < 5\,\mathrm{nK}$. Since the lowest accessible temperature in Ref. [28] is $64\,\mathrm{nK}$, the observation of a pairing gap requires to decrease the temperature or increase the cyclotron frequency and number density.

As mentioned in the Introduction, our system may be viewed as a simulator of analogous phenomena in other fields of physics, such as exciton condensation and chiral condensation in a magnetic field [62, 63, 64]. For example, when the long-range Coulomb attraction between an electron and a hole is screened, the Coulomb attraction can be approximately considered as the contact interaction [115, 116]. Therefore, we can predict from our studies that a pairing gap for an exciton is enhanced by a magnetic field. We expect that our studies will provide important insights into these analogous systems.

Appendix A

Matsubara summation

In this appendix, we perform the Matsubara summation in two cases.

A.1 Mean-field thermodynamic potential

As the first case, we calculate the mean-field thermodynamic potential (3.13). To this end, we need to evaluate the following Matsubara summation:

$$\sum_{i\omega_n} \ln\det G_0^{-1}(k) \tag{A.1}$$

with the inverse mean-field Green function $G_0^{-1}(k)$ given in Eq. (3.14). Now, we introduce convergence factors because the summation is formally divergent. We rewrite Eq. (A.1) as

$$\sum_{i\omega_n} \ln\det G_0^{-1} = \sum_{i\omega_n} \left[\ln(G_0^{-1})_{11} + \ln(G_0^{-1})_{22} + \ln\left(1 - \frac{[(G_0^{-1})_{12}]^2}{(G_0^{-1})_{11}(G_0^{-1})_{22}}\right)\right]. \tag{A.2}$$

According to Ref. [109], convergence factors arise from the equal-time limit of $(G_0)_{11}(\tau) = -\langle \mathrm{T} c_\uparrow(\tau) c_\uparrow^\dagger(0)\rangle$ and $(G_0)_{22}(\tau) = -\langle \mathrm{T} c_\downarrow^\dagger(\tau) c_\downarrow(0)\rangle$, which leads to number densities for each spin components, $n_\uparrow = (G_0)_{11}(\tau \to 0^-)$ and $n_\downarrow = -(G_0)_{22}(\tau \to 0^+)$. Therefore, the first and second term on the right-hand side of Eq. (A.2) are multiplied by $\mathrm{e}^{i\omega_n 0^+}$ and $\mathrm{e}^{-i\omega_n 0^+}$, respectively, while the third term does not need the convergence

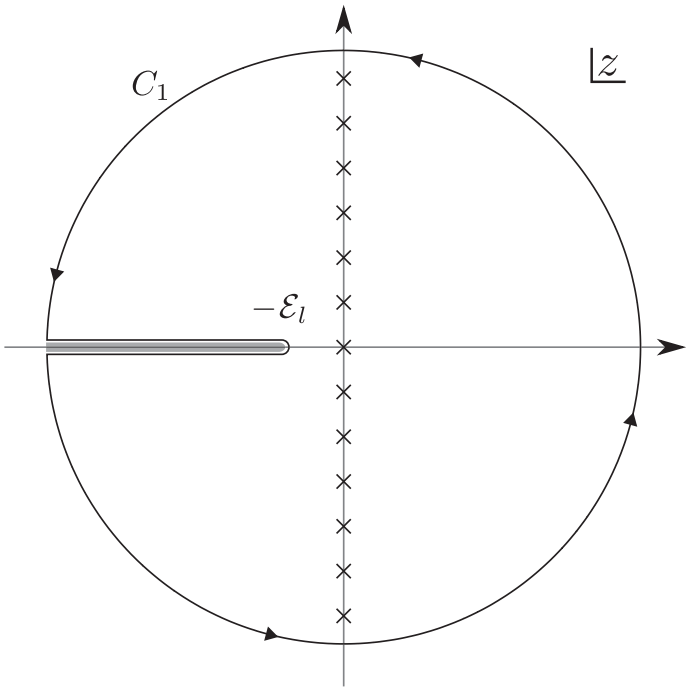

Figure A.1: The integration contour C_1 with a branch cut $\Re z \leq -\mathcal{E}_l$. The Fermi distribution function $n_{\rm F}(z)$ has single poles at $z = i\omega_n$.

factor. Using $(G_0)_{22}(-\omega_n) = -(G_0)_{11}(+\omega_n)$, we can obtain

$$\begin{aligned}\sum_{i\omega_n} \ln\det G_0^{-1} &= \sum_{i\omega_n}\left[2\ln(G_0^{-1})_{11}\mathrm{e}^{i\omega_n 0^+} + \ln\left(1 - \frac{[(G_0^{-1})_{12}]^2}{(G_0^{-1})_{11}(G_0^{-1})_{22}}\right)\right] \\ &= \sum_{i\omega_n}\left[\ln(G_0^{-1})_{11} - \ln(G_0^{-1})_{22} + \ln\det G_0^{-1}\right]\mathrm{e}^{i\omega_n 0^+} \\ &= \sum_{i\omega_n}\left[\ln(i\omega_n - \xi_l) - \ln(i\omega_n + \xi_l) + \ln(i\omega_n - E_l)(i\omega_n + E_l)\right]\mathrm{e}^{i\omega_n 0^+}.\end{aligned} \tag{A.3}$$

We notice that all terms in Eq. (A.3) have the same forms as

$$\sum_{i\omega_n} \ln(i\omega_n + \mathcal{E}_l)\mathrm{e}^{i\omega_n 0^+} \tag{A.4}$$

with $\mathcal{E}_l = \pm\xi_l, \pm E_l$. This summation can be evaluated as a contour integral in the complex plane [102]:

$$\sum_{i\omega_n} \ln(i\omega_n + \mathcal{E}_l)\mathrm{e}^{i\omega_n 0^+} = -\frac{\beta}{2\pi i}\oint_{C_1} dz\, n_{\rm F}(z)\ln(z + \mathcal{E}_l)\mathrm{e}^{z0^+}, \tag{A.5}$$

where the integration contour C_1 is given in Fig. A.1. The Fermi distribution function $n_{\rm F}(z) = 1/(\mathrm{e}^{\beta z}+1)$ ensures convergence for $z \to +\infty$, while the convergence factor e^{z0^+} ensures that for $z \to -\infty$. Therefore, the integral along the perimeter vanishes and we obtain

$$\sum_{i\omega_n} \ln(i\omega_n + \mathcal{E}_l)\mathrm{e}^{i\omega_n 0^+} = -\frac{\beta}{2\pi i}\int_{-\infty}^{\infty} d\omega\, n_{\rm F}(\omega)\left[\ln(\omega+\mathcal{E}_l+i\eta) - \ln(\omega+\mathcal{E}_l-i\eta)\right] \tag{A.6}$$

with a positive infinitesimal η. Here, we have used the fact that the Fermi function $n_{\rm F}(z)$ is continuous across a branch cut $\omega \leq -\mathcal{E}_l$ and the integrand is zero for $\omega > -\mathcal{E}_l$ with $\eta \to 0$. By integrating out by part and using the Dirac identity

$$\lim_{\eta\to 0^+}\frac{1}{z \pm i\eta} = \mp i\pi\delta(z) + \mathcal{P}\frac{1}{z}, \tag{A.7}$$

where $\mathcal{P}(1/z)$ denotes the principal part of $1/z$, we obtain

$$\begin{aligned}\sum_{i\omega_n} \ln(i\omega_n + \mathcal{E}_l)\mathrm{e}^{i\omega_n 0^+} &= -\frac{1}{2\pi i}\int_{-\infty}^{\infty} d\omega\, \ln(1+\mathrm{e}^{-\beta\omega})\left[\frac{1}{\omega+\mathcal{E}_l+i\eta} - \frac{1}{\omega+\mathcal{E}_l-i\eta}\right] \\ &= \int_{-\infty}^{\infty} d\omega\, \ln(1+\mathrm{e}^{-\beta\omega})\delta(\omega+\mathcal{E}_l) \\ &= \ln(1+\mathrm{e}^{\beta\mathcal{E}_l}),\end{aligned} \tag{A.8}$$

which leads to

$$\begin{aligned}\sum_{i\omega_n} \ln\det G_0^{-1}(k) &= \ln(1+\mathrm{e}^{-\beta\xi_l}) - \ln(1+\mathrm{e}^{+\beta\xi_l}) + \ln(1+\mathrm{e}^{-\beta E_l}) + \ln(1+\mathrm{e}^{+\beta E_l}) \\ &= \beta(E_l-\xi_l) + 2\ln(1+\mathrm{e}^{-\beta E_l}).\end{aligned} \tag{A.9}$$

Therefore, the mean-field thermodynamic potential (3.13) becomes

$$\begin{aligned}\Omega_{\rm MF} &= \frac{\Delta_0^2}{g} - \frac{1}{L^2}\sum_{k_x}\sum_{l=0}^{\infty}(E_l-\xi_l)\theta(\Lambda-\epsilon_l) - \frac{2}{\beta L^2}\sum_{k_x}\sum_{l=0}^{\infty}\ln(1+\mathrm{e}^{-\beta E_l}) \\ &= \frac{\Delta_0^2}{g} - \frac{m\omega_B}{2\pi}\sum_{l=0}^{\infty}(E_l-\xi_l)\theta(\Lambda-\epsilon_l) - \frac{m\omega_B}{\pi\beta}\sum_{l=0}^{\infty}\ln(1+\mathrm{e}^{-\beta E_l}),\end{aligned} \tag{A.10}$$

where we have used $\sum_{k_x} 1 = m\omega_B L^2/(2\pi)$ corresponding to the density of state per Landau level. Finally, by taking the limits $\beta, L \to \infty$, we obtain Eq. (3.15).

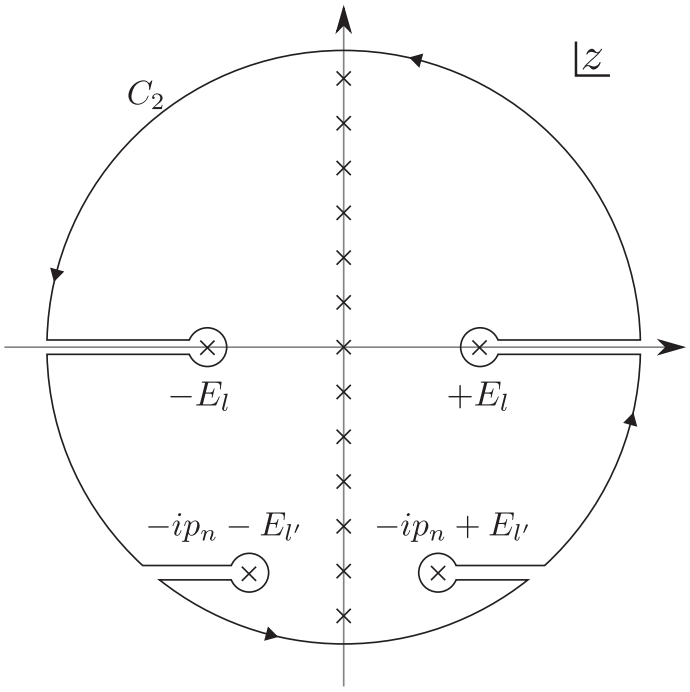

Figure A.2: The integration contour C_2. The Fermi distribution function $n_{\mathrm{F}}(z)$ has single poles at $z = i\omega_n$ and the function $h_{1,2}(z)$ has simple poles at $z = \pm E_l, -ip_n \pm E_{l'}$.

A.2 Inverse fluctuation propagator

Next, we calculate the following Matsubara summations:

$$\frac{1}{\beta}\sum_{i\omega_n} h_{1,2}(i\omega_n) \tag{A.11}$$

with

$$h_1(z) = \frac{(z-\xi_l)(z+ip_n+\xi_{l'})}{(z-E_l)(z+E_l)(z+ip_n-E_{l'})(z+ip_n+E_{l'})}, \tag{A.12}$$

$$h_2(z) = \frac{\Delta_0^2}{(z-E_l)(z+E_l)(z+ip_n-E_{l'})(z+ip_n+E_{l'})}, \tag{A.13}$$

which appear in the calculation of the inverse fluctuation propagator. We replace this summation as a contour integral with the integration contour C_2 (see Fig. A.2) in the complex plane:

$$\frac{1}{\beta}\sum_{i\omega_n} h_{1,2}(i\omega_n) = -\frac{1}{2\pi i}\oint_{C_2} dz\, n_{\mathrm{F}}(z) h_{1,2}(z). \tag{A.14}$$

Unlike the previous section, we do not need to introduce convergence factors because $h_1 \simeq z^{-2}$ and $h_2(z) \simeq z^{-4}$ ensure that the summation is convergent for $|z| \to \infty$. The function $h_{1,2}(z)$ has simple poles at $z = \pm E_l, -ip_n \pm E_{l'}$, and therefore, the residue theorem yields

$$\begin{aligned}\frac{1}{\beta}\sum_{i\omega_n} h_1(i\omega_n) = &\left(\frac{u_l^2 u_{l'}^2}{ip_n - E_l - E_{l'}} - \frac{v_l^2 v_{l'}^2}{ip_n + E_l + E_{l'}}\right)(1 - n_{\rm F}(E_l) - n_{\rm F}(E_{l'})) \\ &+ \left(\frac{v_l^2 u_{l'}^2}{ip_n + E_l - E_{l'}} - \frac{u_l^2 v_{l'}^2}{ip_n - E_l + E_{l'}}\right)(n_{\rm F}(E_l) - n_{\rm F}(E_{l'})), \quad \text{(A.15)} \\ \frac{1}{\beta}\sum_{i\omega_n} h_2(i\omega_n) = &\left(\frac{u_l v_l u_{l'} v_{l'}}{ip_n + E_l + E_{l'}} - \frac{u_l v_l u_{l'} v_{l'}}{ip_n - E_l - E_{l'}}\right)(1 - n_{\rm F}(E_l) - n_{\rm F}(E_{l'})) \\ &+ \left(\frac{u_l v_l u_{l'} v_{l'}}{ip_n + E_l - E_{l'}} - \frac{u_l v_l u_{l'} v_{l'}}{ip_n - E_l + E_{l'}}\right)(n_{\rm F}(E_l) - n_{\rm F}(E_{l'})) \quad \text{(A.16)}\end{aligned}$$

with $n_{\rm F}(-ip_n \pm E_{l'}) = n_{\rm F}(\pm E_{l'})$. Here, we have defined the functions u_l, v_l as

$$u_l^2 = 1 - v_l^2 \equiv \frac{1}{2}\left(1 + \frac{\xi_l}{E_l}\right). \quad \text{(A.17)}$$

Appendix B

Effective action in the Gaussian approximation

In this appendix, we calculate the effective action in the Gaussian approximation and derive the inverse fluctuation propagator $M(p)$. To this end, we introduce quantum fluctuations $\eta(x)$ of the pair field $\Delta(x)$. Setting $\Delta(x) = \Delta_0 + \eta(x)$ yields $\widetilde{\Delta}(k,k') = \Delta_0\delta_{k,k'} + \overline{\eta}(k,k')$ with $\overline{\eta}(k,k') \equiv \int dx\, \chi_k^*(x)\eta(x)\chi_{k'}(x)$ and $G^{-1}(k,k') = G_0^{-1}(k)\delta_{k,k'} + K(k,k')$ with

$$K(k,k') = \begin{bmatrix} 0 & \overline{\eta}(k,k') \\ \overline{\eta}^*(k',k) & 0 \end{bmatrix}. \tag{B.1}$$

We expand the effective action S_{eff} in Eq. (3.11) up to the quadratic order in $\eta(x)$ assumed to be small and smooth, which leads to

$$\begin{aligned}
S_{\text{eff}} &= \int dx\, \frac{|\Delta(x)|^2}{g} - \sum_k \ln\det G_0^{-1}(k) - \mathrm{Tr}\ln[\delta_{k,k'} + G_0(k)K(k,k')] \\
&= \int dx\, \frac{|\Delta(x)|^2}{g} - \sum_k \ln\det G_0^{-1}(k) - \sum_{n=1}^{\infty} \frac{(-1)^{n-1}}{n} \mathrm{Tr}[\{G_0(k)K(k,k')\}^n] \\
&\simeq \beta L^2 \frac{\Delta_0^2}{g} - \sum_k \ln\det G_0^{-1}(k) \\
&\quad + \beta L^2 \frac{\Delta_0}{g}(\widetilde{\eta}(0) + \widetilde{\eta}^*(0)) - \sum_k \mathrm{tr}[G_0(k)K(k,k)] \\
&\quad + \beta L^2 \sum_p \frac{|\widetilde{\eta}(p)|^2}{g} + \frac{1}{2}\sum_k \sum_{k'} \mathrm{tr}[G_0(k)K(k,k')G_0(k')K(k',k)] \\
&\equiv S_{\text{MF}} + S_{\text{G}},
\end{aligned} \tag{B.2}$$

where we have performed the Fourier transformation,

$$\eta(x) = \sum_p \mathrm{e}^{-ip_n\tau + \boldsymbol{p}\cdot\boldsymbol{x}}\widetilde{\eta}(p), \tag{B.3}$$

and have used shorthand notations $(p) \equiv (ip_n, \boldsymbol{p})$, $\sum_p \equiv \sum_{ip_n}\sum_{\boldsymbol{p}}$, where $p_n = 2\pi n/\beta$ ($n \in \mathbb{Z}$) is the bosonic Matsubara frequency. The mean-field action S_{MF} and the Gaussian part S_{G} of the effective action is found to be

$$S_{\mathrm{MF}} = \beta L^2 \frac{\Delta_0^2}{g} - \sum_k \ln\det G_0^{-1}(k) = \beta\Omega_{\mathrm{MF}}, \tag{B.4}$$

$$\begin{aligned} S_{\mathrm{G}} &= \beta L^2 \sum_p \frac{|\widetilde{\eta}(p)|^2}{g} + \frac{1}{2}\sum_k\sum_{k'} \mathrm{tr}[G_0(k)K(k,k')G_0(k')K(k',k)] \\ &= \beta L^2 \sum_p \frac{|\overline{\eta}(p)|^2}{g} + \sum_k\sum_{k'}\Bigg[(G_0)_{11}(k')\overline{\eta}(k',k)(G_0)_{22}(k)\overline{\eta}^*(k',k) \\ &\qquad + \frac{1}{2}\{(G_0)_{12}(k')\overline{\eta}(k',k)(G_0)_{12}(k)\overline{\eta}(k,k') + c.c.\}\Bigg]. \end{aligned} \tag{B.5}$$

The mean-field Green's function $G_0(k)$ is given by

$$G_0(k) = \begin{bmatrix} (G_0)_{11}(k) & (G_0)_{12}(k) \\ (G_0)_{21}(k) & (G_0)_{22}(k) \end{bmatrix} = \frac{1}{(i\omega_n - E_l)(i\omega_n + E_l)} \begin{bmatrix} i\omega_n + \xi_l & -\Delta_0 \\ -\Delta_0 & i\omega_n - \xi_l \end{bmatrix}. \tag{B.6}$$

Before we calculate S_{G}, we show that the first-order term for $\overline{\eta}$ in Eq. (B.2) vanishes. By using $\overline{\eta}(k,k) = L\widetilde{\eta}(0)[F_l(-k_x\ell_B^2)]^2$, we obtain

$$\begin{aligned} &\frac{\Delta_0}{g}(\widetilde{\eta}(0) + \widetilde{\eta}^*(0)) - \frac{1}{\beta L^2}\sum_k \mathrm{tr}\,[G_0(k)K(k,k)] \\ &= (\widetilde{\eta}(0) + \widetilde{\eta}^*(0))\left[\frac{\Delta_0}{g} - \frac{1}{\beta L}\sum_k (G_0)_{12}(k)[F_l(-k_x\ell_B^2)]^2\right] \\ &= (\widetilde{\eta}(0) + \widetilde{\eta}^*(0))\left[\frac{\Delta_0}{g} - \frac{m\omega_B}{2\pi}\sum_{l=0}^{\infty}\frac{1}{\beta}\sum_{i\omega_n}(G_0)_{12}(k)\int dk_x\,[F_l(k_x)]^2\right] \\ &= \frac{m\Delta_0}{4\pi}(\widetilde{\eta}(0) + \widetilde{\eta}^*(0))\left[\ln\left(\frac{2\omega_B}{\epsilon_b}\right) + \psi\left(\frac{1}{2} - \frac{\mu}{\omega_B}\right) - \sum_{l=0}^{\infty}\left(\frac{\omega_B}{E_l}\tanh\left(\frac{\beta E_l}{2}\right) - \frac{\omega_B}{\xi_l}\right)\right] \\ &= 0, \end{aligned} \tag{B.7}$$

where we use the gap equation at finite temperature:

$$\ln\left(\frac{2\omega_B}{\epsilon_b}\right)+\psi\left(\frac{1}{2}-\frac{\mu}{\omega_B}\right)-\omega_B\sum_{l=0}^{\infty}\left(\frac{1}{E_l}\tanh\left(\frac{\beta E_l}{2}\right)-\frac{1}{\xi_l}\right)=0. \tag{B.8}$$

B.1 Gaussian part of the effective action

Firstly, we calculate the element $M_{11}(p)$ of the inverse fluctuation propagator defined as

$$\sum_p M_{11}(p)|\widetilde{\eta}(p)|^2\equiv\sum_p\frac{|\widetilde{\eta}(p)|^2}{g}+\frac{1}{\beta L^2}\sum_k\sum_{k'}(G_0)_{11}(k')\overline{\eta}(k',k)(G_0)_{22}(k)\overline{\eta}^*(k',k). \tag{B.9}$$

By performing the Fourier transformation on $\eta(x)$, the function $\overline{\eta}(k',k)\overline{\eta}^*(k',k)$ becomes

$$\begin{aligned}
&\overline{\eta}(k',k)\overline{\eta}^*(k',k)\\
&\quad=\sum_p\sum_{p'}\widetilde{\eta}(p)\widetilde{\eta}^*(p')\int dx\int dx'\,\mathrm{e}^{-ip_n\tau+ip_{n'}\tau'+i\boldsymbol{p}\cdot\boldsymbol{x}-i\boldsymbol{p}'\cdot\boldsymbol{x}'}\chi^*_{k'}(x)\chi_k(x)\chi^*_k(x')\chi_{k'}(x')\\
&\quad=\sum_p\sum_{p_y}\widetilde{\eta}(p)\widetilde{\eta}^*(ip_n,p_x,p'_y)\delta_{i\omega_{n'},i\omega_n+ip_n}\delta_{k'_x,k_x+p_x}\int dy\int dy'\,\mathrm{e}^{ip_yy-ip'_yy'}\\
&\qquad\times F_l(y-k_x\ell_B^2)F_{l'}(y-(k_x+p_x)\ell_B^2)F_l(y'-k_x\ell_B^2)F_{l'}(y'-(k_x+p_x)\ell_B^2).
\end{aligned} \tag{B.10}$$

Because our system is translationally invariant in the x direction, we obtain

$$\begin{aligned}
&\sum_{k_x}\sum_{k'_x}\overline{\eta}(k',k)\overline{\eta}^*(k',k)\\
&\quad=\sum_p\sum_{p_y}\widetilde{\eta}(p)\widetilde{\eta}^*(ip_n,p_x,p'_y)\delta_{i\omega_{n'},i\omega_n+ip_n}\sum_{k_x}\int dy\int dy'\,\mathrm{e}^{ip_yy-ip'_yy'}\\
&\qquad\times F_l(y-y'-k_x\ell_B^2)F_{l'}(y-y'-(k_x+p_x)\ell_B^2)F_l(-k_x\ell_B^2)F_{l'}(-(k_x+p_x)\ell_B^2)\\
&\quad=\sum_p\sum_{p_y}\widetilde{\eta}(p)\widetilde{\eta}^*(ip_n,p_x,p'_y)\delta_{i\omega_{n'},i\omega_n+ip_n}\sum_{k_x}\int dy\int dy'\,\mathrm{e}^{i(p_y-p'_y)y'+i(p_y+p'_y)y/2}\\
&\qquad\times F_l(y-k_x\ell_B^2)F_{l'}(y-(k_x+p_x)\ell_B^2)F_l(-k_x\ell_B^2)F_{l'}(-(k_x+p_x)\ell_B^2)\\
&\quad=L^2\sum_p|\widetilde{\eta}(p)|^2\delta_{i\omega_{n'},i\omega_n+ip_n}\int\frac{dk_x}{2\pi}\int dy\,\mathrm{e}^{ip_yy}\\
&\qquad\times F_l(y-k_x\ell_B^2)F_{l'}(y-(k_x+p_x)\ell_B^2)F_l(-k_x\ell_B^2)F_{l'}(-(k_x+p_x)\ell_B^2)
\end{aligned}$$

$$= L^2 \frac{m\omega_B}{2\pi} \sum_p |\widetilde{\eta}(p)|^2 \left| \int dy\, \mathrm{e}^{ip_y y} F_l(y) F_{l'}(y - p_x \ell_B^2) \right|^2 \delta_{i\omega_{n'}, i\omega_n + ip_n}$$
$$\equiv L^2 \frac{m\omega_B}{2\pi} \sum_p |\widetilde{\eta}(p)|^2 |I_{l,l'}(\boldsymbol{p})|^2 \delta_{i\omega_{n'}, i\omega_n + ip_n}. \tag{B.11}$$

The overlap $|I_{l,l'}(\boldsymbol{p})|$ was provided in Ref. [72] and, in the next section, we show

$$|I_{l,l'}(\boldsymbol{p})| = \sqrt{\frac{l'!}{l!}} \mathrm{e}^{-|\boldsymbol{p}|^2 \ell_B^2/4} \left(\frac{|\boldsymbol{p}|\ell_B}{\sqrt{2}} \right)^{l-l'} L_{l'}^{l-l'} \left(\frac{\boldsymbol{p}^2 \ell_B^2}{2} \right) \tag{B.12}$$

with the understanding of the following relation [101]:

$$L_l^{l'-l}(z) = \frac{l'!}{l!} (-z)^{l-l'} L_{l'}^{l-l'}(z) \tag{B.13}$$

with the associated Laguerre polynomial $L_n^m(z)$. Performing the fermionic Matsubara summation [see Eq. (A.15)] yields

$$\begin{aligned}
&\frac{1}{\beta L^2} \sum_k \sum_{k'} (G_0)_{11}(k') \overline{\eta}(k', k) (G_0)_{22}(k) \overline{\eta}^*(k', k) \\
&\quad = \frac{m\omega_B}{2\pi} \sum_p |\widetilde{\eta}(p)|^2 \sum_{l=0}^{\infty} \sum_{l'=0}^{\infty} |I_{l,l'}(\boldsymbol{p})|^2 \\
&\qquad \times \frac{1}{\beta} \sum_{i\omega_n} \frac{(i\omega_n + ip_n + \xi_{l'})(i\omega_n - \xi_l)}{(i\omega_n - E_l)(i\omega_n + E_l)(i\omega_n + ip_n - E_{l'})(i\omega_n + ip_n + E_{l'})} \\
&\quad = \frac{m\omega_B}{2\pi} \sum_p |\widetilde{\eta}(p)|^2 \sum_{l=0}^{\infty} \sum_{l'=0}^{\infty} |I_{l,l'}(\boldsymbol{p})|^2 \\
&\qquad \times \left[\left(\frac{u_l^2 u_{l'}^2}{ip_n - E_l - E_{l'}} - \frac{v_l^2 v_{l'}^2}{ip_n + E_l + E_{l'}} \right) (1 - n_{\mathrm{F}}(E_l) - n_{\mathrm{F}}(E_{l'})) \right. \\
&\qquad\quad \left. + \left(\frac{v_l^2 u_{l'}^2}{ip_n + E_l - E_{l'}} - \frac{u_l^2 v_{l'}^2}{ip_n - E_l + E_{l'}} \right) (n_{\mathrm{F}}(E_l) - n_{\mathrm{F}}(E_{l'})) \right] \theta(\Lambda - \epsilon_l),
\end{aligned} \tag{B.14}$$

where an energy cutoff Λ is introduced because the term at $l' = l$ is logarithmically divergent. Therefore, the element $M_{11}(p)$ reads

$$\begin{aligned}
M_{11}(p) = &\frac{m}{4\pi} \left[\log \left(\frac{2\omega_B}{\epsilon_b} \right) + \psi \left(\frac{1}{2} - \frac{\mu}{\omega_B} \right) \right] \\
&+ \frac{m\omega_B}{2\pi} \sum_{l=0}^{\infty} \left[\sum_{l'=0}^{\infty} |I_{l,l'}(\boldsymbol{p})|^2 \right.
\end{aligned}$$

$$\times \left\{ \left(\frac{u_l^2 u_{l'}^2}{ip_n - E_l - E_{l'}} - \frac{v_l^2 v_{l'}^2}{ip_n + E_l + E_{l'}} \right) (1 - n_{\rm F}(E_l) - n_{\rm F}(E_{l'})) \right.$$
$$\left. + \left(\frac{v_l^2 u_{l'}^2}{ip_n + E_l - E_{l'}} - \frac{u_l^2 v_{l'}^2}{ip_n - E_l + E_{l'}} \right) (n_{\rm F}(E_l) - n_{\rm F}(E_{l'})) \right\} + \frac{1}{2\xi_l} \Bigg] \tag{B.15}$$

with the renormalization procedure used to evaluate the mean-field thermodynamic potential (3.15).

Next, we calculate the element $M_{12}(p)$ defined as

$$\sum_p M_{12}(p)\widetilde{\eta}(p)\widetilde{\eta}(-p) \equiv \frac{1}{\beta L^2} \sum_k \sum_{k'} (G_0)_{12}(k)\overline{\eta}(k,k')(G_0)_{12}(k')\overline{\eta}(k',k). \tag{B.16}$$

As with the calculation of the element $M_{11}(p)$, the function $\sum_{k_x} \sum_{k'_x} \overline{\eta}(k',k)\overline{\eta}(k,k')$ is given by

$$\sum_{k_x} \sum_{k'_x} \widetilde{\eta}(k',k)\widetilde{\eta}(k,k') = L^2 \frac{m\omega_B}{2\pi} \sum_p \widetilde{\eta}(p)\widetilde{\eta}(-p)|I_{l,l'}(\boldsymbol{p})|^2 \delta_{i\omega_{n'}, i\omega_n + ip_n}, \tag{B.17}$$

which leads to

$$\begin{aligned} M_{12}(p) &= \frac{m\omega_B}{2\pi} \sum_{l=0}^{\infty} \sum_{l'=0}^{\infty} |I_{l,l'}(\boldsymbol{p})|^2 \\ &\quad \times \frac{1}{\beta} \sum_{i\omega_n} \frac{\Delta_0^2}{(i\omega_n - E_l)(i\omega_n + E_l)(i\omega_n + ip_n - E_{l'})(i\omega_n + ip_n + E_{l'})} \\ &= \frac{m\omega_B}{2\pi} \sum_{l=0}^{\infty} \sum_{l'=0}^{\infty} |I_{l,l'}(\boldsymbol{p})|^2 \\ &\quad \times \left[\left(\frac{u_l v_l u_{l'} v_{l'}}{ip_n + E_l + E_{l'}} - \frac{u_l v_l u_{l'} v_{l'}}{ip_n - E_l - E_{l'}} \right) (1 - n_{\rm F}(E_l) - n_{\rm F}(E_{l'})) \right. \\ &\quad \left. + \left(\frac{u_l v_l u_{l'} v_{l'}}{ip_n + E_l - E_{l'}} - \frac{u_l v_l u_{l'} v_{l'}}{ip_n - E_l + E_{l'}} \right) (n_{\rm F}(E_l) - n_{\rm F}(E_{l'})) \right]. \end{aligned} \tag{B.18}$$

Therefore, we obtain

$$\begin{aligned} S_{\rm G} &= \beta L^2 \sum_p \left[M_{11}(p)|\widetilde{\eta}(p)|^2 + \frac{1}{2} M_{12}(p)(\widetilde{\eta}(p)\widetilde{\eta}(-p) + \widetilde{\eta}^*(-p)\widetilde{\eta}^*(p)) \right] \\ &= \frac{1}{2}\beta L^2 \sum_p \begin{pmatrix} \widetilde{\eta}^*(p) & \widetilde{\eta}(-p) \end{pmatrix} M(p) \begin{pmatrix} \widetilde{\eta}(p) \\ \widetilde{\eta}^*(-p) \end{pmatrix} \end{aligned} \tag{B.19}$$

with $M_{22}(p) \equiv M_{11}(-p), M_{21}(p) \equiv M_{12}(p)$. At the zero-temperature limit $\beta \to \infty$, the inverse fluctuation propagator reduces to

$$M_{11}(p) = \frac{m}{4\pi}\left[\log\left(\frac{2\omega_B}{\epsilon_b}\right) + \psi\left(\frac{1}{2} - \frac{\mu}{\omega_B}\right)\right] + \frac{m\omega_B}{2\pi}\sum_{l=0}^{\infty}\left[\sum_{l'=0}^{\infty}|I_{l,l'}(\boldsymbol{p})|^2\left(\frac{u_l^2u_{l'}^2}{ip_n - E_l - E_{l'}} - \frac{v_l^2v_{l'}^2}{ip_n + E_l + E_{l'}}\right) + \frac{1}{2\xi_l}\right], \tag{B.20a}$$

$$M_{12}(p) = \frac{m\omega_B}{2\pi}\sum_{l=0}^{\infty}\sum_{l'=0}^{\infty}|I_{l,l'}(\boldsymbol{p})|^2\left(\frac{u_lv_lu_{l'}v_{l'}}{ip_n + E_l + E_{l'}} - \frac{u_lv_lu_{l'}v_{l'}}{ip_n - E_l - E_{l'}}\right). \tag{B.20b}$$

B.2 Calculation of the overlap

According to Ref. [72], we review the calculation of the overlap $I_{l,l'}(\boldsymbol{p})$ given by

$$I_{l,l'}(\boldsymbol{p}) = \int dy\, \mathrm{e}^{ip_y y} F_l(y) F_{l'}(y - p_x\ell_B^2). \tag{B.21}$$

To this end, we introduce creation and annihilation operators $c^\dagger, c$ for the harmonic oscillator. These operators satisfy the commutator relation $[c, c^\dagger] = 1$ and the characteristic equations,

$$c^\dagger|l\rangle = \sqrt{l+1}\,|l+1\rangle\,, \tag{B.22}$$

$$c|l\rangle = \begin{cases}\sqrt{l}\,|l-1\rangle & (l \neq 0),\\ 0 & (l = 0),\end{cases} \tag{B.23}$$

where we have defined $|l\rangle$ as $F_l(y) \equiv \langle y|l\rangle$. By expressing the operators $y, d/dy$ in terms of the creation and annihilation operators:

$$y = \frac{\ell_B}{\sqrt{2}}(c^\dagger + c), \tag{B.24}$$

$$\frac{d}{dy} = \frac{1}{\sqrt{2}\ell_B}(c^\dagger - c), \tag{B.25}$$

we obtain

$$\begin{aligned}
I_{l,l'}(\boldsymbol{p}) &= \int dy\, \mathrm{e}^{ip_y y} F_l(y) \mathrm{e}^{-p_y \ell_B^2 \frac{d}{dy}} F_{l'}(y) \\
&= \langle l | \mathrm{e}^{i\frac{p_y \ell_B}{\sqrt{2}}(c^\dagger + c)} \mathrm{e}^{-\frac{p_x \ell_B}{\sqrt{2}}(c^\dagger - c)} | l' \rangle \\
&= \mathrm{e}^{ip_x p_y \ell_B^2/2} \langle l | \mathrm{e}^{-w^* c^\dagger + wc} | l' \rangle \\
&= \mathrm{e}^{ip_x p_y \ell_B^2/2 - \boldsymbol{p}^2 \ell_B^2/4} \langle l | \mathrm{e}^{-w^* c^\dagger} \mathrm{e}^{wc} | l' \rangle \\
&= \mathrm{e}^{ip_x p_y \ell_B^2/2 - \boldsymbol{p}^2 \ell_B^2/4} \sum_{n=0}^{l} \sum_{n'=0}^{l'} \frac{1}{n! n'!} (-w^*)^n w^{n'} \langle l | (c^\dagger)^n c^{n'} | l' \rangle \\
&= \mathrm{e}^{ip_x p_y \ell_B^2/2 - \boldsymbol{p}^2 \ell_B^2/4} \sum_{n=0}^{l} \sum_{n'=0}^{l'} \frac{1}{n! n'!} \sqrt{\frac{l! l'!}{(l-n)!(l'-n')!}} (-w^*)^n w^{n'} \langle l - n | l' - n' \rangle ,
\end{aligned}$$

where $w = (p_x + ip_y)\ell_B/\sqrt{2}$ and we have applied the Baker-Campbell-Hausdorff formula,

$$\mathrm{e}^A \mathrm{e}^B = \mathrm{e}^{A + B + [A,B]/2} \tag{B.26}$$

with $[A,[A,B]] = [B,[A,B]] = 0$. For $l \geq l'$, the overlap becomes

$$\begin{aligned}
I_{l,l'}(\boldsymbol{p}) &= \sqrt{\frac{l'!}{l!}} \mathrm{e}^{ip_x p_y \ell_B^2/2 - \boldsymbol{p}^2 \ell_B^2/4} (-w^*)^{l-l'} \sum_{n'=0}^{l'} \frac{l!}{n'!(l'-n')!(n'+l-l')!} (-|w|^2)^{n'} \\
&= \sqrt{\frac{l'!}{l!}} \mathrm{e}^{ip_x p_y \ell_B^2/2 - \boldsymbol{p}^2 \ell_B^2/4} (-w^*)^{l-l'} L_{l'}^{l-l'}(|w|^2).
\end{aligned} \tag{B.27}$$

On the other hand, the overlap for $l' \geq l$ becomes

$$\begin{aligned}
I_{l,l'}(\boldsymbol{p}) &= \sqrt{\frac{l!}{l'!}} \mathrm{e}^{ip_x p_y \ell_B^2/2 - \boldsymbol{p}^2 \ell_B^2/4} w^{l'-l} L_{l'}^{l-l'}(|w|^2) \\
&= \sqrt{\frac{l'!}{l!}} \mathrm{e}^{ip_x p_y \ell_B^2/2 - \boldsymbol{p}^2 \ell_B^2/4} (-w^*)^{l-l'} L_{l'}^{l-l'}(|w|^2),
\end{aligned} \tag{B.28}$$

where we have used Eq. (B.13), and therefore, we obtain Eq. (B.12). Before moving to the next section, we expand $|I_{l,l'}(\boldsymbol{p})|^2$ up to the quadratic order in $\boldsymbol{p}$. By using

$$L_l^{l-l'}\left(\frac{\boldsymbol{p}^2 \ell_B^2}{2}\right) = \frac{l!}{l'!(l-l')!} - \frac{1}{2} \frac{l!}{(l'-1)!(l-l'+1)!} \boldsymbol{p}^2 \ell_B^2 + \mathcal{O}\left(\boldsymbol{p}^4 \ell_B^4\right), \tag{B.29}$$

we have

$$|I_{l,l'}(\boldsymbol{p})|^2 \simeq \frac{l!}{l'![(l-l')!]^2}\left[\frac{\boldsymbol{p}^2\ell_B^2}{2}\right]^{l-l'}\left[1-\frac{1}{2}\left(1+\frac{2l'}{l-l'+1}\right)\boldsymbol{p}^2\ell_B^2\right]$$
$$= \begin{cases} \dfrac{l}{2}\boldsymbol{p}^2\ell_B^2 & (l'=l-1), \\ 1-\left(l+\dfrac{1}{2}\right)\boldsymbol{p}^2\ell_B^2 & (l'=l), \\ \dfrac{l+1}{2}\boldsymbol{p}^2\ell_B^2 & (l'=l+1), \\ \mathcal{O}(\boldsymbol{p}^4) & (\text{otherwise}). \end{cases} \tag{B.30}$$

B.3 Inverse fluctuation propagator in the low-energy limit

In this section, we compute the inverse fluctuation propagator in the low-energy limit $\omega, \boldsymbol{p} \to 0$ with the analytical continuation $ip_n \to \omega + i0^+$ to obtain physical quantities such as sound velocity and superfluid density. Expanding the elements $M_{11}(p)$ and $M_{12}(p)$ in Eqs. (B.20) up to the quadratic order in $\omega, \boldsymbol{p}$ with Eq. (B.30) yields

$$M_{11}(p) \simeq a_0 + a_1\omega + a_2\omega^2 + b_2\boldsymbol{p}^2, \tag{B.31a}$$
$$M_{12}(p) \simeq a_0' + a_2'\omega^2 + b_2'\boldsymbol{p}^2 \tag{B.31b}$$

with

$$a_0 = \frac{m}{4\pi}\left[\log\left(\frac{2\omega_B}{\epsilon_b}\right)+\psi\left(\frac{1}{2}-\frac{\mu}{\omega_B}\right)\right]-\frac{m\omega_B}{4\pi}\sum_{l=0}^{\infty}\left[\frac{2\xi_l^2+\Delta_0^2}{2E_l^3}-\frac{1}{\xi_l}\right],$$
$$= \frac{m\omega_B}{8\pi}\sum_{l=0}^{\infty}\frac{\Delta_0^2}{E_l^3}, \tag{B.32a}$$
$$a_1 = -\frac{m\omega_B}{8\pi}\sum_{l=0}^{\infty}\frac{\xi_l}{E_l^3}, \tag{B.32b}$$
$$a_2 = -\frac{m\omega_B}{32\pi}\sum_{l=0}^{\infty}\frac{2\xi_l^2+\Delta_0^2}{E_l^5}, \tag{B.32c}$$
$$b_2 = \frac{1}{4\pi}\sum_{l=0}^{\infty}\left[\left(l+\frac{1}{2}\right)\frac{2\xi_l^2+\Delta_0^2}{2E_l^3}-l\frac{u_l^2u_{l-1}^2+v_l^2v_{l-1}^2}{E_l+E_{l-1}}-(l+1)\frac{u_l^2u_{l+1}^2+v_l^2v_{l+1}^2}{E_l+E_{l+1}}\right], \tag{B.32d}$$

$$a_0' = a_0, \tag{B.32e}$$

$$a_2' = \frac{m\omega_B}{32\pi}\sum_{l=0}^{\infty}\frac{\Delta_0^2}{E_l^5}, \tag{B.32f}$$

$$b_2' = -\frac{1}{4\pi}\sum_{l=0}^{\infty}\left[\left(l+\frac{1}{2}\right)\frac{\Delta_0^2}{2E_l^3} - 2l\frac{u_l v_l u_{l-1} v_{l-1}}{E_l + E_{l-1}} - 2(l+1)\frac{u_l v_l u_{l+1} v_{l+1}}{E_l + E_{l+1}}\right], \tag{B.32g}$$

where we have used the relations:

$$u_l v_l = \frac{\Delta_0}{2E_l}, \tag{B.33a}$$

$$u_l^4 + v_l^4 = \frac{2\xi_l^2 + \Delta_0^2}{2E_l^2}, \tag{B.33b}$$

$$u_l^4 - v_l^4 = \frac{\xi_l}{E_l}. \tag{B.33c}$$

We note that we use the gap equation (3.25) to show $a_0 = a_0'$.

List of Publications

1. Takaaki Anzai and Yusuke Nishida, "Two-dimensional Fermi gas in antiparallel magnetic fields," Phys. Rev. A **95**, 051603(R) (2017).

2. Takaaki Anzai and Yusuke Nishida, "Two-dimensional imbalanced Fermi gas in antiparallel magnetic fields," Phys. Rev. A **100**, 043615 (2019).

Acknowledgement

I would like to express my gratitude to my supervisor Prof. Yusuke Nishida for his support and encouragement. I have discussed my research with him ever since I belonged to his laboratory, and this thesis would have not been achieved without insightful comments and fruitful suggestions. I am also grateful to members of Nishida's group and Condensed Matter Theory Group at Tokyo Institute of Technology. In particular, we would like to thank Dr. Yuta Sekino, Dr. Yuki Bando, Mr. Keisuke Fujii, Mr. Takuya Furusawa, and Mr. Tatsuya Amitani for various discussions. I acknowledge the financial support from International Research Center for Nanoscience and Quantum Physics, Tokyo Institute of Technology.

Bibliography

[1] I. Bloch, J. Dalibard, and W. Zwerger, "Many-body physics with ultracold gases," Rev. Mod. Phys. **80**, 885-964 (2008).

[2] *The BCS-BEC Crossover and the Unitary Fermi Gas*, edited by W. Zwerger (Springer, Berlin, 2012).

[3] D. M. Eagles, "Possible pairing without superconductivity at low carrier concentrations in bulk and thin-film superconducting semiconductors," Phys. Rev. **186**, 456 (1969).

[4] A. J. Leggett, *Diatomic molecules and cooper pairs* in *Modern Trends in the Theory of Condensed Matter,* edited by A. Pękalski and J. A. Przystawa (Springer, Berlin, 1980).

[5] A. J. Leggett, "Cooper pairing in spin-polarized Fermi systems," J. Phys. Colloques **41**, C7 (1980).

[6] P. Nozières and S. Schmitt-Rink, "Bose condensation in an attractive fermion gas: From weak to strong coupling superconductivity," J. Low Temp. Phys. **59**, 195 (1985).

[7] K. Miyake, "Fermi liquid theory of dilute submonolayer ^{3}He on thin ^{4}He II film: dimer bound state and Cooper pairs," Prog. Theor. Phys. **69**, 1794 (1983).

[8] M. Randeria, J.-M. Duan, and L.-Y. Shieh, "Bound states, Cooper pairing, and Bose condensation in two dimensions," Phys. Rev. Lett. **62**, 981-984 (1989).

[9] M. Randeria, J.-M. Duan, and L.-Y. Shieh, "Superconductivity in a two-dimensional Fermi gas: Evolution from Cooper pairing to Bose condensation," Phys. Rev. B **41**, 327-343 (1990).

[10] C. A. Regal, M. Greiner, and D. S. Jin, "Observation of resonance condensation of fermionic atom pairs," Phys. Rev. Lett. **92**, 040403 (2004).

[11] M. W. Zwierlein, C. A. Stan, C. H. Schunck, S. M. F. Raupach, A. J. Kerman, and W. Ketterle, "Condensation of pairs of fermionic atoms near a Feshbach resonance," Phys. Rev. Lett. **92**, 120403 (2004).

[12] S. Inouye, M. R. Andrews, J. Stenger, H.-J. Miesner, D. M. Stamper-Kurn, and W. Ketterle, "Observation of Feshbach resonances in a Bose-Einstein condensate," Nature (London) **392**, 151 (1998).

[13] Ph. Courteille, R. S. Freeland, D. J. Heinzen, F. A. van Abeelen, and B. J. Verhaar, "Observation of a Feshbach resonance in cold atom scattering," Phys. Rev. Lett. **81**, 69 (1998).

[14] I. Bloch, "Ultracold quantum gases in optical lattices," Nat. Phys. **1**, 23-30 (2005).

[15] G. Modugno, F. Ferlaino, R. Heidemann, G. Roati, and M. Inguscio, "Production of a Fermi gas of atoms in an optical lattice," Phys. Rev. A **68**, 011601(R) (2003).

[16] K. Martiyanov, V. Makhalov, and A. Turlapov, "Observation of a two-dimensional Fermi gas of atoms," Phys. Rev. Lett. **105**, 030404 (2010).

[17] P. Dyke, E. D. Kuhnle, S. Whitlock, H. Hu, M. Mark, S. Hoinka, M. Lingham, P. Hannaford, and C. J. Vale, "Crossover from 2D to 3D in a weakly interacting Fermi gas," Phys. Rev. Lett. **106**, 105304 (2011).

[18] M. Feld, B. Fröhlich, E. Vogt, M. Koschorreck, and M. Köhl, "Observation of a pairing pseudogap in a two-dimensional Fermi gas," Nature (London) **480**, 75-78 (2011).

[19] B. Fröhlich, M. Feld, E. Vogt, M. Koschorreck, W. Zwerger, and M. Köhl, "Radio-frequency spectroscopy of a strongly interacting two-dimensional Fermi gas," Phys. Rev. Lett. **106**, 105301 (2011).

[20] A. T. Sommer, L. W. Cheuk, M. J. H. Ku, W. S. Bakr, and M. W. Zwierlein, "Evolution of fermion pairing from three to two dimensions," Phys. Rev. Lett. **108**, 045302 (2012).

[21] S. K. Baur, B. Fröhlich, M. Feld, E. Vogt, D. Pertot, M. Koschorreck, and M. Köhl, "Radio-frequency spectra of Feshbach molecules in quasi-two-dimensional geometries," Phys. Rev. A **85**, 061604(R) (2012).

[22] E. Vogt, M. Feld, B. Fröhlich, D. Pertot, M. Koschorreck, and M. Köhl, "Scale invariance and viscosity of a two-dimensional Fermi gas," Phys. Rev. Lett. **108**, 070404 (2012).

[23] Y. Zhang, W. Ong, I. Arakelyan, and J. E. Thomas, "Polaron-to-polaron transitions in the radio-frequency spectrum of a quasi-two-dimensional Fermi gas," Phys. Rev. Lett. **108**, 235302 (2012).

[24] M. Koschorreck, D. Pertot, E. Vogt, B. Fröhlich, M. Feld, and M. Köhl, "Attractive and repulsive Fermi polarons in two dimensions," Nature (London) **485**, 619-622 (2012).

[25] B. Fröhlich, M. Feld, E. Vogt, M. Koschorreck, M. Köhl, C. Berthod, and T. Giamarchi, "Two-dimensional Fermi liquid with attractive interactions," Phys. Rev. Lett. **109**, 130403 (2012).

[26] V. Makhalov, K. Martiyanov, and A. Turlapov, "Ground-state pressure of quasi-2D Fermi and Bose gases," Phys. Rev. Lett. **112**, 045301 (2014).

[27] W. Ong, C. Cheng, I. Arakelyan, and J. E. Thomas, "Spin-imbalanced quasi-two-dimensional Fermi gases," Phys. Rev. Lett. **114**, 110403 (2015).

[28] M. G. Ries, A. N. Wenz, G. Zürn, L. Bayha, I. Boettcher, D. Kedar, P. A. Murthy, M. Neidig, T. Lompe, and S. Jochim, "Observation of pair condensation in the quasi-2D BEC-BCS crossover," Phys. Rev. Lett. **114**, 230401 (2015).

[29] P. A. Murthy, I. Boettcher, L. Bayha, M. Holzmann, D. Kedar, M. Neidig, M. G. Ries, A. N. Wenz, G. Zürn, and S. Jochim, "Observation of the Berezinskii-Kosterlitz-Thouless phase transition in an ultracold Fermi gas," Phys. Rev. Lett. **115**, 010401 (2015).

[30] K. Fenech, P. Dyke, T. Peppler, M. G. Lingham, S. Hoinka, H. Hu, and C. J. Vale, "Thermodynamics of an attractive 2D Fermi gas," Phys. Rev. Lett. **116**, 045302 (2016).

[31] I. Boettcher, L. Bayha, D. Kedar, P. A. Murthy, M. Neidig, M. G. Ries, A. N. Wenz, G. Zürn, S. Jochim, and T. Enss, "Equation of state of ultracold fermions in the 2D BEC-BCS crossover region," Phys. Rev. Lett. **116**, 045303 (2016).

[32] C. Cheng, J. Kangara, I. Arakelyan, and J. E. Thomas, "Fermi gases in the two-dimensional to quasi-two-dimensional crossover," Phys. Rev. A **94**, 031606(R) (2016).

[33] V. L. Berezinskii, "Destruction of long-range order in one-dimensional and two-dimensional systems having a continuous symmetry group I. classical systems," Sov. Phys. JETP **32**, 493 (1971).

[34] V. L. Berezinskii, "Destruction of long-range order in one-dimensional and two-dimensional systems having a continuous symmetry group II. quantum systems," Sov. Phys. JETP **34**, 610 (1972).

[35] J. M. Kosterlitz and D. J. Thouless, "Ordering, metastability and phase transitions in two-dimensional systems," J. Phys. C **6**, 1181 (1973).

[36] J. M. Kosterlitz and D. J. Thouless, "The critical properties of the two-dimensional xy model," J. Phys. C **7**, 1046 (1974).

[37] M. W. Zwierlein, A. Schirotzek, C. H. Schunck, W. Ketterle, "Fermionic superfluidity with imbalanced spin populations," Science **311**, 492 (2006).

[38] G. B. Partridge, W. Li, R. I. Kamar, Y.-a. Liao, and R. G. Hulet, "Pairing and phase separation in a polarized Fermi gas," Science **311**, 503 (2006).

[39] G. J. Conduit, P. H. Conlon, and B. D. Simons, "Superfluidity at the BEC-BCS crossover in two-dimensional Fermi gases with population and mass imbalance," Phys. Rev. A **77**, 053617 (2008).

[40] S. Yin, J.-P. Martikainen, and P. Törmä, "Fulde-Ferrell states and Berezinskii-Kosterlitz-Thouless phase transition in two-dimensional imbalanced Fermi gases," Phys. Rev. B **89**, 014507 (2014).

[41] D. E. Sheehy, "Fulde-Ferrell-Larkin-Ovchinnikov state of two-dimensional imbalanced Fermi gases," Phys. Rev. A **92**, 053631 (2015).

[42] U. Toniolo, B. Mulkerin, X.-J. Liu, and H. Hu, "Larkin-Ovchinnikov superfluidity in a two-dimensional imbalanced atomic Fermi gas," Phys. Rev. A **95**, 013603 (2017).

[43] P. Fulde and R. A. Ferrell, "Superconductivity in a strong spin-exchange field," Phys. Rev. **135**, A550-A563 (1964).

[44] A. I. Larkin and Yu. N. Ovchinnikov, "Nonuniform state of superconductors," Sov. Phys. JETP **20**, 762-769 (1965).

[45] N. R. Cooper, "Rapidly rotating atomic gases," Adv. Phys. **57**, 539 (2008).

[46] A. L. Fetter, "Rotating trapped Bose-Einstein condensates," Rev. Mod. Phys. **81**, 647 (2009).

[47] J. Dalibard, F. Gerbier, G. Juzeliūnas, and P. Öhberg, "Colloquium: Artificial gauge potentials for neutral atoms," Rev. Mod. Phys. **83**, 1523-1543 (2011).

[48] N. Goldman, G. Juzeliūnas, P. Öhberg, and I. B. Spielman, "Light-induced gauge fields for ultracold atoms," Rep. Prog. Phys. **77**, 126401 (2014).

[49] N. R. Cooper, J. Dalibard, and I. B. Spielman, "Topological bands for ultracold atoms," Rev. Mod. Phys. **91**, 015005 (2019).

[50] M. R. Matthews, B. P. Anderson, P. C. Haljan, D. S. Hall, C. E. Wieman, and E. A. Cornell, "Vortices in a Bose-Einstein condensate," Phys. Rev. Lett. **83**, 2498 (1999).

[51] K. W. Madison, F. Chevy, W. Wohlleben, and J. Dalibard, "Vortex formation in a stirred Bose-Einstein condensate," Phys. Rev. Lett. **84**, 806 (2000).

[52] J. R. Abo-Shaeer, C. Raman, J. M. Vogels, and W. Ketterle, "Observation of vortex lattices in Bose-Einstein condensates," Science **292**, 476 (2001).

[53] M. W. Zwierlein, J. R. Abo-Shaeer, A. Schirotzek, C. H. Schunck, and W. Ketterle, "Vortices and superfluidity in a strongly interacting Fermi gas," Nature **435**, 1047 (2005).

[54] Y.-J. Lin, R. L. Compton, A. R. Perry, W. D. Phillips, J. V. Porto, and I. B. Spielman, "Bose-Einstein condensate in a uniform light-induced vector potential," PhysṘev. Lett. **102**, 130401 (2009).

[55] Y.-J. Lin, R. L. Compton, K. Jiménez-García, J. V. Porto, and I. B. Spielman, "Synthetic magnetic fields for ultracold neutral atoms," Nature (London) **462**, 628 (2009).

[56] M. C. Beeler, R. A. Williams, K. Jiménez-García, L. J. LeBlanc, A. R. Perry, and I. B. Spielman, "The spin Hall effect in a quantum gas," Nature (London) **498**, 201-204 (2013).

[57] M. Aidelsburger, M. Atala, M. Lohse, J. T. Barreiro, B. Paredes, and I. Bloch, "Realization of the Hofstadter Hamiltonian with ultracold atoms in optical lattices," Phys. Rev. Lett. **111**, 185301 (2013).

[58] C. J. Kennedy, G. A. Siviloglou, H. Miyake, W. C. Burton, and W. Ketterle, "Spin-orbit coupling and quantum spin Hall effect for neutral atoms without spin flips," Phys. Rev. Lett. **111**, 225301 (2013).

[59] C. L. Kane and E. J. Mele, "Quantum spin Hall effect in graphene," Phys. Rev. Lett. **95**, 226801 (2005).

[60] C. L. Kane and E. J. Mele, "Z_2 topological order and the quantum spin Hall effect," Phys. Rev. Lett. **95**, 146802 (2005).

[61] B. A. Bernevig and S.-C. Zhang, "Quantum spin Hall effect," Phys. Rev. Lett. **96**, 106802 (2006).

[62] J. P. Eisenstein and A. H. MacDonald, "Bose-Einstein condensation of excitons in bilayer electron systems," Nature (London) **432**, 691-694 (2004).

[63] I. A. Shovkovy, "Magnetic catalysis: A review," Lect. Notes Phys. **871**, 13 (2013).

[64] V. A. Miransky and I. A. Shovkovy, "Quantum field theory in a magnetic field: From quantum chromodynamics to graphene and Dirac semimetals," Phys. Rep. **576**, 1-209 (2015).

[65] V. P. Gusynin, V. A. Miransky, and I. A. Shovkovy, "Catalysis of dynamical flavor symmetry breaking by a magnetic field in 2 + 1 dimension," Phys. Rev. Lett. **73**, 3499 (1994).

[66] V. P. Gusynin, V. A. Miransky, and I. A. Shovkovy, "Dynamical flavor symmetry breaking by a magnetic field in 2+1 dimensions," Phys. Rev. D **52**, 4718 (1995).

[67] V. P. Gusynin, V. A. Miransky, and I. A. Shovkovy, "Dimensional reduction and dynamical chiral symmetry breaking by a magnetic field in 3 + 1 dimensions," Phys. Lett. B **349**, 477 (1995).

[68] X.-J. Liu, X. Liu, L. C. Kwek, and C. H. Oh, "Fractional spin Hall effect in atomic Bose gases," Phys. Rev. B **79**, 165301 (2009).

[69] O. Fialko, J. Brand, and U. Zülicke, "Fragility of the fractional quantum spin Hall effect in quantum gases," New J. Phys. **16**, 025006 (2014).

[70] S. Furukawa and M. Ueda, "Global phase diagram of two-component Bose gases in antiparallel magnetic fields," Phys. Rev. A **90**, 033602 (2014).

[71] T. Yoshino, S. Furukawa, S. Higashikawa, and M. Ueda, "Collective modes of vortex lattices in two-component Bose-Einstein condensates under synthetic gauge fields," New J. Phys. **21**, 015001 (2019).

[72] B. Feng, D.-f. Hou, and H.-c. Ren, "Magnetic and inverse magnetic catalysis in the Bose-Einstein condensation of neutral bound pairs," Phys. Rev. D **92**, 065011 (2015).

[73] D. Cocks, P. P. Orth, S. Rachel, M. Buchhold, K. Le Hur, and W. Hofstetter, "Time-reversal-invariant Hofstadter-Hubbard model with ultracold fermions," Phys. Rev. Lett. **109**, 205303 (2012).

[74] L. Wang, H.-H. Hung, and M. Troyer, "Topological phase transition in the Hofstadter-Hubbard model," Phys. Rev. B **90**, 205111 (2014).

[75] M. Iskin, "Attractive Hofstadter-Hubbard model with imbalanced chemical and vector potentials," Phys. Rev. A **91**, 053606 (2015).

[76] R. O. Umucalılar and M. Iskin, "BCS theory of time-reversal-symmetric Hofstadter-Hubbard model," Phys. Rev. Lett. **119**, 085301 (2017).

[77] M. Iskin, "Hofstadter-Hubbard model with opposite magnetic fields: Bardeen-Cooper-Schrieffer pairing and superfluidity in the nearly flat butterfly bands," Phys. Rev. A **96**, 043628 (2017).

[78] S. Peotta and P. Törmä, "Superfluidity in topologically nontrivial flat bands," Nat. Commun. **6**, 8944 (2015).

[79] M. Iskin, "Berezinskii-Kosterlitz-Thouless transition in the time-reversal-symmetric Hofstadter-Hubbard model," Phys. Rev. A **97**, 013618 (2018).

[80] C. Zeng, T. D. Stanescu, C. Zhang, V. W. Scarola, and S. Tewari, "Majorana corner modes with solitons in an attractive Hubbard-Hofstadter model of cold atom optical lattices," Phys. Rev. Lett. **123**, 060402 (2019).

[81] J. Levinsen and M. M. Parish, "Strongly interacting two-dimensional Fermi gases," Annu. Rev. Cold At. Mol. **3**, 1 (2015).

[82] D. S. Petrov and G. V. Shlyapnikov, "Interatomic collisions in a tightly confined Bose gas," Phys. Rev. A. **64**, 012706 (2001).

[83] G. Sarma, "On the influence of a uniform exchange field acting on the spins of the conduction electrons in a superconductor," J. Phys. Chem. Solids **24**, 1029 (1963).

[84] E. Gubankova, A. Schmitt, and F. Wilczek, "Stability conditions and Fermi surface topologies in a superconductor," Phys. Rev. B **74**, 064505 (2006).

[85] L. He and P. Zhuang, "Phase diagram of a cold polarized Fermi gas in two dimensions," Phys. Rev. A **78**, 033613 (2008).

[86] J. Carlson and S. Reddy, "Asymmetric two-component fermion systems in strong coupling," Phys. Rev. Lett. **95**, 060401 (2005).

[87] D. E. Sheehy and L. Radzihovsky, "BEC-BCS crossover in " magnetized " Feshbach-resonantly paired superfluids," Phys. Rev. Lett. **96**, 060401 (2006).

[88] C.-H. Pao, S.-T. Wu, and S.-K. Yip, "Superfluid stability in the BEC-BCS crossover," Phys. Rev. B **73**, 132506 (2006).

[89] H. Hu and X.-J. Liu, "Mean-field phase diagrams of imbalanced Fermi gases near a Feshbach resonance," Phys. Rev. A **73**, 051603(R) (2006).

[90] D. T. Son and M. A. Stephanov, "Phase diagram of a cold polarized Fermi gas," Phys. Rev. A **74**, 013614 (2006).

[91] D. E. Sheehy and L. Radzihovsky, "BEC–BCS crossover, phase transitions and phase separation in polarized resonantly-paired superfluids," Ann. Phys. **322** 1790 (2007).

[92] M. P. A. Fisher, P. B. Weichman, G. Grinstein, and D. S. Fisher, "Boson localization and the superfluid-insulator transition," Phys. Rev. B **40**, 546-570 (1989).

[93] D. Jaksch, C. Bruder, J. I. Cirac, C. W. Gardiner, and P. Zoller, "Cold bosonic atoms in optical lattices," Phys. Rev. Lett. **81**, 3108 (1998).

[94] M. Greiner, O. Mandel, T. Esslinger, T. W. Hänsch, and I. Bloch, "Quantum phase transition from a superfluid to a Mott insulator in a gas of ultracold atoms," Nature **415**, 39 (2002).

[95] T. Stöferle, H. Moritz, C. Schori, M. Köhl, and T. Esslinger, "Transition from a strongly interacting 1D superfluid to a Mott insulator," Phys. Rev. Lett. **92**, 130403 (2004).

[96] I. B. Spielman, W. D. Phillips, and J. V. Porto, "Mott-insulator transition in a two-dimensional atomic Bose gas," Phys. Rev. Lett. **98**, 080404 (2007).

[97] I. B. Spielman, W. D. Phillips, and J. V. Porto, "Condensate fraction in a 2D Bose gas measured across the Mott-insulator transition," Phys. Rev. Lett. **100**, 120402 (2008).

[98] D. van Oosten, P. van der Straten, and H. T. C. Stoof, "Quantum phases in an optical lattice," Phys. Rev. A **63**, 053601 (2001).

[99] See, for example, S. Sachdev, *Quantum Phase Transitions*, 2nd ed. (Cambridge University Press, Cambridge, UK, 2011).

[100] J. Schwinger, "On gauge invariance and vacuum polarization," Phys. Rev. **82**, 664 (1951).

[101] I. S. Gradshteyn and I. M. Ryzhik, *Table of Integrals, Series, and Products,* 7th ed., edited by A. Jeffrey and D. Zwillinger (Academic Press, Burlington, MA, 2007).

[102] See, for example, A. Altland and B. D. Simons, *Condensed Matter Field Theory*, 2nd ed. (Cambridge University Press, Cambridge, UK, 2010).

[103] See, for example, L. D. Landau and L. M. Lifshitz, *Quantum Mechanics*, 3rd ed. (Butterworth-Heinemann, Oxford, UK, 1977).

[104] M. Marini, F. Pistolesi, and G. C. Strinati, "Evolution from BCS superconductivity to Bose condensation: Analytic results for the crossover in three dimensions," Eur. Phys. J. B **1**, 151-159 (1998).

[105] C. N. Yang, "Concept of off-diagonal long-range order and the quantum phases of liquid He and of superconductors," Rev. Mod. Phys. **34**, 694 (1962).

[106] A. J. Leggett, *Quantum Liquids. Bose Condensation and Cooper Pairing in Condensed-Matter Systems*, (Oxford University Press, Oxford, 2006).

[107] L. Salasnich, "Condensate fraction of a two-dimensional attractive Fermi gas," Phys. Rev. A **76**, 015601 (2007).

[108] J. R. Engelbreht, M. Randeria, and C. A. R. Sá de Melo, "BCS to Bose crossover: Broken-symmetry state," Phys. Rev. B. **55**, 22 (1997).

[109] R. B. Diener, R. Sensarma, and M. Randeria, "Quantum fluctuations in the superfluid state of the BCS-BEC crossover," Phys. Rev. A **77**, 023626 (2008).

[110] N. Yoshida and S.-K. Yip, "Larkin-Ovchinnikov state in resonant Fermi gas," Phys. Rev. A **75**, 063601 (2007).

[111] A. Bulgac and M. M. Forbes, "Unitary Fermi supersolid: The Larkin-Ovchinnikov phase," Phys. Rev. Lett. **101**, 215301 (2008).

[112] S. Matsuo, S. Higashitani, Y. Nagato, and K. Nagai, "Phase diagram of the Fulde-Ferrell-Larkin-Ovchinnikov state in a three-dimensional superconductor," J. Phys. Soc. Jpn. **67**, 280-289 (1998).

[113] H. Shimahara, "Structure of the Fulde-Ferrell-Larkin-Ovchinnikov state in two-dimensional superconductors," J. Phys. Soc. Jpn. **67**, 736-739 (1998).

[114] C. A. R. Sá de Melo, M. Randeria, and J. R. Engelbrecht, "Crossover from BCS to Bose superconductivity: Transition temperature and time-dependent Ginzburg-Landau theory," Phys. Rev. Lett. **71**, 3202 (1993).

[115] K. Yamashita, K. Asano, and T. Ohashi, "Quantum condensation in electron–hole bilayers with density imbalance," J. Phys. Soc. Jpn. **79**, 033001 (2010).

[116] M. P. Mink, H. T. C. Stoof, R. A. Duine, and A. H. MacDonald, "Influence of remote bands on exciton condensation in double-layer graphene," Phys. Rev. B **84**, 155409 (2011).